End of Degree Project
Degree in Industrial Technologies Engineering

Analytical study of a hovering magnetic system (Levitron)

Author: Alfonso García-Agúndez Blanco
Tutors: Antonio González Fernández
Manuel Toscano Jiménez

Applied Physics III Department
Higher Technical School of Engineering
University of Seville

Seville, 2017

End of Degree Project
Degree in Industrial Technologies Engineering

Analytical study of a hovering magnetic system (Levitron)

Author:
Alfonso García-Agúndez Blanco

Tutors:
Prof. Dr. Antonio González Fernández

Prof. Dr. Manuel Toscano Jiménez

Applied Physics III Department
Higher Technical School of Engineering
University of Seville
Seville, 2017

End of Degree Project: Analytical study of a hovering magnetic system (Levitron)

Author: Alfonso García-Agúndez Blanco

Tutors: Antonio González Fernández
Manuel Toscano Jiménez

El tribunal nombrado para juzgar el Proyecto arriba indicado, compuesto por los siguientes miembros:

Presidente:

Vocales:

Secretario:

Acuerdan otorgarle la calificación de:

El Secretario del Tribunal

Fecha:

Agradecimientos

Quiero dar las gracias, en primer lugar, a mis padres, que dan todo por mi bienestar y buscan por encima de cualquier cosa la felicidad de sus hijos. No hay palabras para agradecer todo vuestro esfuerzo diario. También agradecer a mis hermanos por compartir su día a día conmigo apoyándome y dándome cariño.

A mis amigos, tanto a los de siempre como a los que he tenido la oportunidad de conocer en la Escuela, por ser mi segunda familia estos años. Especialmente, gracias a aquellos que han apostado por mi siempre y a los que se han interesado en el día a día sobre la marcha del trabajo, preguntándome e interesándose por el progreso.

Gracias a Antonio por su total implicación en el trabajo desde el día que me ofreció el tema, por las reuniones de todos los jueves, por transmitirme conocimientos de diversas áreas (desde electromagnetismo hasta cuaterniones) y por el continuo interés mostrado.

Gracias a Manuel, por transmitirme su entusiasmo también desde el primer día, por orientarme y aconsejarme en distintos puntos del trabajo y por confiar en mi, dándome tranquilidad y seguridad.

Por último, quiero mencionar a Paula, que junto a mis padres, es la persona que ha seguido conmigo la evolución de este trabajo desde el inicio. Agradecerle sus consejos, sobre todo de programación, y el apoyo diario.

Abstract (English)

The scope of this project is to perform an analytical study of the hovering magnetic system, known as Levitron. Firstly, we will start with an introduction where we explain how the toy works, the typical elements of the kit and its history. In chapter 2, the analytical study starts: we begin describing the free motion, in absence of the external magnetic field and solely submitted to the action of gravity, using the Classic Euler angles. Nevertheless, the use of these angles leads to a singularity that we need to avoid, so in chapter 3 we present the Tait-Bryan angles to solve this problem.

In chapter 4 we obtain the expressions for the magnetic field generated by the base, and in chapter 5 we outline Earnshaw's Theorem and study the static stability by means of the potential energy of the system.

In chapter 6, we derive the equations of motion using vector mechanics, and in chapter 7 the same is done using the Lagrangian and Hamiltonian formulation of the analytical mechanics.

Once the equations of the system are obtained, we define nondimensional variables in chapter 8 to perform the numerical simulations. In chapter 9 we study the linear stability of the system, obtaining the stability region for which stable hovering is possible and the normal modes. In chapter 10 we analyze the linear and nonlinear coupling, and numerically simulate the trajectory of the spinning top considering different initial conditions that reproduce real situations when one plays with the toy.

In chapter 11, we present the constants of the motion of the system, and in chapter 12 a simple model considering air friction is shown. Finally, chapter 13 contains some instructions to master the toy and we attach a flowchart where we describe the usual situations that a player has to face to achieve levitation.

Lastly, we include three addendums: the first contains the experimental adjustment of the magnetic field generated by the base in the $0Z_1$ axis; the second is dedicated to the quaternions, containing the main properties of its algebra and the set of equations of the system in terms of the Euler parameters; and finally, in the third we study the dynamics of three systems that share some of the characteristics of the hovering magnetic device.

Resumen

El objetivo de este proyecto es llevar a cabo un estudio analítico del sistema de levitación magnética, conocido como Levitron. En primer lugar, se va a empezar haciendo una introducción explicando el funcionamiento del juguete, los elementos típicos que conforman el kit para jugar y su historia. En el capítulo 2 comienza el estudio analítico: se empieza describiendo el movimiento de la peonza como sólido libre, en ausencia de campo magnético externo y sometida únicamente a la acción de la gravedad, utilizando los ángulos clásicos de Euler. Sin embargo, veremos que el uso de estos ángulos produce una singularidad que nos obligará a presentar, en el capítulo 3, los ángulos de Tait-Byan para solucionarlo.

En el capítulo 4 obtenemos las expresiones del campo magnético creado por la base, y en el capítulo 5 enunciamos el Teorema de Earnshaw y se estudia la estabilidad estática del sistema por medio de su energía potencial.

En el capítulo 6, se obtienen las ecuaciones de movimiento utilizando la mecánica vectorial, y en el capítulo 7 se obtienen las ecuaciones del sistema empleando la formulación Lagrangiana y Hamiltoniana de la mecánica analítica.

Una vez obtenidas las ecuaciones, se introducen variables adimensionales en el capítulo 8 para llevar a cabo la simulación numérica de los posteriores apartados. En el capítulo 9 estudiamos la estabilidad lineal del sistema, obteniendo la región de estabilidad en la que es posible la levitación y los modos normales de movimiento. En el capítulo 10, analizamos el acoplamiento lineal y no lineal y simulamos numéricamente la trayectoria considerando distintas condiciones iniciales que intentan reproducir situaciones reales que se dan a la hora de jugar.

En el capítulo 11 presentamos las constantes de movimiento del sistema, y en el capítulo 12 se elabora un sencillo modelo para tener en cuenta el efecto de la fricción del aire sobre la peonza. Finalmente, en el capítulo 13 se añaden algunas instrucciones para dominar el juguete y se adjunta un diagrama de flujo donde se describen las situaciones habituales a las que un jugador se enfrenta cuando intenta hacer levitar la peonza.

Por último, se adjuntan tres anexos: el primero contiene el ajuste experimental del campo magnético en el eje $0Z_1$; el segundo está dedicado a los cuaterniones, incluyendo las propiedades más importantes y el sistema con las ecuaciones de movimiento en término de los parámetros de Euler; y en el tercero, se estudia la dinámica de tres sistemas que guardan analogías con el sistema de levitación magnética.

Index

LIST OF FIGURES

1 INTRODUCTION

1.1 What is a Levitron?

The **hovering magnetic device** consists on a permanent magnetic top and its corresponding **magnetic base** plate, with a ring-shape or others alternate geometric configurations. In specific conditions and under top rotation the magnetic, gyroscopic and gravitational forces are balanced, and the top remains in levitation. The stabilizing rotational speed of the hovering top decreases due to air friction, becoming gradually slower, so that the hovering phenomenon fails within two minutes unless external power is supplied to sustain rotation.

Figure 1-1: Levitron toy.

This method, with moving permanent magnets, **is quite distinct from other versions which use changing electromagnetic fields**, levitating various items in a permanent way. This kind of device isn't in the scope of this study.

Figure 1-2: Versions of the toy with changing electromagnetic fields.

The most known brand of spin-stabilized magnetic levitation device is **Levitron**. **Levitron®** is a brand of levitating toys and gifts in science and educational markets marketed by Creative Gifts Inc. and Fascination Toys & Gifts.

The typical contents of a Levitron kit are:

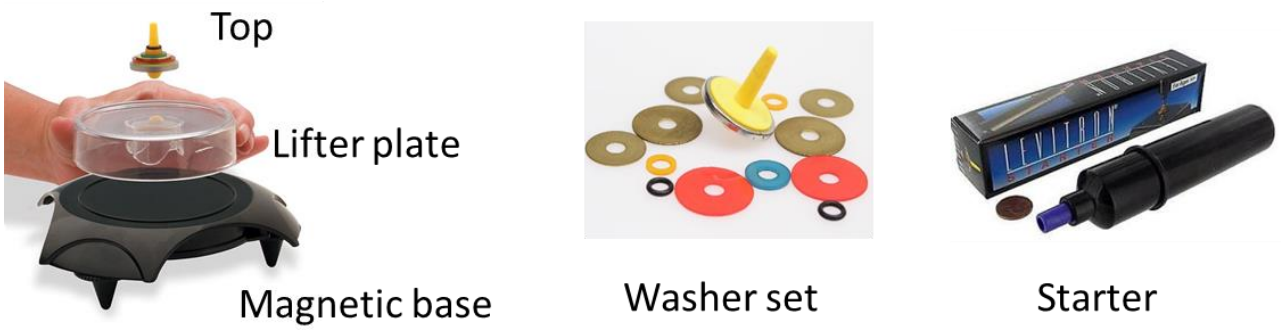

Figure 1-3: Contents of a Levitron kit.

1.2 How does it work?

In order to achieve the hovering, a plastic lifter plate is placed on top of the magnetic base, and the top is spun on the plate with a rotational speed between 25-50 rotations per second (1500-3000 rpm). If too slow, the top falls over and flies off sideways; if too fast it does not orient itself to follow the magnetic field lines as it moves, and slides off. Since it can be difficult to spin the top fast enough by hand, Creative Gifts makes a battery-powered, hand held device to spin the top with an electric motor. Next, the plate is lifted by hand until, if conditions are right, the top rises above it to an equilibrium point. The top must also be weighted with washers of various sizes supplied in the kit. If too heavy it will not rise above the plate; if too light it flies off. After a few minutes, the top falls when air friction slows it below a lower critical speed.

Figure 1-4: View of the base magnet and legs.

The top is a rotationally symmetric rigid body with mass m, polar and transversal moments of inertia I_Z and I_X, angular momentum with respect to the center of mass $\vec{L}_G$ and angular speed $\vec{\omega}$ whose centre of mass G is located at $\vec{r} = \{x, y, z\}$. It can be regarded as a magnetic dipole with magnetic moment $\vec{\mu}$ centered in $\vec{r}$ and directed along its axis of symmetry. The gradients of the magnetic field $B(r)$ compensate for the gravitational force by generating a repulsive force that acts on $\vec{\mu}$ in the presence of $\vec{L}_G$ (whose gyroscopic effect prevents the top from overturning and falling) and must provide the mechanism for the top to levitate in a stable way above the base.

1.3 Levitron's history

According to [1], the first spin-stabilized permanent magnet levitation device was invented (1976) and patented (1983) by inventor Roy Harrigan, of Vermont. In the mid-1990s, Seattle entrepreneur Bill Hones, who was himself exploring the possibility of permanent magnet levitation, discovered Harrigan's patent. Hones subsequently contacted Harrigan and later met him. Upon Hones' request, Harrigan permitted him to borrow his

prototype with the understanding that they were entering into a business arrangement. Hones, with the help of his father, a Physicist and employee at Los Alamos National Laboratory, analyzed the physics of the prototype, and then filed for an "improvement patent". In 1984, independent of Roy Harrigan, inventor Joseph Chieffo, of Pennsylvania, also discovered spin-stabilized magnetic levitation. Chieffo then developed his own spin-stabilized magnetic levitation device and attempted to obtain a patent thereon. Employing an attorney to conduct a U.S. Patent and Trademark records search, Chieffo was informed of the existence of the Harrigan patent; he thus concluded his efforts to secure a patent. In a final assessment, Chieffo's attorney noted that his device, although apparently unpatentable, could be marketed without infringing upon the Harrigan patent. In 1988, Chieffo marketed his device in kit form. Contrasting with the dished supporting magnet of the Harrigan invention, the base magnet of this latter device was rectangular and planar of upper surface, not unlike the base magnet of Hones' later-patented device, the now-popular Physics toy known as the Levitron.

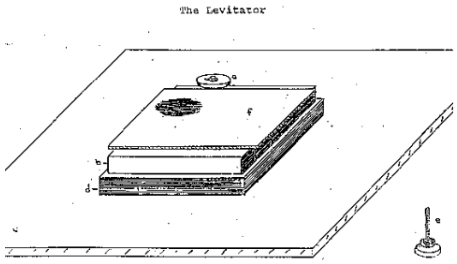

Figure 1-5: Levitator system with rectangular base.

In the 1990s, Michael and Karen Sherlock formed the company they named "UFO" in New Mexico to market the Levitron under an oral agreement in partnership with Hones' company, Creative Gifts, Inc. Efforts to formalize the agreement in writing fell apart and grew acrimonious after UFO's principals learned about the device's earlier invention by Harrigan, and redesigned their website to incorporate the exposé-style article "THE HIDDEN HISTORY OF THE LEVITRON!" [2], which accused Hones of stealing the invention from Harrigan. Creative Gifts, in turn, filed a trademark infringement suit in United States District Court of New Mexico against UFO and its owners. At trial and on appeal to the Tenth Circuit Creative Gifts' trademark claims were upheld, and all of UFO's counterclaims were rejected after UFO, which had been representing itself as a "pro se" defendant, was sanctioned by the court for abuse of discovery. The appeals court, noting that UFO had submitted a one-page opening brief with no citations to the record or discussion of the relevant law, commented in its ruling, "they have shot themselves in the foot."

Note that in this moment (2017) it's not possible to buy a Levitron device.

This magnet-mechanical problem has been studied by several authors. M. V. Berry, in [3], describes the system using adiabatic approximations and provides the mass interval in which stable hovering is achieved. Genta et al. [4] provides an analytical expression to compute the lower and upper stable rotational speed bounds and Dullin et al. [5] and Gov et al. [6] find the stability range where hovering is possible. Moreover, A. T. Pérez et al. [7] analyze the misalignment between the magnetic dipole moment and the mechanical axis of the top, and achieve stable levitation for hours and even days using an alternating magnetic field.

2 FREE MOTION. DESCRIPTION WITH EULER ANGLES

We begin our dynamical analysis describing the motion of the spinning top with the classical Euler angles, in absence of the external magnetic field and solely submitted to the action of gravity. Euler's equations are particularised for the case of inertial symmetry in the body (like our spinning top), where two of the principal moments of inertia are the same. We then analyse the free-motion, the constants of the motion and give a geometric visualization by means of the axoids (body and space cones).

2.1. Euler angles

To describe the orientation of the body, there are twelve choices in which no two adjacent rotation indices are the same. A sequence is given by three numbers, which represent each of the rotations (1 denotes a rotation about a X axis, 2 about a Y axis and 3 is a transformation about a Z axis).

These twelve sets are called Euler angles sequences and they can be classified into two main categories. Depending on the application, one select the most suitable set, such that the sequence used gives a better physical visualization or leads to fewer singularities.

- The first category group the transformations where the first and third indices are the same.
- The second group consists of rotations where the first and the third indices are different. These are usually known as Tait-Bryan angles.

The most common used Euler angle sequence is the 3-1-3 sequence, which is beforehand the most suitable choice to visualize the orientation of the body with respect the fixed coordinate system. In the 3-1-3 transformation, the rotation angles ϕ, θ and ψ are known as the precession, nutation and spin angles, respectively.

2.1.1. Rotation {21}: Precession angle ϕ

Starting in the fixed frame, our first rotation is counterclockwise (if we look down the axis) through an angle ϕ about the Z_1-axis. The new frame is numbered as '2' and its unit vectors are $\vec{\imath}_2$, $\vec{\jmath}_2$ and $\vec{k}_2$. The relation between frames '1' and '2' is given by

$$\begin{aligned} \vec{\imath}_2 &= \cos(\phi)\,\vec{\imath}_1 + \sin(\phi)\,\vec{\jmath}_1 \\ \vec{\jmath}_2 &= -\sin(\phi)\,\vec{\imath}_1 + \cos(\phi)\,\vec{\jmath}_1 \\ \vec{k}_1 &= \vec{k}_2 \end{aligned} \tag{2.1}$$

2.1.2. Rotation {32}: Tilt angle θ

The second rotation is counterclockwise (if we look down the axis) through an angle θ about the X_2-axis, changing from frame '2' to '3'. The unit vectors are $\vec{\imath}_3$, $\vec{\jmath}_3$ and $\vec{k}_3$. The transformation of coordinates can be represented as follows:

$$\begin{aligned} \vec{\imath}_3 &= \vec{\imath}_2 \\ \vec{\jmath}_3 &= \cos(\theta)\,\vec{\jmath}_2 + \sin(\theta)\,\vec{k}_2 \\ \vec{k}_3 &= -\sin(\theta)\,\vec{\jmath}_2 + \cos(\theta)\,\vec{k}_2 \end{aligned} \tag{2.2}$$

2.1.3. Rotation {43}: Roll angle ψ

The third rotation is counterclockwise (if we look down the axis) through an angle ψ about the Z_3-axis. The new frame is the body frame '4' and the transformation is given by

$$\begin{aligned} \vec{\imath}_4 &= \cos(\psi)\,\vec{\imath}_3 + \sin(\psi)\,\vec{\jmath}_3 \\ \vec{\jmath}_4 &= -\sin(\psi)\,\vec{\imath}_3 + \cos(\psi)\,\vec{\jmath}_3 \\ \vec{k}_4 &= \vec{k}_3 \end{aligned} \tag{2.3}$$

In figure 2-1, we can see the successive rotations

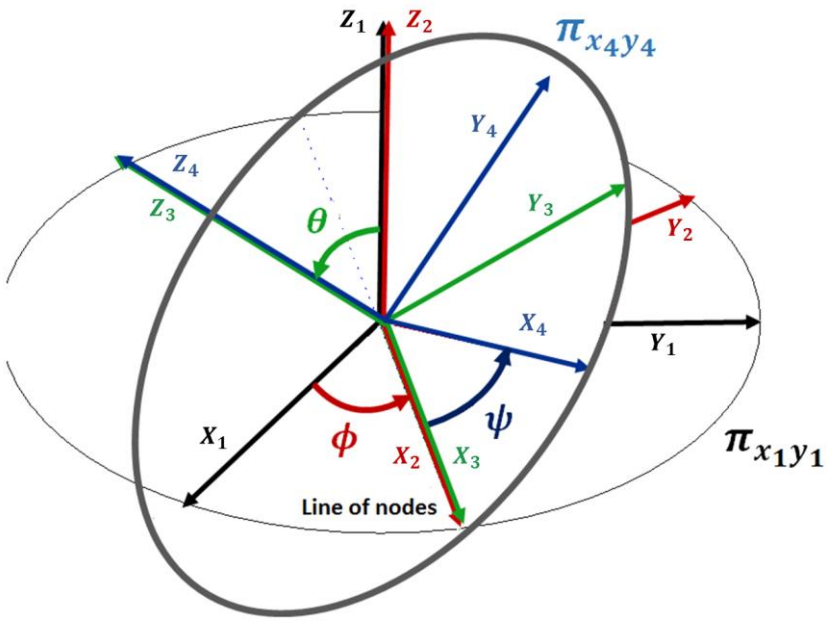

Figure 2-1: Classical Euler angles.

The line of nodes is given by the instersection of the planes $\boldsymbol{\pi_{x_1y_1}}$(which contains the axis X_1 and Y_1 of the fixed frame '1') and $\boldsymbol{\pi_{x_4y_4}}$.

To obtain the combined transformation from the frame '1' to the local frame '4', we combine the three previous rotations,

$$\{X_4\} = \boldsymbol{R_T}\{X_1\} \tag{2.4}$$

with $\boldsymbol{R_T}$ being

$$\boldsymbol{R_T = R_\psi R_\theta R_\phi} = \begin{pmatrix} \cos\psi\cos\phi - \cos\theta\sin\phi\sin\psi & \cos\psi\sin\phi + \cos\theta\cos\phi\sin\psi & \sin\psi\sin\theta \\ -\sin\psi\cos\phi - \cos\theta\sin\phi\cos\psi & -\sin\psi\sin\phi + \cos\phi\cos\theta\cos\psi & \cos\psi\sin\theta \\ \sin\theta\sin\phi & -\sin\theta\cos\phi & \cos\theta \end{pmatrix} \quad (2.5)$$

2.2. Angular velocity

The angular velocity of the top with respect the fixed frame '1' is given by the composition of the previous rotations:

$$\vec{\omega} = \vec{\omega}_{41} = \vec{\omega}_{43} + \vec{\omega}_{32} + \vec{\omega}_{21} = \dot{\phi}\vec{k}_1 + \dot{\theta}\vec{j}_2 + \dot{\psi}\vec{k}_3 \quad (2.6)$$

with its components being

$$\begin{aligned} \omega_X &= \dot{\theta}\cos(\psi) - \dot{\phi}\ \sin(\theta)\sin(\psi) \\ \omega_Y &= -\dot{\theta}\sin(\psi) - \dot{\phi}\ \sin(\theta)\cos(\psi) \\ \omega_Z &= \dot{\psi} + \dot{\phi}\cos(\theta) \end{aligned} \quad (2.7)$$

Inverse relations give

$$\begin{aligned} \dot{\phi} &= -\frac{\omega_X\sin(\psi) + \omega_Y\cos(\psi)}{\sin(\theta)} \\ \dot{\theta} &= \omega_X\cos(\psi) - \omega_Y\sin(\psi) \\ \dot{\psi} &= \omega_Z + \frac{\cos(\theta)}{\sin(\theta)}(\omega_X\sin(\psi) + \omega_Y\cos(\psi)) \end{aligned} \quad (2.8)$$

Note that the presence of the sine functions in the denominators of equations (2.8) leads to a singularity when $\theta = 0°$. This value of θ corresponds with the spinning top in vertical position, with its local axis aligned with the OZ_1-axis. This fact obscures the description of the problem with these angles, as we are not able to perform numerical integrations with θ around this value. Consequently, in chapter 3 we derive the matrix of rotation for the known 'Gimbal set', that corresponds with a yaw-pitch-rolling sequence.

2.3. Free motion with inertial symmetry

The motion of the hovering spinning top, in absence of external magnetic field and in presence of gravity, is going to be analyzed.

The translational equations are straightforward, as we are only considering the gravity force. Newton's second law imply the conservation of the horizontal components of linear momentum ($\vec{C}_{hor} = \overrightarrow{CTE}$), and the z-component of the center of mass of the body describes a parabolic path.

$$m\ddot{x} = 0 \tag{2.9}$$

$$m\ddot{y} = 0 \tag{2.10}$$

$$m\ddot{z} = -mg \tag{2.11}$$

For the rotational motion we use Euler's equations projected in the body frame, which in absence of external moments, are

$$I_X\,\dot{\omega}_X - (I_Y - I_Z)\omega_Y\omega_Z = M_X = 0 \tag{2.12}$$

$$I_Y\,\dot{\omega}_Y - (I_Z - I_X)\omega_X\omega_Z = M_Y = 0 \tag{2.13}$$

$$I_Z\dot{\omega}_Z - (I_X - I_Y)\omega_X\omega_Y = M_Z = 0 \tag{2.14}$$

Considering the case of inertial symmetry in the body and that two principal moments of inertia are the same ($I_X = I_Y$), equations (2.12-2.14) simplify to

$$I_X\,\dot{\omega}_X - (I_X - I_Z)\omega_Y\omega_Z = 0 \tag{2.15}$$

$$I_X\,\dot{\omega}_Y - (I_Z - I_X)\omega_X\omega_Z = 0 \tag{2.16}$$

$$I_Z\dot{\omega}_Z = 0 \tag{2.17}$$

We can see that ω_Z is a first constant of the motion. Introducing the constant Ω

$$\Omega = \frac{I_Z - I_X}{I_X}\omega_Z \tag{2.18}$$

equations (2.15-2.16) can be written as

$$\dot{\omega}_X + \Omega\omega_Y = 0 \tag{2.19}$$

$$\dot{\omega}_Y - \Omega\omega_X = 0 \tag{2.20}$$

In matrix format,

$$\begin{pmatrix}\dot{\omega}_X\\ \dot{\omega}_Y\end{pmatrix} = -\begin{pmatrix}0 & \Omega\\ -\Omega & 0\end{pmatrix}\begin{pmatrix}\omega_X\\ \omega_Y\end{pmatrix} \tag{2.21}$$

The coefficient matrix is skew symmetric and proportional to the rotation constant Ω, which is sign of a gyroscopic behavior.

A first way to solve the set is to find the time derivative of eq. (2.19):

$$\ddot{\omega}_X = -\Omega\dot{\omega}_Y \tag{2.22}$$

and substitute for $\dot{\omega}_Y$

$$\ddot{\omega}_X = -\Omega^2 \omega_X \tag{2.23}$$

A solution for ω_X and ω_Y is

$$\omega_X = A\cos(\Omega t) \tag{2.24}$$

$$\omega_Y = A\sin(\Omega t) \tag{2.25}$$

The magnitude of the vector $\vec{\omega}_{XY} = \omega_X \vec{\imath}_1 + \omega_Y \vec{\jmath}_1$ is therefore another integral of motion. It represents the magnitude of the projection of the angular velocity vector on the XY plane. This constancy can be also proved by multiplying eq. (2.19) by ω_Y and eq. (2.20) by ω_X and adding both equations:

$$\omega_X \dot{\omega}_X + \omega_Y \dot{\omega}_Y = \frac{1}{2}\frac{d}{dt}(\omega_X^2 + \omega_Y^2) = 0 \rightarrow \omega_{XY} = \sqrt{\omega_X^2 + \omega_Y^2} = CTE \tag{2.26}$$

The combination of the two first integrals yields to a third conserved quantity, thus

$$|\vec{\omega}|^2 = \omega_X^2 + \omega_Y^2 + \omega_Z^2 = CTE \tag{2.27}$$

so that the magnitude of the angular velocity vector is also constant.

With the previous results, we can compute the kinetic moment $\vec{L}_G$ and the rotational kinetic energy T_{Rot}:

$$\vec{L}_G = I_X \omega_X \vec{\imath}_1 + I_X \omega_Y \vec{\jmath}_1 + I_Z \omega_Z \vec{k}_1 = \overrightarrow{CTE} \tag{2.28}$$

$$2T_{Rot} = \vec{\omega} \cdot \vec{L}_G = \omega_X^2 + \omega_Y^2 + \omega_Z^2 = CTE \tag{2.29}$$

Denoting the projection of the angular momentum vector onto the XY plane as $L_{G_{HOR}}$

$$L_{G_{HOR}} = I_X \sqrt{\omega_X^2 + \omega_Y^2} = I_X \omega_{XY} \tag{2.30}$$

one can observe that this magnitude is also constant and that lies along the same line of ω_{XY}. Hence, vectors $\vec{k}_4, \vec{L}_G$ and $\vec{\omega}$ must lie on the same plane. Defining the unit vector $\vec{u}_{XY}$ such that $\vec{L}_{G_{HOR}} = L_{G_{HOR}} \vec{u}_{XY}$, this plane is defined by $\vec{k}_1$ and $\vec{u}_{XY}$.

Figure 2-2 summarizes most of the previous ideas.

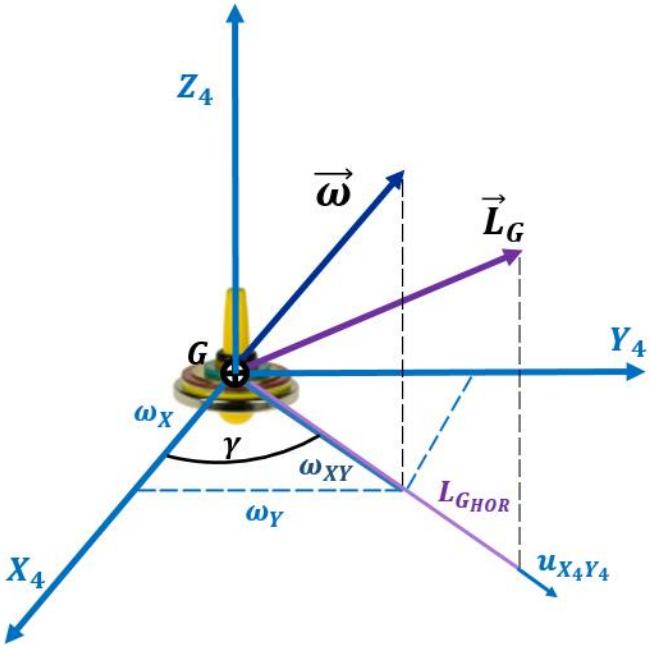

Figure 2-2: Important magnitudes in the free-motion analysis.

The motion can be seen as the rotation of this plane. The rotation is about the angular momentum vector $\vec{L}_G$, as both the magnitude and direction of this vector are constant.

The rotation of the angular velocity vector can also be described as the motion of two imaginary cones, known as axoids or body and space cones, on top of each other. The body cone is fixed to the body, and it is generated by the rotation of the angular velocity vector about the spin and symmetry axis $\vec{k}_4$. The space cone is fixed in the inertial space and is generated by the rotation of the angular velocity vector about the angular momentum vector. The cones generated are right circular due to the inertial symmetry.

Introducing the angles α and β (see figure 2-3)

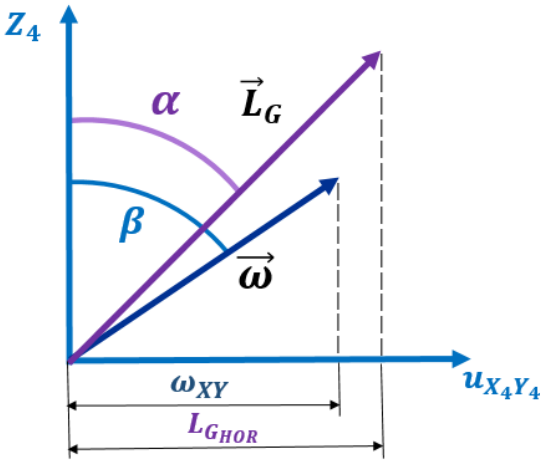

Figure 2-3: Angles α and β.

they can be expressed as

$$\tan\alpha = \frac{L_{G_{HOR}}}{L_{G_Z}} = \frac{I_X \omega_{XY}}{I_Z \omega_Z} = constant \tag{2.31}$$

$$\tan\beta = \frac{\omega_{XY}}{\omega_Z} = constant \tag{2.32}$$

The values of α and β depend on the mass moment of inertia I_X and I_Z:

- For a flat body, such a disk, we have $I_X < I_Z \rightarrow \alpha < \beta$.
- For a slender body, such as a rod or rugby ball, $I_X > I_Z \rightarrow \alpha > \beta$

When viewed from the body-fixed frame, $\vec{\omega}$ generates the body cone, which has an apex angle of β around Z_4. When viewed from the inertial frame, it generates the space cone with an apex angle $|\beta - \alpha|$. In the case of our spinning top, which it is a flat body (from this point forward, we are going to consider $I_Z \simeq 2\, I_X$), the space cone rolls inside the body cone, as it can be seen in figure 2-4.

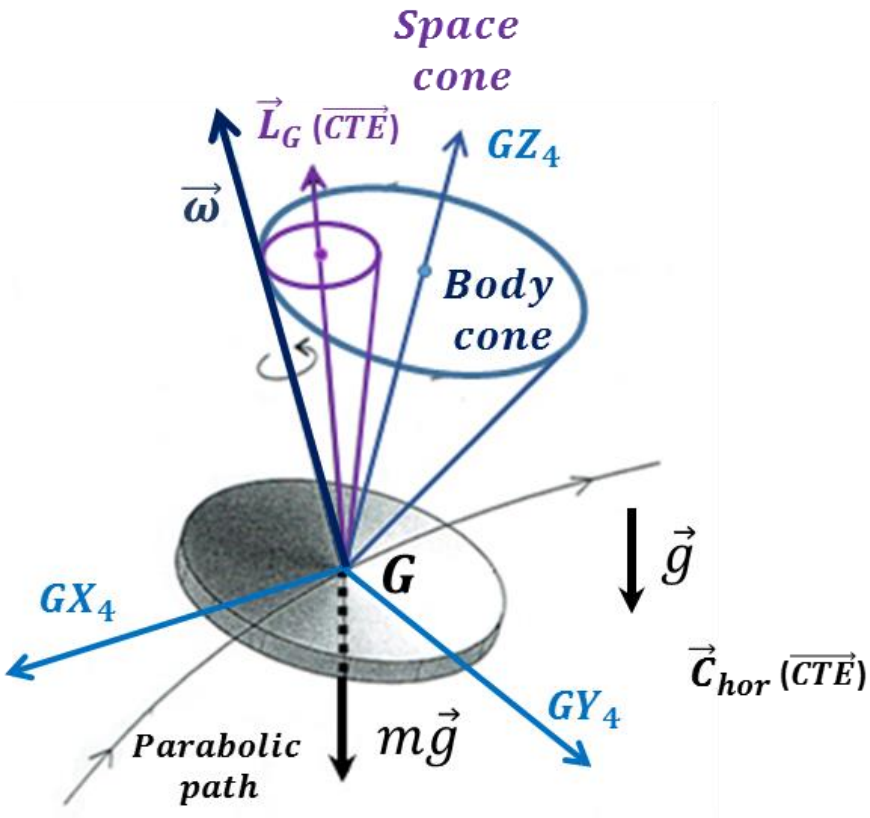

Figure 2-4: Body and space cones.

If a slender body was considered, the body and space cones would lie outside of each other.

We next address the issue of the rate at which ω_{XY} rotates, which is the same as the rate with which the described plane rotates and the body cone is swept, and is denoted as $\dot{\gamma}$. From figure 2-2, it can be seen that γ is the angle $\vec{\omega}_{XY}$ with the X_4 axis:

$$\tan\gamma = \frac{\sin\gamma}{\cos\gamma} = \frac{\omega_Y}{\omega_X} \tag{2.33}$$

The time derivative of both sides yields

$$\frac{\cos\gamma\,(\dot{\gamma}\cos\gamma) - \sin\gamma(-\dot{\gamma}\sin\gamma)}{\cos^2\gamma} = \frac{\omega_X\dot{\omega}_Y - \omega_Y\dot{\omega}_X}{\omega_X^2} \tag{2.34}$$

Using equations (2.24) and (2.25), one obtains

$$\frac{\dot{\gamma}}{\cos^2\gamma} = \frac{\Omega(\omega_X^2 + \omega_Y^2)}{\omega_X^2} = \frac{\Omega}{\frac{\omega_X^2}{(\omega_X^2 + \omega_Y^2)}} \tag{2.35}$$

From figure 2-2, it can be seen that

$$\cos\gamma = \frac{\omega_X}{\sqrt{\omega_X^2 + \omega_Y^2}} \tag{2.36}$$

which leads to the result that $\dot{\gamma} = \Omega$.

3 TAIT-BRYAN ANGLES

In this chapter, we are going to derive a matrix which completely describes the relative orientation between the fixed global system and the top system, which comoves with the top. As we saw in the previous chapter, the 3-1-3 transformation provides the best visualization of the problem but leads to singularities when $\theta = 0°$.

In order to characterize the position of the top, Euler angles are going to be used following a yaw-pitch-roll sequence which moves the singularity to $\theta = \frac{\pi}{2}$, that corresponds with the top overturned and not hovering.

This sequence is usually used in inertial navigation (planes, ships, submarines…), photography or imaging (in drones) and many other applications.

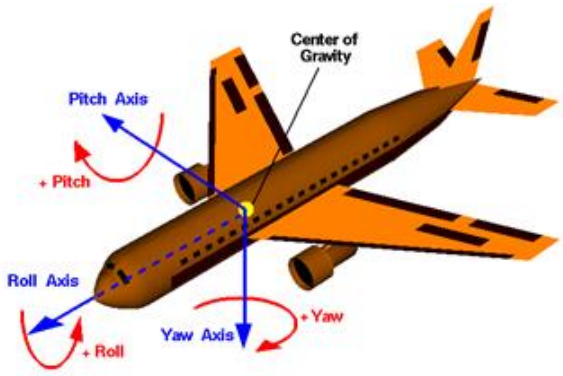

Figure 3-1: Yaw-pitch-roll sequence used in navigation.

3.1. Yaw-pitch-roll sequence

3.1.1. Rotation {21}: ϕ angle

Starting from the fixed frame '1', we move to frame '2' by means of a counterclockwise rotation through an angle ϕ about $OX_1 = OX_2$ axis.

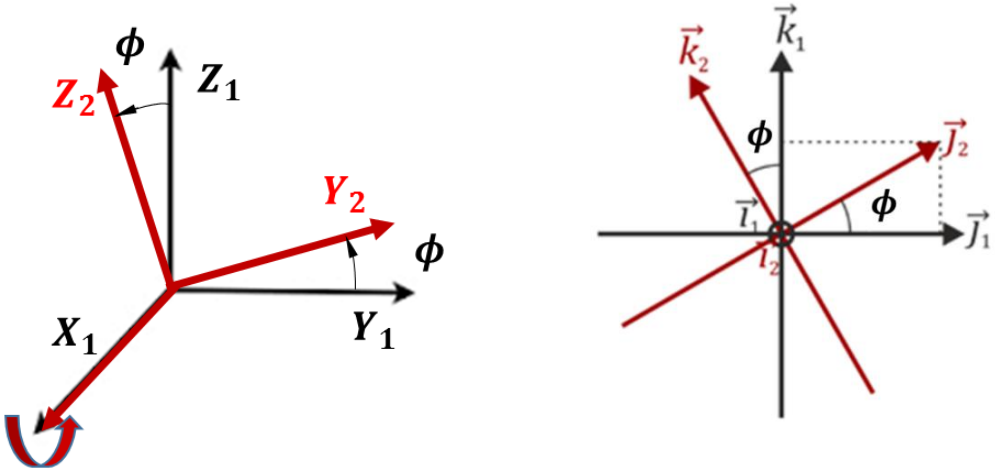

Figure 3-2: Rotation {21}.

The relation between the two systems due to this rotation is:

$$\begin{aligned}\vec{\imath}_2 &= \vec{\imath}_1\\ \vec{\jmath}_2 &= \cos(\phi)\,\vec{\jmath}_1 + \sin(\phi)\,\vec{k}_1\\ \vec{k}_2 &= -\sin(\phi)\,\vec{\jmath}_1 + \cos(\phi)\,\vec{k}_1\end{aligned} \tag{3.1}$$

with the inverse relation

$$\begin{aligned}\vec{\imath}_1 &= \vec{\imath}_2\\ \vec{\jmath}_1 &= \cos(\phi)\,\vec{\jmath}_2 - \sin(\phi)\,\vec{k}_2\\ \vec{k}_1 &= \sin(\phi)\,\vec{\jmath}_2 + \cos(\phi)\,\vec{k}_2\end{aligned} \tag{3.2}$$

Angular velocity of this rotation $\vec{\omega}_{21}$ is

$$\vec{\omega}_{21} = \dot{\phi}\,\vec{\imath}_1 = \dot{\phi}\vec{\imath}_2 \tag{3.3}$$

3.1.2. Rotation {32}: θ angle

We arrive to frame '3' making a counterclockwise rotation through an angle θ about $OY_2 = OY_3$ axis (line of nodes).

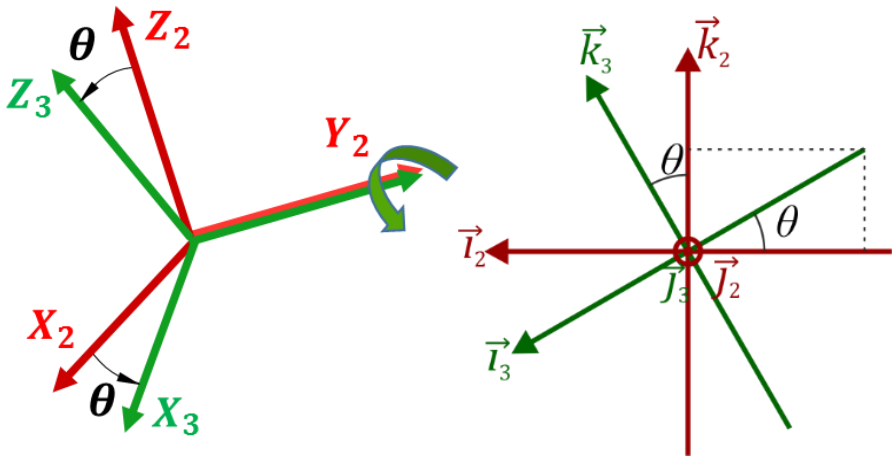

Figure 3-3: Rotation {32}.

The relation between both bases in this rotation is

$$\begin{aligned}\vec{\imath}_3 &= \cos(\theta)\,\vec{\imath}_2 - \sin(\theta)\,\vec{k}_2\\ \vec{\jmath}_3 &= \vec{\jmath}_2\\ \vec{k}_3 &= \sin(\theta)\,\vec{\imath}_2 + \cos(\theta)\,\vec{k}_2\end{aligned} \tag{3.4}$$

with the inverse relation

$$\begin{aligned}\vec{\imath}_2 &= \cos(\theta)\,\vec{\imath}_3 + \sin(\theta)\,\vec{k}_3\\ \vec{\jmath}_2 &= \vec{\jmath}_3\\ \vec{k}_2 &= -\sin(\theta)\,\vec{\imath}_3 + \cos(\theta)\,\vec{k}_3\end{aligned} \tag{3.5}$$

Angular velocity of this rotation, $\vec{\omega}_{32}$ is given by

$$\vec{\omega}_{32} = \dot{\theta}\vec{\jmath}_2 = \dot{\theta}\vec{\jmath}_3 \tag{3.6}$$

3.1.3. Rotation {43}: ψ angle

The last rotation leads to the body-frame '4' by means of a counterclockwise rotation ψ about $OZ_3 = OZ_4$ axis.

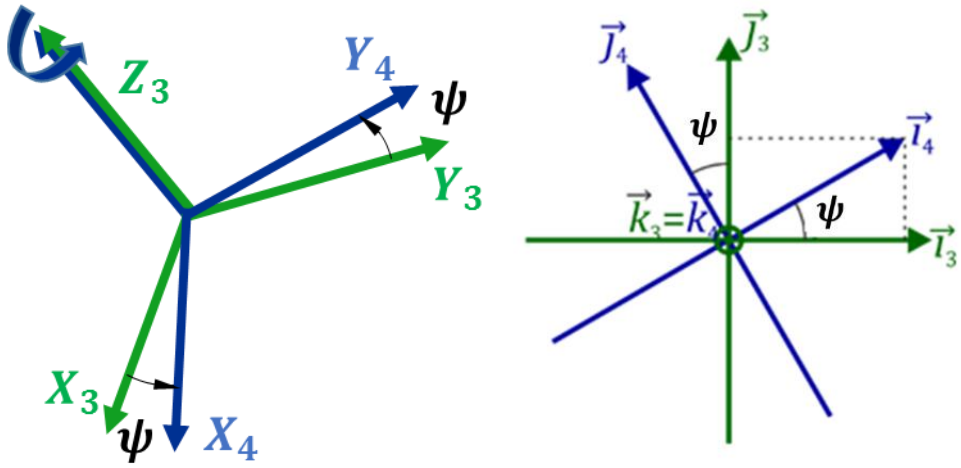

Figure 3-4: Rotation {43}.

The relation between both bases is given by

$$\begin{aligned}\vec{\imath}_4 &= \cos(\psi)\,\vec{\imath}_3 + \sin(\psi)\,\vec{\jmath}_3\\ \vec{\jmath}_4 &= -\sin(\psi)\,\vec{\imath}_3 + \cos(\psi)\,\vec{\jmath}_3\\ \vec{k}_4 &= \vec{k}_3\end{aligned} \tag{3.7}$$

and

$$\begin{aligned}\vec{\imath}_3 &= \cos(\psi)\,\vec{\imath}_4 - \sin(\psi)\,\vec{\jmath}_4\\ \vec{\jmath}_3 &= \sin(\psi)\,\vec{\imath}_4 + \cos(\psi)\,\vec{\jmath}_4\\ \vec{k}_3 &= \vec{k}_4\end{aligned} \tag{3.8}$$

The angular velocity corresponding with the last rotation is given by $\vec{\omega}_{43}$

$$\vec{\omega}_{43} = \dot{\psi}\vec{k}_3 = \dot{\psi}\vec{k}_4 \tag{3.9}$$

As we did with the 3-1-3 transformation, the objective is to obtain the combined rotation matrix $\boldsymbol{R_T}$ which completely describes the relative orientation between the fixed and local frames:

$$\{X_1\} = \boldsymbol{R_T}\{X_4\} \tag{3.10}$$

with $\boldsymbol{R_T}$

$$\boldsymbol{R_T} = \begin{pmatrix} \cos\theta\cos\psi & -\cos\theta\sin\psi & \sin\theta \\ \sin\phi\sin\theta\cos\psi + \cos\phi\sin\psi & -\sin\phi\sin\theta\sin\psi + \cos\phi\cos\psi & -\sin\phi\cos\theta \\ -\cos\phi\sin\theta\cos\psi + \sin\phi\sin\psi & \cos\phi\sin\theta\sin\psi + \sin\phi\cos\psi & \cos\phi\cos\theta \end{pmatrix} \tag{3.11}$$

Because of the rotational symmetry of the spinning top, we are going to use frame '3' in the next chapters. Therefore, we give the expression of matrix $\boldsymbol{R_3}$, which relates frames '1' and '3':

$$\{X_1\} = \boldsymbol{R_3}\{X_3\} \tag{3.12}$$

$$\boldsymbol{R_3} = \begin{pmatrix} \cos\theta & 0 & \sin\theta \\ \sin\phi\sin\theta & \cos\phi & -\sin\phi\cos\theta \\ -\cos\phi\sin\theta & \sin\phi & \cos\phi\cos\theta \end{pmatrix} \tag{3.13}$$

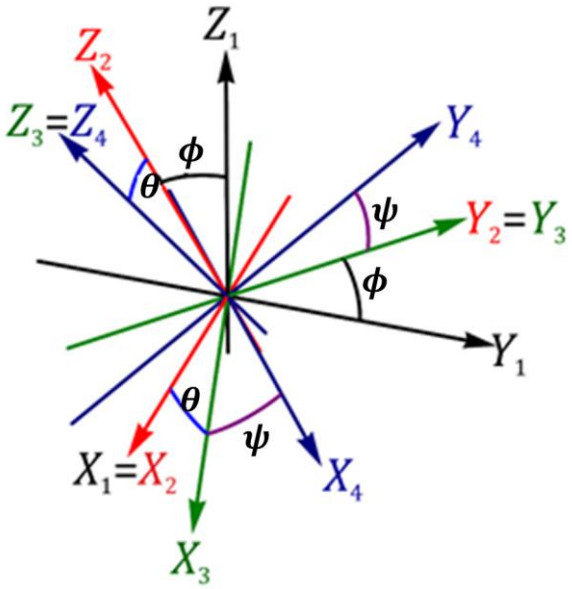

Figure 3-5: Successive rotations and different frames.

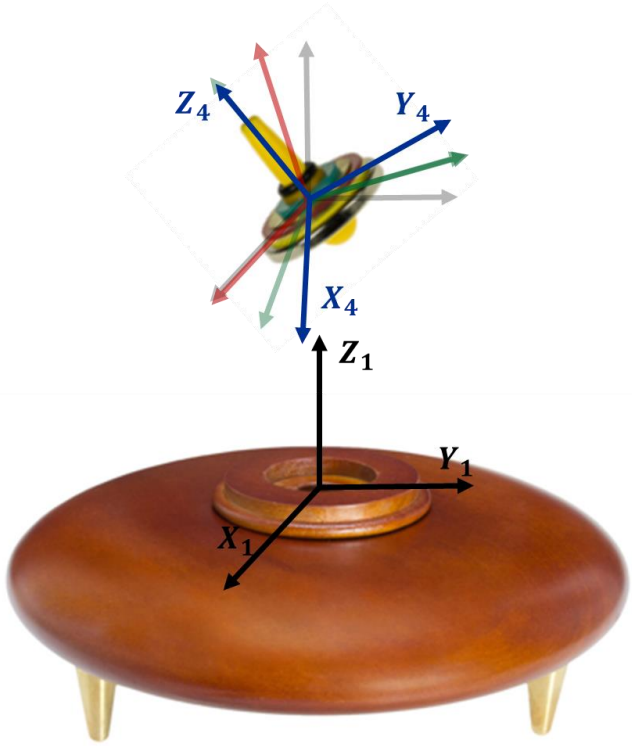

Figure 3-6: Fixed frame '1' and body frame '4' in the real toy.

Despite the numerical advantage provided by the yaw-pitch-roll sequence, there are disadvantages. These angles provide a worse visualization of the problem than the 3-1-3 transformation. In the description with the 'Classical Euler angles', the angle between $\vec{k}_4$ and $\vec{k}_1$ is θ and it represents the nutation motion. In this case, visualization is not so clear and the nutation motion is given by a combination of ϕ and θ. This can be seen computing the dot product $\vec{k}_4 \cdot \vec{k}_1$:

$$\vec{k}_4 \cdot \vec{k}_1 = \cos\phi \cos\theta = \cos\delta \tag{3.14}$$

Therefore, the angle between both vectors is given by

$$\delta = \arccos(\cos\phi \cos\theta) \tag{3.15}$$

3.2. Angular velocity $\vec{\omega}$

The angular velocity of the top with respect to the fixed frame '1' is given by the composition of the previous rotations:

$$\vec{\omega} = \vec{\omega}_{41} = \vec{\omega}_{43} + \vec{\omega}_{32} + \vec{\omega}_{21} = \dot{\psi}\vec{k}_3 + \dot{\theta}\vec{j}_3 + \dot{\phi}\vec{\imath}_2 \tag{3.16}$$

Expressed in the frame '3', we have

$$\vec{\omega}|_3 = \vec{\omega}_{41}|_3 = \dot{\psi}\vec{k}_3 + \dot{\theta}\vec{j}_3 + \dot{\phi}\left(\cos(\theta)\,\vec{\imath}_3 + \sin(\theta)\,\vec{k}_3\right) = \dot{\phi}\cos(\theta)\,\vec{\imath}_3 + \dot{\theta}\vec{j}_3 + \left(\dot{\psi} + \dot{\phi}\sin(\theta)\right)\vec{k}_3 \tag{3.17}$$

or, in components

$$\begin{aligned} \omega_X &= \dot{\phi}\cos(\theta) \\ \omega_Y &= \dot{\theta} \\ \omega_Z &= \dot{\psi} + \dot{\phi}\sin(\theta) \end{aligned} \tag{3.18}$$

The inverse relation provides

$$\begin{aligned} \dot{\theta} &= \omega_Y \\ \dot{\phi} &= \frac{\omega_X}{\cos(\theta)} \\ \dot{\psi} &= \omega_Z - \omega_X \tan(\theta) \end{aligned} \tag{3.19}$$

Note that equations (3.19) are regular for $\theta = 0°$.

Arrived to this point, it is important to make a clarification between $\vec{\omega}_{31}$ and $\vec{\omega}|_3$, because the nomenclature might be confusing:

- On the one hand, $\vec{\omega}|_3 = \vec{\omega}_{41}|_3$ is the angular velocity of the top with respect to the frame '1', expressed in the frame '3', as we have just seen.
- On the other hand, $\vec{\omega}_{31}$is the angular velocity of the frame '3' with respect to the fixed frame '1'. Vectors at base 3 move with respect to the fixed frame with an angular velocity which is different to that of the top, being the difference the angular velocity of the top around its own axis. Its expression will be necessary in chapter 6 and it is given by

$$\vec{\omega}_{31} = \vec{\omega}_{32} + \vec{\omega}_{21} = \dot{\theta}\vec{J}_3 + \dot{\phi}\vec{\imath}_2 \tag{3.20}$$

To take advantage of the rotational symmetry of the top, $\vec{\omega}_{31}$ is going to be expressed precisely at base '3':

$$\vec{\omega}_{31}|_3 = \vec{\Omega} = \dot{\phi}\cos(\theta)\,\vec{\imath}_3 + \dot{\theta}\vec{J}_3 + \dot{\phi}\sin(\theta)\,\vec{k}_3 \tag{3.21}$$

The components of $\vec{\omega}_{31}$can be written in terms of the components of the angular velocity ω_X, ω_Y of the top as follows:

$$\begin{aligned} \Omega_X &= \dot{\phi}\cos(\theta) = \omega_X \\ \Omega_Y &= \dot{\theta} = \omega_Y \\ \Omega_Z &= \dot{\phi}\sin(\theta) = \omega_X \tan(\theta) \end{aligned} \tag{3.22}$$

3.3. Kinetic moment $\vec{L}_G$

Assuming rotational symmetry of the spinning top about its axis (which coincides with the direction of the magnetic pole), the inertia moment tensor of the dipole can be written, in a system of coordinates that moves with the top, as:

$$\bar{\bar{I}} = \begin{pmatrix} I_X & 0 & 0 \\ 0 & I_X & 0 \\ 0 & 0 & I_Z \end{pmatrix} \tag{3.23}$$

Due to the rotational symmetry of the top, this expression is also valid in the frame '3'.

Assimilating the top to a disk of mass m and radius r, the inertia tensor can be written as

$$\bar{\bar{I}} = \frac{1}{4} mr^2 \begin{pmatrix} 1 & 0 & 0 \\ 0 & 1 & 0 \\ 0 & 0 & 2 \end{pmatrix} \tag{3.24}$$

Thus, the kinetic moment is related with the angular velocity through the inertia tensor. Its expression, in frame '3', is

$$\vec{L}_G\big|_3 = \bar{\bar{I}}\big|_3 \cdot \vec{\omega}|_3 \tag{3.25}$$

and we get

$$\vec{L}_G\big|_3 = \begin{pmatrix} I_X & 0 & 0 \\ 0 & I_X & 0 \\ 0 & 0 & I_Z \end{pmatrix} \begin{pmatrix} \dot{\phi}\cos(\theta) \\ \dot{\theta} \\ \dot{\psi} + \dot{\phi}\,\mathrm{sen}(\theta) \end{pmatrix} = \begin{pmatrix} I_X\dot{\phi}\cos(\theta) \\ I_X\dot{\theta} \\ I_Z\big(\dot{\psi} + \dot{\phi}\sin(\theta)\big) \end{pmatrix} \tag{3.26}$$

3.4. Kinetic energy *T*

To compute the total kinetic energy, we have to consider the translational and rotational contributions

$$T = T_T + T_R \tag{3.27}$$

The translational kinetic energy T_T is given by

$$T_T = \frac{1}{2} m v_G^2 = \frac{1}{2} m(\dot{x}^2 + \dot{y}^2 + \dot{z}^2) \tag{3.28}$$

On the other hand, the rotational kinetic energy T_R is

$$T_R = \frac{1}{2}\vec{\omega}^{\,T} \cdot \bar{\bar{I}} \cdot \vec{\omega} = \frac{1}{2}\,\vec{\omega} \cdot \vec{L}_G = \frac{1}{2}(\dot{\phi}\cos(\theta) \quad \dot{\theta} \quad \dot{\psi} + \dot{\phi}\sin(\theta)) \cdot \begin{pmatrix} I_X\dot{\phi}\cos(\theta) \\ I_X\dot{\theta} \\ I_z\big(\dot{\psi} + \dot{\phi}\sin(\theta)\big) \end{pmatrix} \tag{3.29}$$

obtaining

$$T_R = \frac{1}{2} I_X \left(\dot{\theta}^2 + \dot{\phi}^2\cos^2(\theta)\right) + \frac{1}{2} I_Z(\dot{\psi} + \dot{\phi}\sin(\theta))^2 \tag{3.30}$$

Therefore, we have

$$T = \frac{1}{2} m(\dot{x}^2 + \dot{y}^2 + \dot{z}^2) + \frac{1}{2} I_X \left(\dot{\theta}^2 + \dot{\phi}^2\cos^2(\theta)\right) + \frac{1}{2} I_Z(\dot{\psi} + \dot{\phi}\sin(\theta))^2 \tag{3.31}$$

4 MAGNETIC FIELD

Before obtaining the expression of the magnetic field created by the base, some of the key aspects of the theory of the magnetic fields are going to be remembered:

- The magnetic field created by a bar magnet form lines without extremes. The direction of the magnetic field is taken to be outward from the north pole and in to the south pole of the magnet.

- The magnetic field produced by a circular bar magnet is similar to that of a cylindrical coil with the same diameter. Therefore, if the thickness of the bar magnet tends to zero and becomes a magnetized disk, its magnetic field is equivalent to the field to that of a current loop.

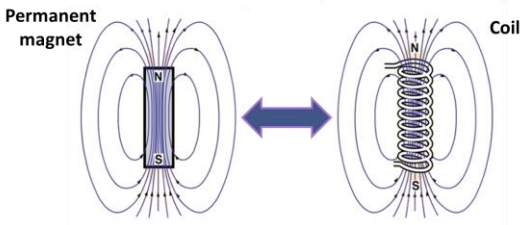

Figure 4-1: Analogy between permanent magnet and coil.

4.1. Magnetic field at Z-axis

In this way, if the base were a magnetized disk we could consider it as a closed current-carrying segment. Since it has a circular bore can be modelled as a superposition of two concentrical circular loops. The expression of the magnetic field produced by a line current is given by the Biot-Savart law:

$$\vec{B}(\vec{r}) = \frac{\mu_0}{4\pi} \oint \frac{I d\vec{r} \times (\vec{r} - \vec{r}')}{|\vec{r} - \vec{r}'|^3} \tag{4.1}$$

If we apply the law on the centerline of a current loop and integrate the z-component, we get:

$$\vec{B}_0(z) = \frac{\mu_0 I}{2} \frac{R^2}{(R^2 + z^2)^{3/2}} \vec{k}_1 \tag{4.2}$$

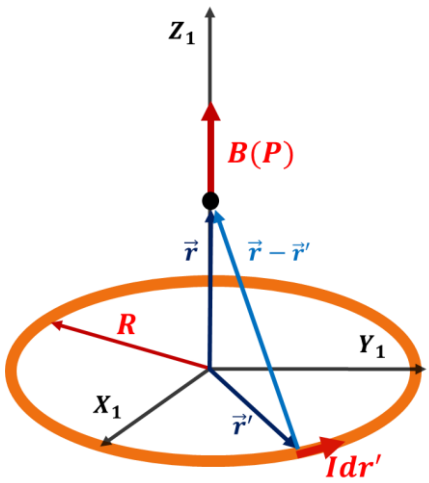

Figure 4-2: Magnetic field created by a current loop in the Z-axis.

In the case of the Levitron, as we have seen in chapter 1, the base magnet consists of an annulus shaped magnetized block. In this way, it can be modeled as two concentric current loops of radius a and b, being a the inner radius and b the outer radius of the annulus. To take into account the central hole of the annulus (which does not contribute to the magnetic field along the axis), the outer ring is going to be modeled as a loop that transports a counterclockwise current intensity I, whereas the inner ring is going to be considered as a loop along which a clockwise current intensity I flows.

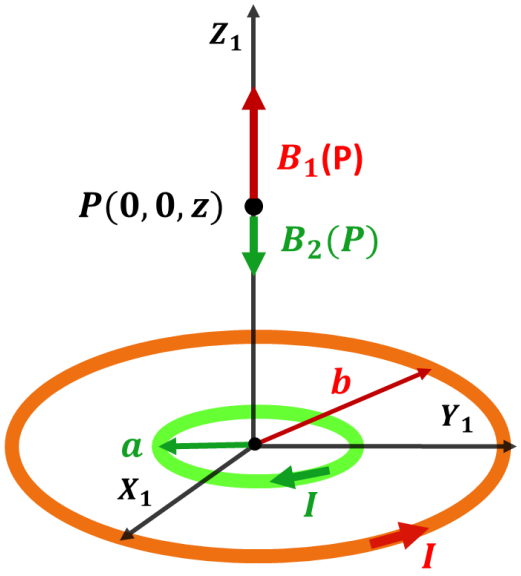

Figure 4-3: Magnetic field created by two concentric loops in the Z-axis.

Considering a generic point P of the Z-axis, the use of the right-hand rule allows us to see that the contributions of the two current loops to the magnetic field at this point have opposite senses, so that the inner loop weakens the magnetic field of the outer ring (in the same way the central hole is a desmagnetized area in the base magnet).

Thus, the analytical expression for the magnetic field along the Z-axis is given by:

$$\vec{B}_0(z) = \frac{\mu_0 I}{2}\left(\frac{b^2}{(b^2+z^2)^{3/2}} - \frac{a^2}{(a^2+z^2)^{3/2}}\right)\vec{k}_1 \tag{4.3}$$

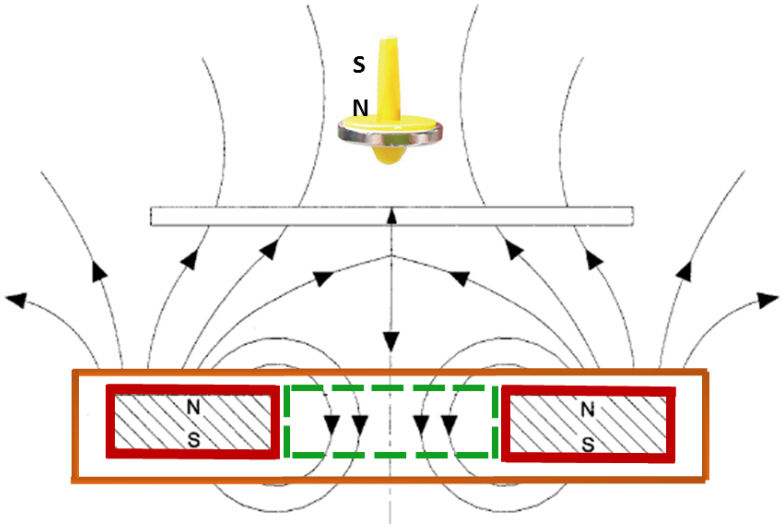

Figure 4-4: Section of the magnetic base of the system.

In order to study the behavior of the system, it is necessary to experimentally measure the magnetic field along the Z-axis and try to make a regression adjustment between the experimental data and the analytical expression given by the theory. We have to take into account some details to do this:

- First of all, the base is not a perfect annulus. The central hole can be considered as a circle of radius $a = 25$ mm, but we cannot measure the radius of the outer loop b directly on the base.
- The second thing to consider is that our analytical model consists of two concentric rings placed on a plane, whereas the base magnet is a block with height. If we want to make an adjustment between the experimental data and the analytical model, it will be necessary a variable change working with $z - z_0$.

The magnetic field produced by the base was measured in the work 'Efectos de pequeñas corrientes de aire sobre un Levitron' [8] using a teslameter. A table with the experimental data and the detailed attainment of the parameters for the adjustment are attached at addendum I. The expression of $\vec{B}_0(z)$ is therefore

$$\vec{B}_0(z) = A\left(\frac{b^2}{(b^2 + (z - z_0)^2)^{3/2}} - \frac{a^2}{(a^2 + (z - z_0)^2)^{3/2}}\right)\vec{k}_1 \tag{4.4}$$

with $b = 67.6864$ mm, $z_0 = -11.4067$ mm, $A = 1.9608 \cdot$ mT $\cdot$ m

4.2. Magnetic field near the Z-axis

The magnetic field caused by the magnetized base acting on the dipole fulfils Maxwell's equations for magnetostatics:

$$\nabla \cdot \vec{B} = 0 \qquad \nabla \times \vec{B} = \vec{0} \tag{4.5}$$

Moreover, we assume cylindrical symmetry of the magnetic field about the OZ_1 axis. Using cylindrical coordinates, it can be written as:

$$\vec{B} = B_\rho(\rho, z)\vec{u}_\rho + B_z(\rho, z)\vec{k}_1 \tag{4.6}$$

Where

$$\rho = \sqrt{x^2 + y^2} \qquad \vec{u}_\rho = \frac{x}{\rho}\vec{\imath}_1 + \frac{y}{\rho}\vec{\jmath}_1 \tag{4.7}$$

The magnetostatic equations lead to the following set:

$$\frac{1}{\rho}\frac{\partial}{\partial \rho}(\rho B_\rho) + \frac{\partial B_z}{\partial z} = 0 \qquad \frac{\partial B_\rho}{\partial z} - \frac{\partial B_\rho}{\partial z} = 0 \tag{4.8}$$

As we know the magnetic field along the Z-axis of the system, we can integrate these equations in order to determine the field at points near the axis of the system. The following procedure is going to be performed:

1. We start with the expression of the magnetic field created by the base along the Z-axis, given by eq. (4.4). Because of the symmetry of the system, this field can only be vertical

$$\vec{B}(0, z) = B_0(z)\vec{k} \tag{4.9}$$

2. Considering points near the axis, i.e, with $\rho \ll 1$, at these points B_z approximately equals to the field at the points of the Z-axis, so we can do

$$\frac{\partial}{\partial\rho}(\rho B_\rho) = -\rho\frac{\partial B_z}{\partial z} = -\rho\frac{\mathrm{d}B_0}{\mathrm{d}z} \tag{4.10}$$

and integrate once

$$\rho B_\rho = -\frac{\rho^2}{2}\frac{\mathrm{d}B_0}{\mathrm{d}z} \quad \Rightarrow \quad B_\rho = -\frac{\rho}{2}\frac{\mathrm{d}B_0}{\mathrm{d}z} \quad (\rho \ll 1) \tag{4.11}$$

3. This result can be taken to the second equation and integrate again

$$\frac{\partial B_z}{\partial\rho} = \frac{\partial B_\rho}{\partial z} = -\frac{\rho}{2}\frac{\mathrm{d}^2B_0}{\mathrm{d}z^2} \quad \Rightarrow \quad B_z = B_0(z) - \frac{\rho^2}{4}\frac{\mathrm{d}^2B_0}{\mathrm{d}z^2} \tag{4.12}$$

4. Procedure can be repeated indefinitely. In general, it results in

$$B_z = \sum_{n=0}^{\infty} a_n\rho^{2n} \qquad a_n = \frac{(-1)^n}{2^{2n}n!^2}\frac{\mathrm{d}^{2n}B_0}{\mathrm{d}z^{2n}} \tag{4.13}$$

and

$$B_\rho = \sum_{n=0}^{\infty} b_n\rho^{2n+1} \qquad b_n = \frac{(-1)^{n+1}}{2^{2n+1}n!\,(n+1)!}\frac{\mathrm{d}^{(2n+1)}B_0}{\mathrm{d}z^{(2n+1)}} \tag{4.14}$$

Nevertheless, for points near the Z-axis (in which we are interested), the first two approximations are enough and the magnetic field can be written as

$$\vec{B} \simeq -\frac{\rho}{2}\frac{\mathrm{d}B_0}{\mathrm{d}z}\vec{u}_\rho + \left(B_0 - \frac{\rho^2}{4}\frac{\mathrm{d}^2B_0}{\mathrm{d}z^2}\right)\vec{k} \tag{4.15}$$

In Cartesian coordinates, we have

$$\vec{B} \simeq -\frac{1}{2}\frac{\mathrm{d}B_0}{\mathrm{d}z}(x\vec{\imath}_1 + y\vec{\jmath}_1) + \left(B_0 - \frac{(x^2+y^2)}{4}\frac{\mathrm{d}^2B_0}{\mathrm{d}z^2}\right)\vec{k}_1 \tag{4.16}$$

Using primes for the derivatives with respect to z, the expression (4.16) can be slightly shortened

$$\vec{B} \simeq -\frac{1}{2}B_0'(x\vec{\imath}_1 + y\vec{\jmath}_1) + \left(B_0 - \frac{(x^2+y^2)}{4}\mathrm{B}_0''\right)\vec{k}_1 \tag{4.17}$$

We could have obtained the same result working with a scalar potential $V(r)$ since outside the base the magnetic field is curl-free. Some authors of the bibliography ([3] and [5]) prefer to work with a notation using a potential instead of the components of the magnetic field. We show here the correspondence between both formulations.

The base produces a static magnetic field, which does not change in intensity or direction over time. Therefore,

it can be written as the gradient of a scalar potential:

$$\vec{B}(\vec{r}) = -\nabla V(r) \tag{4.18}$$

The fulfilment of Maxwell's equations provides that the potential must be a harmonic function

$$\nabla^2 V(r) = 0. \tag{4.19}$$

The cylindrical symmetry therefore requires that:

$$V(r) = V_0(z) + \rho V_1(z) + \rho^2 V_2(z) + \cdots, \tag{4.20}$$

The Laplacian of the potential, in cylindrical coordinates, is:

$$\nabla^2 V(r) = \frac{1}{\rho}\frac{\partial}{\partial \rho}\left(\rho \frac{\partial V(r)}{\partial \rho}\right) + \frac{1}{\rho^2}\frac{\partial^2 V(r)}{\partial \varphi^2} + \frac{\partial^2 V(r)}{\partial z^2} \tag{4.21}$$

Therefore, Laplace equation provides that

$$\nabla^2 V(r) = V_0''(z) + \rho V_1''(z) + V_1(z)\Delta\rho + \rho^2 V_2''(z) + V_2(z)\Delta\rho^2 + \cdots = 0 \tag{4.22}$$

Following Dulling et al. [5], we use the formula $\Delta\rho^n = n^2\rho^{n-2}$ and set the terms with equal powers of ρ equal to zero, obtaining

$$\begin{cases} V_j(z) = 0 \text{ for j odd} \\ V_{2j+2}(z) = -\left(\dfrac{1}{(2j+2)^2}\right) V_{2j+2}''(z) \text{ for j even} \end{cases} \tag{4.23}$$

Introducing the notation

$$\phi_k(z) = \frac{\mathrm{d}^k V_0(z)}{\mathrm{d}z^k} \tag{4.24}$$

we obtain

$$V(r) = \phi_0(z) - \frac{\rho^2}{4}\phi_2(z) + \cdots \tag{4.25}$$

The magnetic field therefore becomes

$$\vec{B} = -\nabla V(r) = \begin{pmatrix} \dfrac{x}{2}\phi_2(z) + O(\rho^3) \\ \dfrac{y}{2}\phi_2(z) + O(\rho^3) \\ -\phi_1(z) + \dfrac{\rho^2}{4}\phi_3(z) + O(\rho^4) \end{pmatrix} \tag{4.26}$$

Taking into account that the potential generated by a disk of outer radius b with a hole of radius a is given by

$$V_0(z) = 2\pi z\left(\frac{1}{(a^2+z^2)^{1/2}} - \frac{1}{(b^2+z^2)^{1/2}}\right) \tag{4.27}$$

and substituting $V_0(z)$ in ϕ_1, ϕ_2 and ϕ_3, we get the same expression of the magnetic field.

The derivatives of $B_0(z)$ are shown below, as we will need its expressions in the next chapters:

$$\frac{\mathrm{d}B_0}{\mathrm{d}z} = 3A\left(\frac{a^2 z}{(a^2+z^2)^{\frac{5}{2}}} - \frac{b^2 z}{(b^2+z^2)^{\frac{5}{2}}}\right) \tag{4.28}$$

$$\frac{\mathrm{d}^2 B_0}{\mathrm{d}z^2} = 3A\left(\frac{a^2}{(a^2+z^2)^{\frac{5}{2}}} - \frac{b^2}{(b^2+z^2)^{\frac{5}{2}}} + \frac{5b^2 z^2}{(b^2+z^2)^{\frac{7}{2}}} - \frac{5a^2 z^2}{(a^2+z^2)^{\frac{7}{2}}}\right) \tag{4.29}$$

$$\frac{\mathrm{d}^3 B_0}{\mathrm{d}z^3} = 3A\left(\frac{15b^2 z}{(b^2+z^2)^{\frac{7}{2}}} - \frac{15a^2 z}{(a^2+z^2)^{\frac{7}{2}}} + \frac{35a^2 z^3}{(a^2+z^2)^{\frac{9}{2}}} - \frac{35b^2 z^3}{(b^2+z^2)^{\frac{9}{2}}}\right) \tag{4.30}$$

We have to keep in mind that the expression of $\vec{B}$ is valid for points verifying $\rho \ll 1$, i.e, for small values of x and y. The studies of the next chapters are therefore limited due to this restriction, although their validity is good as the stable hovering of the spinning top takes place near the Z_1axis. Also note that large variations in ϕ, θ and ψ are permitted, as no restriction concerning these angles has been done.

4.3. Spinning top: magnetic dipole

So far, we have given the expressions of the magnetic field created by the base, but we must not forget the other essential element of the system. As a first approximation, the spinning top can be seen as a magnetic dipole of magnetic moment $\vec{\mu}$, which represents the magnetization of the dipole.

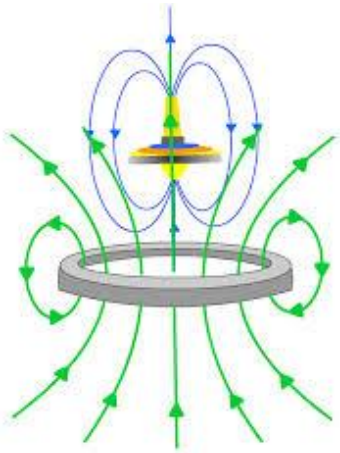

Figure 4-5: Ilustration of the magnetic field created by the base and the top.

5 STUDY OF THE STATIC STABILITY

It is well known that stable passive magnetic levitation is impossible except for a few cases: such result is commonly referred to as the Earnshaw's theorem.

Theorem 5.1.1: Earnshaw's theorem

A collection of point charges cannot be maintained in a stable stationary equilibrium configuration solely by the electrostatic interaction of the charges.

Also the exceptions are well known: superconductors, electrodynamic systems, diamagnetic materials and the systems in which the magnetic field changes in time. Nevertheless, our spinning top can hover (although not much time) in the stationary magnetic field generated by the permanent magnetized base. This apparently violates the physical laws stated by Earnshaw.

5.1. Potential energy of the system: validation of Earnshaw's Theorem

For a vector field to have a stable equilibrium point, the potential of the field must have a minimum at that point. Nevertheless, following Gauss' law, which states that the divergence of any possible electric or magnetic force field is zero at free space, the potential U of these types of forces $\vec{F}$ satisfy Laplace equation:

$$\nabla \cdot \vec{F} = -\nabla^2 U = 0 \tag{5.1}$$

If this equation is verified, the potential has no maximums or minimums but saddle points, characterized by the existence of an instability at least in one direction. Therefore, there are no stable equilibrium points.

To compute the potential energy of the top, we have to include gravitational and magnetic contributions. The gravitational potential energy is just mgz taking the Z-axis as vertically upwards. On the other hand, the magnetic energy of the magnetic dipole $\vec{\mu}$ in a magnetic field $\vec{B}$ (denoted as U_{magn}) is $-\vec{\mu} \cdot \vec{B}$, so that the moment tends to align with the magnetic field:

$$U = U_{grav} + U_{magn} = mgz - \vec{\mu} \cdot \vec{B} = mgz + \mu \left(B_x \sin(\theta) - B_y \sin(\phi) \cos(\theta) + B_z \cos(\phi) \cos(\theta) \right) \tag{5.2}$$

The first term of the equation verifies Laplace equation. Moreover, if we assume that $\vec{\mu}$ has constant direction and invoke Maxwell's equations for magnetostatics $\nabla \cdot \vec{B} = 0$ and $\nabla \times \vec{B} = \vec{0}$, we have

$$\nabla^2 \vec{B} = \nabla\left(\nabla \cdot \vec{B}\right) - \nabla \times (\nabla \times \vec{B}) = \vec{0} \tag{5.3}$$

and therefore

$$\nabla^2 U = 0 \tag{5.4}$$

Hence, there is no point at space where the dipole keeps at stable position.

5.2. Alignment between $\vec{\mu}$ and $\vec{B}$

Nevertheless, if we study the situation with the alignment between the magnetic moment $\vec{\mu}$ and the external magnetic field $\vec{B}$, the result changes.

Following Gov et al. [6], the physical principle underlying the operation of the hovering magnetic top relies on the so-called 'adiabatic approximation', idea that is tackled by Berry in [3]. As the top is launched, its magnetic moment points antiparallel to the magnetization of the base in order to supply the repulsive magnetic force which will act against the gravitational pull. As the top hovers, it experiences lateral oscillations $\Omega_{lateral}$ which are slow compared to its precession $\Omega_{precession}$. The latter, itself, is small compared to the top's spin Ω_{spin}.

Since $\Omega_{spin} \gg \Omega_{precession}$, the top can be considered as fast and acts like a fast classical top. Furthermore, as $\Omega_{precession} \gg \Omega_{lateral}$ this spin may be considered as experiencing a slowly rotating magnetic field. Under these circumstances the spin precesses around the local direction of the magnetic field $\vec{B}$ (adiabatic approximation) and, on the average, its magnetic moment $\vec{\mu}$ points antiparallel to the local magnetic field lines.

The mechanism that provides this alignment between $\vec{\mu}$ and $\vec{B}$ is the gyroscopic effect of the spinning top, which outweights horizontal instabilities.

In view of this discussion, the magnetic interaction energy $-\vec{\mu} \cdot \vec{B}$, considering the alignment of both vectors, is now given by

$$U = -k\left|\vec{B}\right|^2 = -k(B_x^2 + B_y^2 + B_z^2) \tag{5.5}$$

Computing the laplacian

$$\nabla^2\left|\vec{B}\right|^2 = 2\left(|\nabla B_x|^2 + \left|\nabla B_y\right|^2 + |\nabla B_z|^2 + B_x\nabla^2 B_x + B_y\nabla^2 B_y + B_z\nabla^2 B_z\right) \tag{5.6}$$

and considering eq. (5.3), we have

$$\nabla^2\left|\vec{B}\right|^2 = 2\left(|\nabla B_x|^2 + \left|\nabla B_y\right|^2 + |\nabla B_z|^2\right) \tag{5.7}$$

where one can deduce that $\nabla^2\left|\vec{B}\right|^2 \geq 0$, which means that the laplacian of the potential energy is always positive. Therefore, our system can be stable in all directions (but not unstable in all directions) and saddle points are also possible, situation in which the system is stable in some directions and unstable in others.

5.3. Equilibrium at OZ_1 axis

Considering the cylindrical symmetry of the magnetic field, we are going to study equilibrium points on the OZ_1 axis of symmetry (a more complex model of the field might lead to a ring of equilibrium points). The condition that $(0, z_e)$ be an equilibrium point is:

$$\begin{cases} F_z = 0 = -\dfrac{\partial U(0,z_e)}{\partial z} = -mg + \vec{\mu} \cdot \dfrac{\partial \vec{B}(0,z_e)}{\partial z} \\ F_\rho = 0 = -\dfrac{\partial U(0,z_e)}{\partial \rho} = \vec{\mu} \cdot \dfrac{\partial \vec{B}(0,z_e)}{\partial \rho} \end{cases} \tag{5.8}$$

The conditions for this equilibrium to be stable are

$$\frac{\partial^2 U(0,z_e)}{\partial z^2} > 0$$
$$\frac{\partial^2 U(0,z_e)}{\partial \rho^2} > 0 \tag{5.9}$$

Note that in the second equation in (5.9) we are using the second derivative with respect to ρ, despite we only work with the first derivative in the approximation of points near the axis.

Following Kirk T. McDonald [9], we can learn several things from equations (5.8) and (5.9). Taking into account that a cylindrically symmetric magnetic field has a radial component B_ρ that grows linearly with radius near the axis, while its axial component B_z drops off quadratically with radius, the second eq. in (5.8) tells us that the magnetic dipole moment must be either **parallel or antiparallel** to the (axial) magnetic field at the equilibrium point. We desire the equilibrium point to be above the source of the magnetic field, so the device can operate on a tabletop. Then magnitude of the magnetic field will decrease with increasing height, so if the axial magnetic field is positive, then $\frac{\partial B_z}{\partial z} < 0$ will be negative, and the first eq. in (5.8) tells us that the magnetic dipole must be **antiparallel** to field to obtain an upward force to balance that of gravity.

Since magnetic dipoles prefer to be parallel to an applied magnetic field, there must be some mechanism to insure that if the dipole is initially antiparallel it will remain so. Spinning the dipole rapidly about its axis has this effect.

To study the equilibrium points, the potential energy at OZ_1 axis is going to be analised. Therefore, $\vec{\mu} = -\mu\vec{k}_1$ and $\vec{B} = B_0(z)\vec{k}_1$ and the expression for U is

$$U = mgz + \mu A\left(\frac{b^2}{(b^2+(z-z_0)^2)^{3/2}} - \frac{a^2}{(a^2+(z-z_0)^2)^{3/2}}\right) \tag{5.10}$$

The following dimensionless variables are going to be introduced:

$$\gamma = \frac{b}{a}$$
$$B_0 = \frac{A}{a}$$
$$\beta = \frac{\mu B_0}{mga} \tag{5.11}$$
$$z^* = \frac{z-z_0}{a}$$

The expression then becomes

$$U^* = z^* + \beta B_0^*(z^*) = z^* + \beta\left(\frac{\gamma^2}{\left(\gamma^2+z^{*2}\right)^{\frac{3}{2}}} - \frac{1}{\left(1+z^{*2}\right)^{\frac{3}{2}}}\right) \tag{5.12}$$

In figure 5-1, potential energy is plotted for different values of the parameter β.

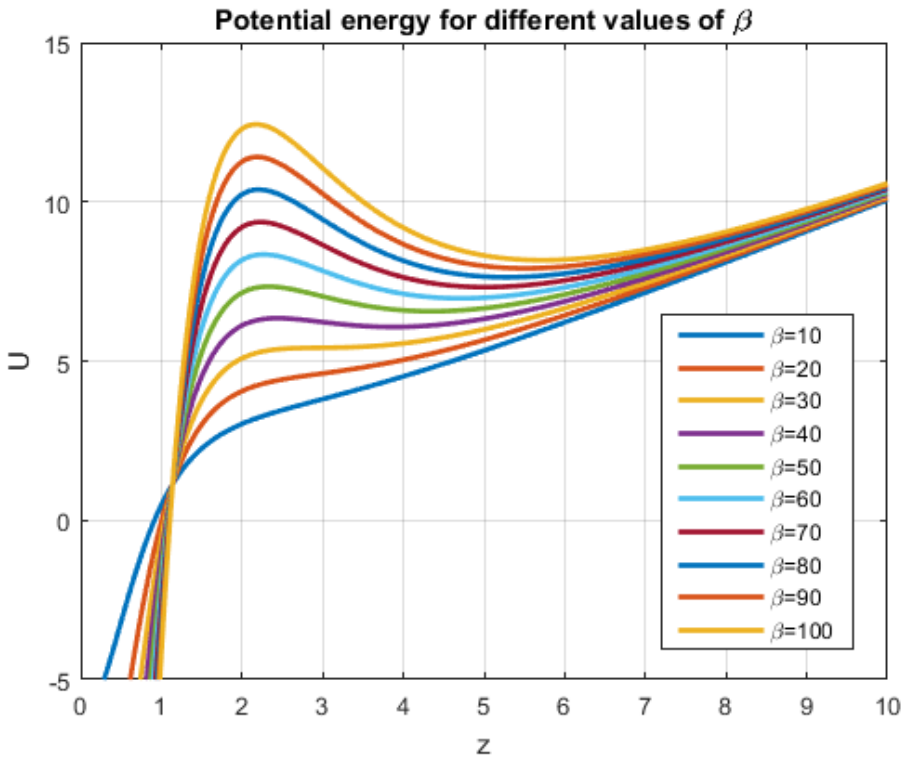

Figure 5-1: Potential energy for different values of β.

We can look for the minimum value of β for which a stable static equilibrium position can exist. Computing the first and second derivatives of U^* with respect to z^*, this value corresponds to the curve where the minimum and the maximum in the potential energy coalesce, becoming this stationary point also an inflexion point.

$$\frac{dU^*}{dz^*} = 1 + \beta B_0^{*\prime}(z^*) = 1 + 3\beta\left(\frac{1}{\left(1+z^{*2}\right)^{\frac{5}{2}}} - \frac{\gamma^2}{\left(\gamma^2+z^{*2}\right)^{\frac{5}{2}}}\right) \tag{5.13}$$

$$\frac{d^2U^*}{dz^{*2}} = \beta B_0^{*\prime\prime}(z^*) = 3\beta\left(\frac{1}{\left(1+z^{*2}\right)^{\frac{5}{2}}} - \frac{\gamma^2}{\left(\gamma^2+z^{*2}\right)^{\frac{5}{2}}} + \frac{5\gamma^2 z^{*2}}{\left(\gamma^2+z^{*2}\right)^{\frac{7}{2}}} - \frac{5z^2}{\left(1+z^{*2}\right)^{\frac{7}{2}}}\right) \tag{5.14}$$

and solving the set of equations

$$\begin{cases} \dfrac{dU^*}{dz^*} = 0 \\ \dfrac{d^2U^*}{dz^{*2}} = 0 \end{cases} \tag{5.15}$$

we get the value of z^* for which the curve $U^*(\beta, z^*)$ has an inflexion point.

Parameter β verifies the relation

$$\beta = -\frac{1}{B_0^{*\prime}(z^*)} \tag{5.16}$$

The solutions are $z^* = 2.9235$ and $\beta_{min} = 30.4311$. In figure 5-2 we can see the potential energy for β_{min}. This minimum value of z corresponds to 7.31 cm. Below this height levitation is not possible.

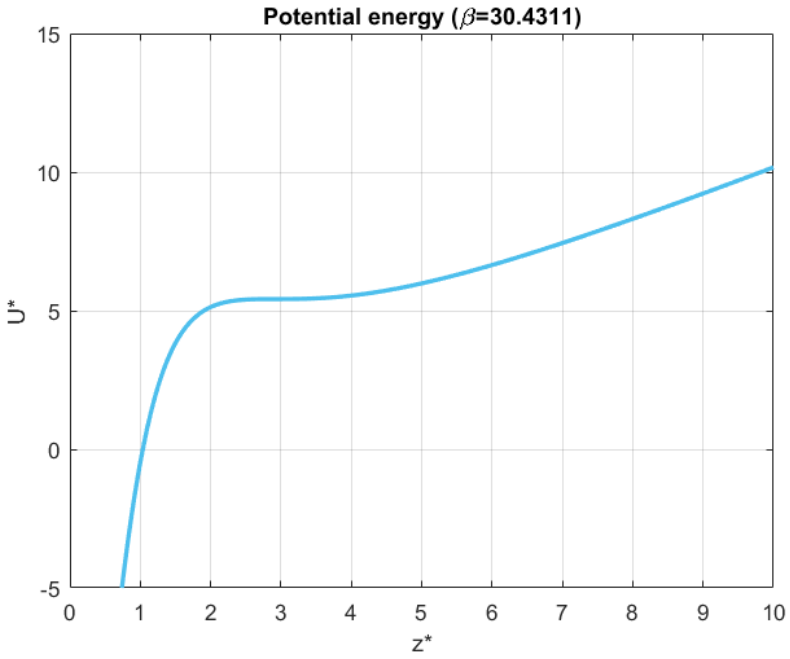

Figure 5-2: Potential energy for β_{min}

From the definition of the parameter β, we can see that β_{min} provides the minimum ratio $\frac{\mu}{m}$ in order to have a stable equilibrium. Moreover, if we assume a constant value of the magnetic moment μ, one can see that the only variable in the definition of β is the mass of the spinning top m. This mass can be changed by the player adding the washers described in the Introduction, so that a correct election is of great importance to achieve the hovering of the top.

6 ANALYSIS WITH VECTOR MECHANICS

The motion of the hovering top is governed by the equation of the dynamics, that is, Newton's second law and Euler's second law.

$$m\vec{a}_G = \vec{F} \qquad \frac{\mathrm{d}\vec{L}_G}{\mathrm{d}t} = \vec{M}_G \tag{6.1}$$

where G is the center of mass of the dipole.

6.1. Translational motion: Newton's second law

As the top hovers over the magnetized plate, it is submitted to the gravity and magnetic force:

$$\vec{F} = m\vec{g} + \nabla\left(\vec{\mu} \cdot \vec{B}\right) \tag{6.2}$$

The application of Newton's second law provides the following vectorial equation:

$$\vec{F} = m\vec{g} + \nabla\left(\vec{\mu} \cdot \vec{B}\right) = m\vec{a}_G \tag{6.3}$$

To compute the magnetic force, we need the dot product $\vec{\mu} \cdot \vec{B}$. As we saw in the previous chapters, $\vec{\mu}$ has the same direction as the unit vector $\vec{k}_4$, pointing downwards. This unit vector, expressed in frame '1', is given by:

$$\vec{k}_4 = \begin{pmatrix} \sin(\theta) \\ -\sin(\phi)\cos(\theta) \\ \cos(\phi)\cos(\theta) \end{pmatrix} \tag{6.4}$$

The dot product $\vec{\mu} \cdot \vec{B}$ is therefore

$$\vec{\mu} \cdot \vec{B} = -\mu\left(B_x \sin(\theta) - B_y \sin(\phi)\cos(\theta) + B_z \cos(\theta)\cos(\phi)\right) \tag{6.5}$$

$$\vec{F} = m\vec{g} + \nabla\left(\vec{\mu} \cdot \vec{B}\right) = \begin{pmatrix} 0 \\ 0 \\ -\mathrm{mg} \end{pmatrix} - \mu \begin{pmatrix} \frac{\partial B_x}{\partial x}\sin(\theta) - \frac{\partial B_y}{\partial x}\sin(\phi)\cos(\theta) + \frac{\partial B_z}{\partial x}\cos(\phi)\cos(\theta) \\ \frac{\partial B_x}{\partial y}\sin(\theta) - \frac{\partial B_y}{\partial y}\sin(\phi)\cos(\theta) + \frac{\partial B_z}{\partial y}\cos(\phi)\cos(\theta) \\ \frac{\partial B_x}{\partial z}\sin(\theta) - \frac{\partial B_y}{\partial z}\sin(\phi)\cos(\phi) + \frac{\partial B_z}{\partial y}\cos(\phi)\cos(\theta) \end{pmatrix} \tag{6.6}$$

Thus, the equilibrium of forces applied to the top leads to the following three scalar equations:

$$m\ddot{x} = -\mu\left(\frac{\partial B_x}{\partial x}\sin(\theta) - \frac{\partial B_y}{\partial x}\sin(\phi)\cos(\theta) + \frac{\partial B_z}{\partial x}\cos(\phi)\cos(\theta)\right) \tag{6.7}$$

$$m\ddot{y} = -\mu\left(\frac{\partial B_x}{\partial y}\sin(\theta) - \frac{\partial B_y}{\partial y}\sin(\phi)\cos(\theta) + \frac{\partial B_z}{\partial y}\cos(\phi)\cos(\theta)\right) \tag{6.8}$$

$$m\ddot{z} = -mg - \mu\left(\frac{\partial B_x}{\partial z}\sin(\theta) - \frac{\partial B_y}{\partial z}\sin(\phi)\cos(\phi) + \frac{\partial B_z}{\partial y}\cos(\phi)\cos(\theta)\right) \tag{6.9}$$

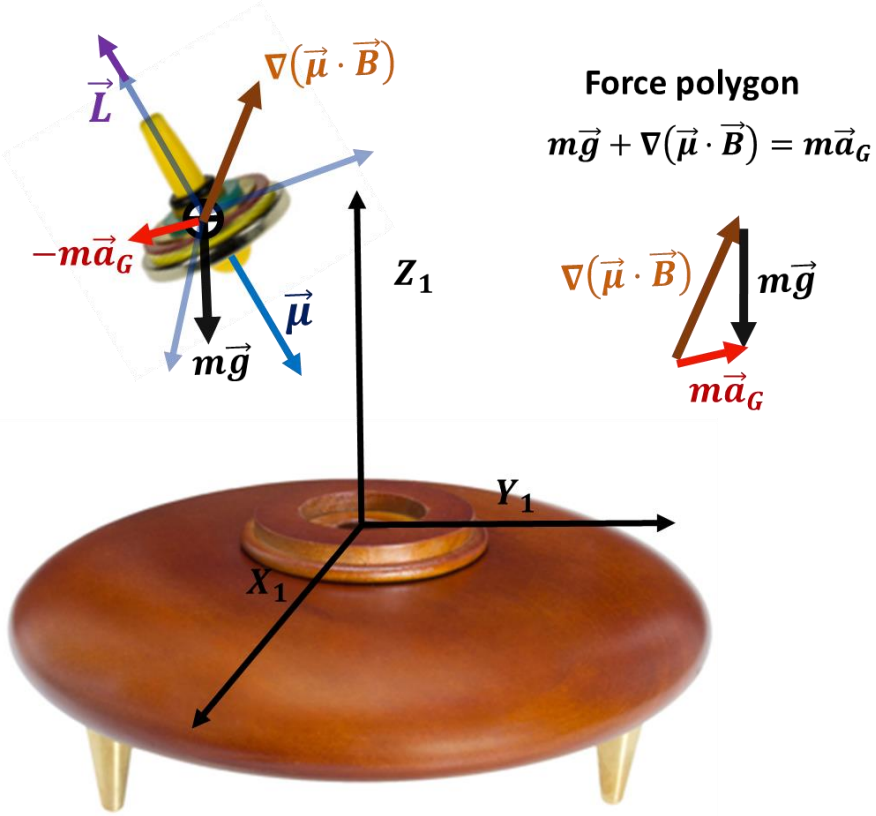

Figure 6-1: Free body diagram of the top

The previous expressions can be rewritten as a first order set using the three components of the center of mass velocity:

$$\begin{cases} \dot{x} = v_x \\ \dot{y} = v_y \\ \dot{z} = v_z \end{cases} \tag{6.10}$$

$$\begin{cases} \dot{v}_x = \dfrac{1}{m}\dfrac{\partial}{\partial x}(B_x\mu_x + B_y\mu_y + B_z\mu_z) \\ \dot{v}_y = \dfrac{1}{m}\dfrac{\partial}{\partial y}(B_x\mu_x + B_y\mu_y + B_z\mu_z) \\ \dot{v}_z = -g + \dfrac{1}{m}\dfrac{\partial}{\partial z}(B_x\mu_x + B_y\mu_y + B_z\mu_z) \end{cases} \tag{6.11}$$

6.2. Rotational motion: Modified Euler's equations

The resultant torque acting on the center of mass is only caused by the magnetic field, because the weight of the top is applied at G. The magnetic torque can be related to the characteristics of the dipole by magnetic dipole moment define above.

Watching the figure, we can see that the torque exerted by the magnetic field $\vec{M}_G$ tends to align the magnetic dipole moment $\vec{\mu}$ with the magnetic field $\vec{B}$, so this represents its lowest energy configuration.

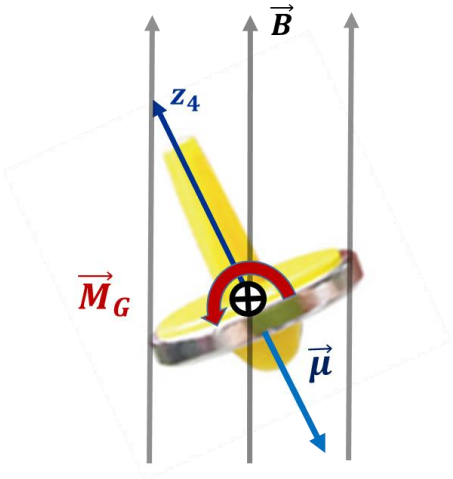

Figure 6-2: Magnetic torque acting on the spinning top.

Considering the torque as a vector quantity, it can be written as the vector product:

$$\vec{M}_G = \vec{\mu} \times \vec{B} \tag{6.12}$$

Applying the angular momentum theorem, we have:

$$\frac{\mathrm{d}\vec{L}_G}{\mathrm{d}t} = \vec{M}_G \tag{6.13}$$

Because of the rotational symmetry of the spinning top, it is highly recommendable the expression of the vector equation using frame '3', which allows us to work with an easier set of equations. When we take advantage of this rotational symmetry, these equations are known as the **Modified Euler's equations**

$$\left.\frac{\mathrm{d}\vec{L}_G}{\mathrm{d}t}\right|_1 = \left.\frac{\mathrm{d}\vec{L}_G}{\mathrm{d}t}\right|_3 + \vec{\omega}_{31} \times \vec{L}_G = \vec{\mu}|_3 \times \vec{B}|_3 \tag{6.14}$$

To compute the absolute time derivative of the angular momentum of the top, we need to know the time derivative of $\vec{L}_G$ in the frame '3' and the angular velocity of this frame with respect to the fixed frame '1'. Both vectors were computed in chapters 3.3 and 3.1, respectively.

$$\left.\frac{\mathrm{d}\vec{L}_G}{\mathrm{d}t}\right|_3 = \begin{pmatrix} I_X\left(\ddot{\phi}\cos(\theta) - \dot{\phi}\,\dot{\theta}\sin(\theta)\right) \\ I_X\ddot{\theta} \\ I_Z\left(\ddot{\psi} + \ddot{\phi}\sin(\theta) + \dot{\phi}\dot{\theta}\cos(\theta)\right) \end{pmatrix} \tag{6.15}$$

The cross product between both vectors is given by

$$\vec{\omega}_{31}|_3 \times \vec{L}_G\big|_3 = \begin{vmatrix} \vec{\imath}_3 & \vec{\jmath}_3 & \vec{k}_3 \\ \dot{\phi}\cos(\theta) & \dot{\theta} & \dot{\phi}\sin(\theta) \\ I_X\dot{\phi}\cos(\theta) & I_X\dot{\theta} & I_Z\big(\dot{\psi}+\dot{\phi}\sin(\theta)\big) \end{vmatrix} = \begin{pmatrix} I_Z\dot{\theta}\big(\dot{\psi}+\dot{\phi}\sin(\theta)\big) - I_X\dot{\phi}\dot{\theta}\sin(\theta) \\ I_X\dot{\phi}^2\sin(\theta)\cos(\theta) - I_Z\,\dot{\phi}\big(\dot{\psi}+\dot{\phi}\sin(\theta)\big)\cos(\theta) \\ 0 \end{pmatrix} \tag{6.16}$$

On the other hand, the magnetic torque is

$$\vec{M}_G = \vec{\mu}|_3 \times \vec{B}\big|_3 = -\mu\vec{k}_3 \times \vec{B}\big|_3 = -\mu B_Y\vec{\imath}_3 - \mu B_X\vec{\jmath}_3 \tag{6.17}$$

where B_X and B_Y are the components in the frame '3'. Projecting in this frame, we get

$$\begin{aligned} B_X = \vec{B}\cdot\vec{\imath}_3 &= \vec{B}\cdot\Big(\cos(\theta)\,\vec{\imath}_1 - \sin(\theta)\big(-\sin(\phi)\,\vec{\jmath}_1 + \cos(\phi)\,\vec{k}_1\big)\Big) \\ &= B_x\cos(\theta) + B_y\sin(\theta)\sin(\phi) - B_z\sin(\theta)\cos(\phi) \end{aligned} \tag{6.18}$$

$$B_Y = \vec{B}\cdot\vec{\jmath}_3 = \vec{B}\cdot\big(\cos(\phi)\,\vec{\jmath}_1 + \sin(\phi)\,\vec{k}_1\big) = B_y\cos(\phi) + B_z\sin(\phi) \tag{6.19}$$

where B_x, B_y and B_z are the components of the field derived in chapter 4.2.

The torque is therefore

$$\vec{M}_G = \begin{pmatrix} \mu\big(B_y\cos(\phi) + B_z\sin(\phi)\big) \\ \mu\big(B_z\cos(\phi)\sin(\theta) - B_x\cos(\theta) - B_y\sin(\phi)\sin(\theta)\big) \\ 0 \end{pmatrix} \tag{6.20}$$

Substituting these expressions in eq. (6.14), we get the following second order differential equation set

$$I_X\ddot{\phi}\cos(\theta) + (I_Z - 2I_X)\dot{\phi}\dot{\theta}\sin(\theta) + I_Z\dot{\theta}\dot{\psi} - \mu\big(B_y\cos(\phi) + B_z\sin(\phi)\big) = 0 \tag{6.21}$$

$$\begin{aligned} I_X\ddot{\theta} + (I_X - I_Z)\dot{\phi}^2\sin(\theta)\cos(\theta) - I_Z\dot{\phi}\dot{\psi}\cos(\theta) \\ + \mu\big(B_x\cos(\theta) + B_y\sin(\phi)\sin(\theta) - B_z\cos(\phi)\sin(\theta)\big) = 0 \end{aligned} \tag{6.22}$$

$$\frac{d}{dt}\Big(I_z\big(\dot{\psi}+\dot{\phi}\sin(\theta)\big)\Big) = 0 \tag{6.23}$$

As it was done with the translational motion, we can rewrite the second order differential equations set as a first order set using the components of the angular velocity ω_X, ω_Y, ω_Z.

$$\left.\frac{\mathrm{d}\vec{L}_G}{\mathrm{d}t}\right|_1 = \left.\frac{\mathrm{d}\vec{L}_G}{\mathrm{d}t}\right|_3 + \vec{\omega}_{31}\times\vec{L}_G = I_X(\dot{\omega}_X\vec{\imath}_3 + \dot{\omega}_Y\vec{\jmath}_3) + I_Z\dot{\omega}_Z\vec{k}_3 + \begin{vmatrix} \vec{\imath}_3 & \vec{\jmath}_3 & \vec{k}_3 \\ \omega_X & \omega_Y & \omega_X\tan(\theta) \\ I_X\omega_X & I_X\omega_Y & I_Z\omega_Z \end{vmatrix} \tag{6.24}$$

Solving and separating in components, we have

$$\begin{cases} I_X\,\dot{\omega}_X + \omega_Y(I_Z\omega_Z - I_X\omega_X\tan(\theta)) &= M_X \\ I_X\,\dot{\omega}_Y - \omega_X(I_Z\omega_Z - I_X\omega_X\tan(\theta)) &= M_Y \\ I_Z\dot{\omega}_Z &= M_Z \end{cases} \tag{6.25}$$

The first-order set is therefore

$$\begin{cases} \dot{\phi} = \dfrac{\omega_X}{\cos(\theta)} \\ \dot{\theta} = \omega_Y \\ \dot{\psi} = \omega_Z - \omega_X\tan(\theta) \end{cases} \tag{6.26}$$

$$\begin{cases} I_X\,\dot{\omega}_X + \omega_Y(I_Z\omega_Z - I_X\omega_X\tan(\theta)) &= \mu\big(B_y\cos(\phi) + B_z\sin(\phi)\big) \\ I_X\,\dot{\omega}_Y - \omega_X(I_Z\omega_Z - I_X\omega_X\tan(\theta)) &= -\mu\big(B_x\cos(\theta) + B_y\sin(\theta)\sin(\phi) - B_z\sin(\theta)\cos(\phi)\big) \\ I_Z\dot{\omega}_Z &= 0 \end{cases} \tag{6.27}$$

Taking advantage of the fact that the torque equation has been used to describe the motion of the spinning dipole about its center of mass, we are going to obtain briefly the spin precession.

In the limit of large spin angular velocity ω, the angular momentum $\vec{L}_G$ may be approximated by

$$\vec{L}_G = I_Z\vec{\omega} = I_Z\omega\frac{\vec{\mu}}{\mu} \tag{6.28}$$

Then, the torque equation

$$\frac{\mathrm{d}\vec{L}_G}{\mathrm{d}t} = \vec{\mu}\times\vec{B} \tag{6.29}$$

can be rewritten as

$$\frac{\mathrm{d}\vec{\mu}}{\mathrm{d}t} = -\frac{\mu\vec{B}}{I_Z\omega}\times\vec{\mu} \tag{6.30}$$

Thus, one can see that the motion of the dipole relative to its center of mass consists of a precession about the local direction of the magnetic field with an angular velocity

$$\Omega_{prec} = -\frac{\mu B}{I_Z\omega} \tag{6.31}$$

7 ANALYSIS WITH ANALYTICAL MECHANICS

In the previous chapters a description of the system using vector quantities of motion was made using Newton and Euler laws.

By contrast, there is an alternative formulation of classical mechanics that uses scalar properties of motion (such as its kinetic and potential energy) to describe the system as a whole: **analytical mechanics**.

We are going to derive the equations of motion of the Levitron using the two dominant branches of analytical mechanics: the Lagrangian formulation, using generalized coordinates and the corresponding generalized velocities, and the Hamiltonian mechanics, which uses coordinates and corresponding conjugate momenta.

7.1. Lagrange's equations

Lagrange equations for a system without friction are:

$$\frac{d}{dt}\left(\frac{\partial \mathcal{L}}{\partial \dot{q}_k}\right) - \frac{\partial \mathcal{L}}{\partial q_k} = 0 \tag{7.1}$$

where q_k denotes each of the generalized coordinates, i.e $q_k = \{x, y, z, \phi, \theta, \psi\}$ and $\mathcal{L}$ is the Lagrangian of the system, which is given by

$$\mathcal{L} = \mathrm{T} - \mathrm{U} \tag{7.2}$$

Substituting the expressions of T and U obtained in the previous chapters, we have

$$\mathcal{L} = \frac{1}{2}m(\dot{x}^2 + \dot{y}^2 + \dot{z}^2) + \frac{1}{2}I_X\left(\dot{\theta}^2 + \dot{\phi}^2\cos^2(\theta)\right) + \frac{1}{2}I_Z(\dot{\psi} + \dot{\phi}\sin(\theta))^2 - mgz - \mu\left(B_x\sin(\theta) - B_y\sin(\phi)\cos(\theta) + B_z\cos(\phi)\cos(\theta)\right) \tag{7.3}$$

Computing the partial derivatives for each of the coordinates,

$\boldsymbol{q = x}$

$$\frac{\partial \mathcal{L}}{\partial \dot{x}} = m\dot{x} \rightarrow \frac{d}{dt}\left(\frac{\partial \mathcal{L}}{\partial \dot{y}}\right) = m\ddot{x} \tag{7.4}$$

$$\frac{\partial \mathcal{L}}{\partial x} = -\mu\left(\frac{\partial B_x}{\partial x}\sin(\theta) - \frac{\partial B_y}{\partial x}\cos(\phi)\sin(\theta) + \frac{\partial B_z}{\partial x}\cos(\phi)\cos(\theta)\right) \tag{7.5}$$

$\boldsymbol{q = y}$

$$\frac{\partial \mathcal{L}}{\partial \dot{y}} = m\dot{y} \rightarrow \frac{d}{dt}\left(\frac{\partial \mathcal{L}}{\partial \dot{y}}\right) = m\ddot{y} \tag{7.6}$$

$$\frac{\partial \mathcal{L}}{\partial y} = -\mu\left(\frac{\partial B_x}{\partial y}\sin(\theta) - \frac{\partial B_y}{\partial y}\cos(\phi)\sin(\theta) + \frac{\partial B_z}{\partial y}\cos(\phi)\cos(\theta)\right) \tag{7.7}$$

$\boldsymbol{q = z}$

$$\frac{\partial \mathcal{L}}{\partial \dot{z}} = m\dot{z} \rightarrow \frac{d}{dt}\left(\frac{\partial \mathcal{L}}{\partial \dot{y}}\right) = m\ddot{z} \tag{7.8}$$

$$\frac{\partial \mathcal{L}}{\partial z} = -\mu \left(\frac{\partial B_x}{\partial z}\sin(\theta) - \frac{\partial B_y}{\partial z}\sin(\phi)\cos(\theta) + \frac{\partial B_z}{\partial y}\cos(\phi)\cos(\theta)\right) - mg \tag{7.9}$$

$\boldsymbol{q = \phi}$

$$\frac{\partial \mathcal{L}}{\partial \dot{\phi}} = I_X\dot{\phi}\cos^2(\theta) + I_z(\dot{\psi} + \dot{\phi}\sin(\theta))\sin(\theta) \tag{7.10}$$

$$\begin{aligned}\frac{d}{dt}\left(\frac{\partial \mathcal{L}}{\partial \dot{\phi}}\right) = {} & I_X\ddot{\phi}\cos^2(\theta) - 2I_X\dot{\phi}\dot{\theta}\sin(\theta)\cos(\theta) + I_z\left(\ddot{\psi} + \ddot{\phi}\sin(\theta) + \dot{\phi}\dot{\theta}\cos(\theta)\right)\sin(\theta) \\ & + I_z\dot{\theta}(\dot{\psi} + \dot{\phi}\sin(\theta))\cos(\theta)\end{aligned} \tag{7.11}$$

$$\frac{\partial \mathcal{L}}{\partial \phi} = -\mu\left(-B_y\cos(\phi)\cos(\theta) - B_z\sin(\phi)\cos(\theta)\right) \tag{7.12}$$

$\boldsymbol{q = \theta}$

$$\frac{\partial \mathcal{L}}{\partial \dot{\theta}} = I_X\dot{\theta} \rightarrow \frac{d}{dt}\left(\frac{\partial \mathcal{L}}{\partial \dot{\theta}}\right) = I_X\ddot{\theta} \tag{7.13}$$

$$\begin{aligned}\frac{\partial \mathcal{L}}{\partial \theta} = {} & -I_X\dot{\phi}^2\sin(\theta)\cos(\theta) + I_z\dot{\phi}\dot{\psi}\cos(\theta) \\ & + I_z\dot{\phi}^2\sin(\theta)\cos(\theta) \\ & - \mu(B_x\cos(\theta) + B_y\sin(\phi)\sin(\theta) - B_z\cos(\phi)\sin(\theta))\end{aligned} \tag{7.14}$$

$\boldsymbol{q = \psi}$

$$\frac{\partial \mathcal{L}}{\partial \dot{\psi}} = I_z(\dot{\psi} + \dot{\phi}\sin(\theta)) \tag{7.15}$$

$$\frac{\partial \mathcal{L}}{\partial \psi} = 0 \tag{7.16}$$

We obtain the following six equations:

$$m\ddot{x} + \mu\left(\frac{\partial B_x}{\partial x}\sin(\theta) - \frac{\partial B_y}{\partial x}cos(\phi)\,sin(\theta) + \frac{\partial B_z}{\partial x}cos(\phi)\,cos(\theta)\right) = 0 \tag{7.17}$$

$$m\ddot{y} + \mu\left(\frac{\partial B_x}{\partial y}\sin(\theta) - \frac{\partial B_y}{\partial y}\cos(\phi)\sin(\theta) + \frac{\partial B_z}{\partial y}\cos(\phi)\cos(\theta)\right) = 0 \tag{7.18}$$

$$m\ddot{z} + \mu\left(\frac{\partial B_x}{\partial z}sin(\theta) - \frac{\partial B_y}{\partial z}cos(\theta)\,sin(\phi) + \frac{\partial B_z}{\partial z}cos(\phi)\,cos(\theta)\right) + mg = 0 \tag{7.19}$$

$$\begin{aligned}\left(I_X\cos^2(\theta) + I_Z sin^2(\theta)\right)\ddot{\phi} + I_Z\,\ddot{\psi}\,sin(\theta) + (I_Z - I_X)\dot{\phi}\dot{\theta}\,sin(2\theta)\\ + I_Z\dot{\psi}\dot{\theta}\,cos(\theta) + \mu\left(-B_y\,cos(\phi)\,cos(\theta) - B_z\,sin(\phi)\,cos(\theta)\right) = 0\end{aligned} \tag{7.20}$$

$$\begin{aligned}I_X\ddot{\theta} + (I_X - I_Z)\dot{\phi}^2\,sin(\theta)\,cos(\theta) - I_Z\dot{\phi}\dot{\psi}\,cos(\theta)\\ + \mu\left(B_x\,cos(\theta) + B_y\,sin(\phi)\,sin(\theta) - B_z\,cos(\phi)\,sin(\theta)\right) = 0\end{aligned} \tag{7.21}$$

$$\frac{d}{dt}\left(I_z\left(\dot{\psi} + \dot{\phi}\sin(\theta)\right)\right) = 0 \tag{7.22}$$

The use of the Lagrange's equations has led to a set of second-order differential equations. However, if one compares these expressions with the set obtained using vectorial mechanics, they are all the same with the exception of the fourth one. In the lagrangian formulation, terms depending on $\ddot{\phi}$ and $\ddot{\psi}$ appear, whereas in the vector mechanics analysis each equation has only one second derivative. The use of eq. (7.22) allows us to find the relation between $\ddot{\psi}$ and $\ddot{\phi}$:

$$\frac{d}{dt}\left(I_z\left(\dot{\psi} + \dot{\phi}\sin(\theta)\right)\right) = 0 \rightarrow \ddot{\psi} = -\ddot{\phi}\sin(\theta) - \dot{\phi}\dot{\theta}\,cos(\theta) \tag{7.23}$$

Substituting in eq. (7.20), we get

$$I_X\ddot{\phi}\cos(\theta) + (I_Z - 2I_X)\dot{\phi}\dot{\theta}\sin(\theta) + I_Z\dot{\theta}\dot{\psi} - \mu\left(B_y\cos(\phi) + B_z\sin(\phi)\right) = 0 \tag{7.24}$$

which exactly corresponds with the expression obtained using vectorial mechanics. Thus, we have arrived to the same result with both formulations.

7.2. Hamilton's equations

The time evolution of the system can be defined by Hamilton's equations:

$$\frac{d\boldsymbol{p}}{dt} = -\frac{\partial\mathcal{H}}{\partial\boldsymbol{q}} \tag{7.25}$$

$$\frac{d\boldsymbol{q}}{dt} = \frac{\partial\mathcal{H}}{\partial\boldsymbol{p}} \tag{7.26}$$

where $\boldsymbol{q} = \{x\ y\ z\ \phi\ \theta\ \psi\}$ is the generalized coordinates vector and $\boldsymbol{p} = \{p_x\ p_y\ p_z\ p_\phi\ p_\theta\ p_\psi\}$ the conjugate momenta vector.

The first step is creating the Hamiltonian:

$$\mathcal{H} = \dot{\boldsymbol{q}}^{\boldsymbol{T}}\boldsymbol{p} - \mathcal{L} \tag{7.27}$$

where $\mathcal{L}$ is the Lagrangian, whose expression was shown in the previous chapter.

To obtain the conjugate momenta vector $\boldsymbol{p}$, the derivatives of the Lagrangian with respect the generalized velocities were calculated for the Lagrange's equations:

$$p_x = \frac{\partial \mathcal{L}}{\partial \dot{x}} = m\dot{x} \tag{7.28}$$

$$p_y = \frac{\partial \mathcal{L}}{\partial \dot{y}} = m\dot{y} \tag{7.29}$$

$$p_z = \frac{\partial \mathcal{L}}{\partial \dot{z}} = m\dot{z} \tag{7.30}$$

$$p_\phi = \frac{\partial \mathcal{L}}{\partial \dot{\phi}} = I_X\dot{\phi}\cos^2(\theta) + I_z(\dot{\psi} + \dot{\phi}\sin(\theta))\sin(\theta) \tag{7.31}$$

$$p_\theta = \frac{\partial \mathcal{L}}{\partial \dot{\theta}} = I_X\dot{\theta} \tag{7.32}$$

$$p_\psi = \frac{\partial \mathcal{L}}{\partial \dot{\psi}} = I_z(\dot{\psi} + \dot{\phi}\sin(\theta)) \tag{7.33}$$

We can rewrite the vector $\dot{\boldsymbol{q}}$ in terms of the conjugate momenta. The generalized velocities $\dot{x}$, $\dot{y}$, $\dot{z}$ and $\dot{\theta}$ are found easily from the equations above:

$$\begin{aligned} \dot{x} &= \frac{p_x}{m} \\ \dot{y} &= \frac{p_y}{m} \\ \dot{z} &= \frac{p_z}{m} \\ \dot{\theta} &= \frac{p_\theta}{I_X} \end{aligned} \tag{7.34}$$

The generalized velocities $\dot{\phi}$ and $\dot{\psi}$ as a function of the conjugate momenta can be obtained solving the following set of equations:

$$p_\phi = I_X\dot{\phi}\cos^2(\theta) + I_z(\dot{\psi} + \dot{\phi}\sin(\theta))\sin(\theta) \tag{7.35}$$

$$p_\psi = I_z\big(\dot{\psi} + \dot{\phi}\sin(\theta)\big) \tag{7.36}$$

Inverse relations give

$$\dot{\phi} = \frac{p_\phi - p_\psi \sin(\theta)}{I_x \cos^2(\theta)} \tag{7.37}$$

$$\dot{\psi} = \frac{p_\psi}{I_z} - \frac{p_\phi - p_\psi \sin(\theta)}{I_x \cos^2(\theta)} \sin(\theta) \tag{7.38}$$

Therefore, the generalized velocities vector and the Lagrangian, in terms of the conjugate momenta, are:

$$\dot{\boldsymbol{q}}^{\boldsymbol{T}} = \begin{pmatrix} \dot{x} & \dot{y} & \dot{z} & \dot{\phi} & \dot{\theta} & \dot{\psi} \end{pmatrix} \tag{7.39}$$

$$\dot{\boldsymbol{q}}^{\boldsymbol{T}} = \left(\frac{p_x}{m}, \frac{p_y}{m}, \frac{p_z}{m}, \frac{p_\phi - p_\psi \sin(\theta)}{I_x \cos^2(\theta)}, \frac{p_\theta}{I_X}, \frac{p_\psi}{I_z} - \frac{p_\phi - p_\psi \sin(\theta)}{I_x \cos^2(\theta)} \sin(\theta) \right) \tag{7.40}$$

$$\begin{aligned} \mathcal{L} = {} & \frac{1}{2m}\left(p_x^2 + p_y^2 + p_z^2\right) + \frac{1}{2} I_x \left(\frac{p_\theta^2}{I_X^2} + \frac{\left(p_\phi - p_\psi \, sin(\theta)\right)^2}{I_x^2 cos^2(\theta)} \right) \\ & + \frac{1}{2} I_z \left(\frac{p_\psi}{I_z} - \frac{p_\phi - p_\psi \, sin(\theta)}{I_x cos^2(\theta)} sin(\theta) + \frac{p_\phi - p_\psi \, sin(\theta)}{I_x cos^2(\theta)} sin(\theta) \right)^2 - U \end{aligned} \tag{7.41}$$

Substituting these expressions in eq. (7.27), we obtain the expression of the Hamiltonian $\mathcal{H}$

$$\mathcal{H} = \dot{\boldsymbol{q}}^{\boldsymbol{T}} \boldsymbol{p} - \mathcal{L} = \left(\frac{p_x}{m}, \frac{p_y}{m}, \frac{p_z}{m}, \frac{p_\phi - p_\psi \sin(\theta)}{I_x \cos^2(\theta)}, \frac{p_\theta}{I_X}, \frac{p_\psi}{I_z} - \frac{p_\phi - p_\psi \sin(\theta)}{I_x \cos^2(\theta)} \sin(\theta) \right) \begin{pmatrix} p_x \\ p_y \\ p_z \\ p_\phi \\ p_\theta \\ p_\psi \end{pmatrix} - \mathcal{L} \tag{7.42}$$

$$\begin{aligned} \mathcal{H} = {} & \frac{1}{2m}\left(p_x^2 + p_y^2 + p_z^2\right) + \frac{p_\theta^2}{2I_x} + \frac{\left(p_\phi - p_\psi \, sin(\theta)\right)^2}{2I_x cos^2(\theta)} + \frac{p_\psi^2}{2I_z} + mgz \\ & + \mu\left(B_x \, sin(\theta) - B_y sin(\phi) \, cos(\theta) + B_z \, cos(\phi) \, cos(\theta)\right) \end{aligned} \tag{7.43}$$

The use of Hamilton's equations leads to

$$\dot{x} = \frac{p_x}{m} \tag{7.44}$$

$$\dot{y} = \frac{p_y}{m} \tag{7.45}$$

$$\dot{z} = \frac{p_z}{m} \tag{7.46}$$

$$\dot{\phi} = \frac{p_\phi - p_\psi \, sin(\theta)}{I_x cos^2(\theta)} \tag{7.47}$$

$$\dot{\theta} = \frac{p_\theta}{I_X} \tag{7.48}$$

$$\dot{\psi} = \frac{p_\psi}{I_z} - \frac{p_\phi - p_\psi \sin(\theta)}{I_x \cos^2(\theta)} \sin(\theta) \tag{7.49}$$

$$\dot{p}_x = -\mu \left(\frac{\partial B_x}{\partial x} \sin(\theta) - \frac{\partial B_y}{\partial x} \sin(\phi) \cos(\theta) + \frac{\partial B_z}{\partial x} \cos(\phi) \cos(\theta) \right) \tag{7.50}$$

$$\dot{p}_y = -\mu \left(\frac{\partial B_x}{\partial y} \sin(\theta) - \frac{\partial B_y}{\partial y} \sin(\phi) \cos(\theta) + \frac{\partial B_z}{\partial y} \cos(\phi) \cos(\theta) \right) \tag{7.51}$$

$$\dot{p}_z = -\mu \left(\frac{\partial B_x}{\partial z} \sin(\theta) - \frac{\partial B_y}{\partial z} \sin(\phi) \cos(\theta) + \frac{\partial B_z}{\partial z} \cos(\phi) \cos(\theta) \right) - mg \tag{7.52}$$

$$\dot{p}_\phi = -\mu \big(-B_y \cos(\phi) \cos(\theta) - B_z \sin(\phi) \cos(\theta) \big) \tag{7.53}$$

$$\dot{p}_\theta = \frac{\big(p_\psi \sin(\theta) - p_\phi\big)\big(p_\phi \sin(\theta) - p_\psi\big)}{I_x \cos^3(\theta)} - \mu \big(B_x \cos(\theta) + B_y \sin(\phi) \sin(\theta) - B_z \cos(\phi) \sin(\theta) \big) \tag{7.54}$$

$$\dot{p_\psi} = 0 \tag{7.55}$$

As we can see from the previous set, Hamilton's equations provide 12 first-order differential equations. Despite we have reduced the order of the system (Lagrange's equations are second-order) Hamilton's equations do not reduce the difficulty of finding an explicit solution of the nonlinear system.

Nevertheless, they offer other advantage over Lagrange's equations: because the coordinate ψ does not occur in the Hamiltonian, the corresponding momentum is conserved, and that coordinate can be ignored in the other equations of the set. Effectively, this reduces the problem from 6 coordinates to 5 coordinates. In the Lagrangian framework, of course the result that the corresponding momentum is conserved still follows immediately, but all the generalized velocities still occur in the Lagrangian - we still have to solve a system of equations in 6 coordinates.

8 NONDIMENSIONALIZATION AND SUMMARY OF EQUATIONS

To perform numerical integrations it is convenient to define dimensionless variables, whose values will typically be of the order of unity.

8.1. Introduction of nondimensional variables

We choose as unit of time t_0

$$t_0 = \sqrt{a/g} \tag{8.1}$$

which is the free-fall time. It is recalled that a is the inner radius of the base, which will be constantly used in order to get the nondimensional variables.

Note that the problem has another characteristic timescale because of the fast spin of the top, but for simplicity we opt to work only with t_0.

First of all, we define the units used to get the dimensionless variables. These variables are obtained dividing real variables by these units, and will be denoted with an asterisk *.

One must mention that choosing different scales for the variables, simpler equations can be obtained. Nevertheless, for simplicity we have chosen the same scale for all of them.

$$\begin{gathered}
[x, y, z\,] = a \\
\left[v_x, v_y, v_z\,\right] = \frac{a}{t_0} = a\sqrt{g/a} \\
[\phi, \theta, \psi] = 1 \\
\left[\dot{\phi}, \dot{\theta}, \dot{\psi}\right] = \frac{1}{t_0} = \sqrt{g/a} \\
\left[\omega_x, \omega_y, \omega_z\,\right] = \frac{1}{t_0} = \sqrt{g/a} \\
\left[\dot{\omega}_x, \dot{\omega}_y, \dot{\omega}_z\right] = \frac{1}{t_0^2} = g/a \\
\left[p_x, p_y, p_z\,\right] = \frac{ma}{t_0} = ma\sqrt{g/a} \\
\left[p_\phi, p_\theta, p_\psi\,\right] = \frac{ma^2}{t_0} = ma^2\sqrt{g/a} \\
\left[\dot{p}_x, \dot{p}_y, \dot{p}_z\right] = \frac{ma}{t_0^2} = mg \\
\left[\dot{p}_\phi, \dot{p}_\theta, \dot{p}_\psi\right] = \frac{ma^2}{t_0^2} = mga
\end{gathered} \tag{8.2}$$

It is also necessary to define the following parameters. Some of them were introduced in chapter 5 in order to

have a nondimensional expression for the potential energy:

$$\begin{gathered}\gamma = \frac{b}{a} \\ B_0 = \frac{A}{a} \\ \beta = \frac{\mu B_0}{mga} \\ \sigma = \frac{I_z}{I_x} = 2 \\ R = \frac{ma^2}{I_x} = \frac{ma^2}{\frac{1}{4}mr^2} = 16\end{gathered} \tag{8.3}$$

To obtain the value of R, it has been used the relation $\frac{a}{r} = 2$, obtained by simple inspection of the toy.

8.2. Summary of equations

8.2.1. Vectorial mechanics

$$\dot{x}^* = v_x^* \tag{8.4}$$

$$\dot{y}^* = v_y^* \tag{8.5}$$

$$\dot{z}^* = v_z^* \tag{8.6}$$

$$\dot{\phi}^* = \frac{\omega_x^*}{\cos(\theta^*)} \tag{8.7}$$

$$\dot{\theta}^* = \omega_y^* \tag{8.8}$$

$$\dot{\psi}^* = \omega_z^* - \omega_x^* \tan(\theta^*) \tag{8.9}$$

$$\dot{v_x^*} = \beta\left(\frac{1}{2}\frac{dB_0^*}{dz^*}\sin(\theta^*) + \frac{x^*}{2}\frac{d^2B_0^*}{dz^{*2}}\cos(\phi^*)\cos(\theta^*)\right) \tag{8.10}$$

$$\dot{v_y^*} = -\beta\left(\frac{1}{2}\frac{dB_0^*}{dz^*}\sin(\phi^*)\cos(\theta^*) - \frac{y^*}{2}\frac{d^2B_0^*}{dz^{*2}}\cos(\phi^*)\cos(\theta^*)\right) \tag{8.11}$$

$$\begin{aligned}\dot{v_z^*} = -1 - \beta\Bigg(&-\frac{1}{2}x^*\frac{d^2B_0^*}{dz^{*2}}\sin(\theta^*) \\ &+\frac{1}{2}y^*\frac{d^2B_0^*}{dz^{*2}}\sin(\phi^*)\cos(\theta^*) \\ &+\frac{dB_0^*}{dz^*}\cos(\phi^*)\cos(\theta^*) - \frac{x^{*2}+y^{*2}}{4}\frac{d^3B_0^*}{dz^{*3}}\cos(\phi^*)\cos(\theta^*)\Bigg)\end{aligned} \tag{8.12}$$

$$\dot{\omega_x^*} = \beta R\left(-\frac{1}{2}y^*\frac{dB_0^*}{dz^*}\cos(\phi^*) + B_0^*\sin(\phi^*) - \frac{x^{*2}+y^{*2}}{4}\frac{d^2B_0^*}{dz^{*2}}\sin(\phi^*)\right) - \omega_y^*(\sigma\omega_z^* - \omega_x^*\tan(\theta^*)) \tag{8.13}$$

$$\dot{\omega_y^*} = -\beta R\left(-\frac{1}{2}x^*\frac{dB_0^*}{dz^*}\cos(\theta^*) - \frac{1}{2}y^*\frac{dB_0^*}{dz^*}\sin(\theta^*)\sin(\phi^*) - B_0^*\sin(\theta^*)\cos(\phi^*) + \frac{x^{*2}+y^{*2}}{4}\frac{d^2B_0^*}{dz^{*2}}\sin(\theta^*)\cos(\phi^*)\right) + \omega_x^*(\sigma\omega_z^* - \omega_x^*\tan(\theta^*)) \tag{8.14}$$

$$\dot{\omega_z^*} = 0 \tag{8.15}$$

8.2.2. Hamilton's equations

$$\dot{x}^* = p_x^* \tag{8.16}$$

$$\dot{y}^* = p_y^* \tag{8.17}$$

$$\dot{z}^* = p_z^* \tag{8.18}$$

$$\dot{\phi}^* = R\frac{p_\phi^* - p_\psi^*\sin(\theta^*)}{\cos^2(\theta^*)} \tag{8.19}$$

$$\dot{\theta}^* = Rp_\theta^* \tag{8.20}$$

$$\dot{\psi}^* = \frac{R}{\sigma}p_\psi^* - R\frac{\sin(\theta^*)}{\cos^2(\theta^*)}\left(p_\phi^* - p_\psi^*\sin(\theta^*)\right) \tag{8.21}$$

$$\dot{p_x^*} = -\beta\left(-\frac{1}{2}\frac{dB_0^*}{dz^*}\sin(\theta^*) - \frac{x^*}{2}\frac{d^2B_0^*}{dz^{*2}}\cos(\phi^*)\cos(\theta^*)\right) \tag{8.22}$$

$$\dot{p_y^*} = -\beta\left(\frac{1}{2}\frac{dB_0^*}{dz^*}\sin(\phi^*)\cos(\theta^*) - \frac{y^*}{2}\frac{d^2B_0^*}{dz^{*2}}\cos(\phi^*)\cos(\theta^*)\right) \tag{8.23}$$

$$\dot{p_z^*} = -1 - \beta\left(-\frac{1}{2}x^*\frac{d^2B_0^*}{dz^{*2}}\sin(\theta^*) + \frac{1}{2}y^*\frac{d^2B_0^*}{dz^{*2}}\sin(\phi^*)\cos(\theta^*) + \frac{dB_0^*}{dz^*}\cos(\phi^*)\cos(\theta^*) - \frac{x^{*2}+y^{*2}}{4}\frac{d^3B_0^*}{dz^{*3}}\cos(\phi^*)\cos(\theta^*)\right) \tag{8.24}$$

$$\dot{p_\phi^*} = -\beta\left(\frac{1}{2}y^*\frac{dB_0^*}{dz^*}\cos(\phi^*)\cos(\theta^*) - B_0^*\sin(\phi^*)\cos(\theta^*) + \frac{x^{*2}+y^{*2}}{4}\frac{d^2B_0^*}{dz^{*2}}\sin(\phi^*)\cos(\theta^*)\right) \tag{8.25}$$

$$\dot{p_\theta^*} = \frac{R}{\cos^3(\theta^*)}\left(p_\psi^*\sin(\theta^*) - p_\phi^*\right)\left(p_\phi^*\sin(\theta^*) - p_\psi^*\right) - \beta\left(-\frac{1}{2}x^*\frac{dB_0^*}{dz^*}\cos(\theta^*) - \frac{1}{2}y^*\frac{dB_0^*}{dz^*}\sin(\phi^*)\sin(\theta^*) - B_0^*\cos(\phi^*)\sin(\theta^*) + \frac{x^{*2}+y^{*2}}{4}\frac{d^2B_0^*}{dz^{*2}}\cos(\phi^*)\sin(\theta^*)\right) \tag{8.26}$$

$$\dot{p_\psi^*} = 0 \tag{8.27}$$

In both cases, the nondimensional expression of B_0^* and its derivatives with respect to z^* are

$$B_0^* = \left(\frac{\gamma^2}{(\gamma^2+z^{*2})^{3/2}} - \frac{1}{(1+z^{*2})^{3/2}}\right) \tag{8.28}$$

$$\frac{\mathrm{d}B_0^*}{\mathrm{d}z^*} = 3\left(\frac{z^*}{\left(1+z^{*2}\right)^{\frac{5}{2}}} - \frac{\gamma^2 z^*}{\left(\gamma^2+z^{*2}\right)^{\frac{5}{2}}}\right) \tag{8.29}$$

$$\frac{\mathrm{d}^2B_0^*}{\mathrm{d}z^{*2}} = 3\left(\frac{1}{\left(1+z^{*2}\right)^{\frac{5}{2}}} - \frac{\gamma^2}{\left(\gamma^2+z^{*2}\right)^{\frac{5}{2}}} + \frac{5\gamma^2 z^{*2}}{\left(\gamma^2+z^{*2}\right)^{\frac{7}{2}}} - \frac{5z^{*2}}{\left(1+z^{*2}\right)^{\frac{7}{2}}}\right) \tag{8.30}$$

$$\frac{\mathrm{d}^3B_0^*}{\mathrm{d}z^{*3}} = 3\left(\frac{15\gamma^2 z^*}{\left(\gamma^2+z^{*2}\right)^{\frac{7}{2}}} - \frac{15z^*}{\left(1+z^{*2}\right)^{\frac{7}{2}}} + \frac{35z^{*3}}{\left(1+z^{*2}\right)^{\frac{9}{2}}} - \frac{35\gamma^2 z^{*3}}{\left(\gamma^2+z^{*2}\right)^{\frac{9}{2}}}\right) \tag{8.31}$$

From this point forward, the asterisk * is supressed in order to ease the notation.

The objective of the next chapters is study the Hamiltonian set of equations, ignoring the trivial equations for ψ and using p_ψ as a parameter.

9 STUDY OF THE LINEAR SYSTEM

9.1. Position of equilibrium

The positions of equilibrium of the spinning top, in the Hamiltoninan formulation, are given by the set

$$I = \{x = y = 0;\ z = z_e;\ \phi = \theta = 0;\ \ p_x = p_y = 0;\ p_z = 0;\ p_\phi = p_\theta = 0\} \tag{9.1}$$

We must check that the time derivatives of each of the variables used to define I are equal to zero at each point in the set I. For example, $\dot{x} = p_x$, and since $p_x = 0$ on I, it follows that $\dot{x} = 0$. The same can be done for the rest of variables.

As ψ is a cyclic coordinate, its corresponding conjugate momenta is a constant of the motion that can be treated as a parameter. The value of ψ, if it was necessary, could be obtained later.

At this position, the spinning top has its center of mass at rest at the z-axis, and it is spinning with its local axis Z_4 fixed along the OZ_1-axis.

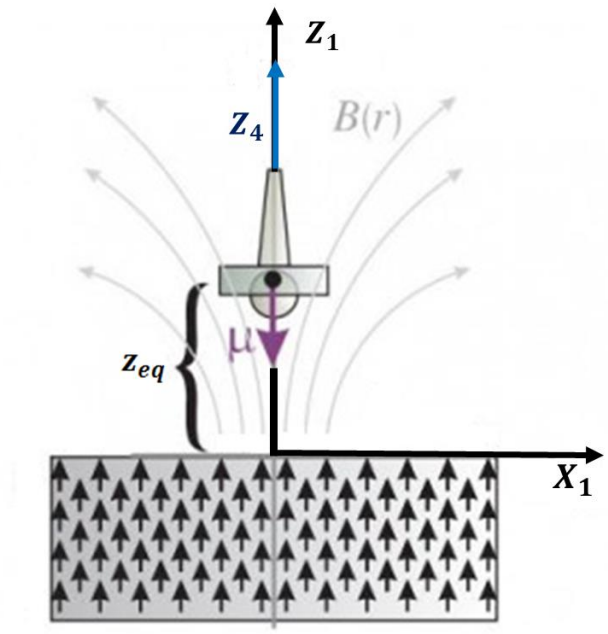

Figure 9-1: Equilibrium points, given by $z = z_e$

9.2. Linearization about the equilibrium position

We now define the local variables $\bar{q}_i = q_i - q_{i_e}$, $\bar{p}_i = p_i - p_{i_e}$ and Taylor expand each of the equations of motion about the equilibrium position given by I, retaining the linear terms. This leads to the linear system

$$\begin{cases} \dot{\bar{x}} = \dfrac{\overline{p_x}}{m} \\ \dot{\bar{y}} = \dfrac{\overline{p_y}}{m} \\ \dot{\bar{z}} = \dfrac{\overline{p_z}}{m} \\ \dot{\bar{\phi}} = \dfrac{\overline{p_\phi}}{I_X} - \dfrac{p_\psi}{I_X}\bar{\theta} \\ \dot{\bar{\theta}} = \dfrac{\overline{p_\theta}}{I_X} \\ \dot{\overline{p_x}} = \dfrac{\mu B_0'(z_e)}{2}\bar{\theta} + \dfrac{\mu B_0''(z_e)}{2}\bar{x} \\ \dot{\overline{p_y}} = \dfrac{-\mu B_0'(z_e)}{2}\bar{\phi} + \dfrac{\mu B_0''(z_e)}{2}\bar{y} \\ \dot{\overline{p_z}} = -\mu B_0''(z_e)\bar{z} \\ \dot{\overline{p_z}} = -\mu B_0''(z_e)\bar{z} \\ \dot{\overline{p_\phi}} = \dfrac{-\mu B_0'(z_e)}{2}\bar{y} + \mu B_0(z_e)\bar{\phi} \\ \dot{\overline{p_\theta}} = \dfrac{\mu B_0'(z_e)}{2}\bar{x} + \left(\mu B_0(z_e) - \dfrac{p_\psi^2}{I_X}\right)\bar{\theta} + \dfrac{p_\psi}{I_X}\overline{p_\phi} \end{cases} \tag{9.2}$$

In matrix format, the set of equations can be written as

$$\dot{\bar{\boldsymbol{q}}} = \boldsymbol{L}\,\bar{\boldsymbol{q}} \tag{93}$$

where L is the matrix that gathers all the coefficients of the linearization

$$\begin{pmatrix} \dot{\bar{x}} \\ \dot{\bar{y}} \\ \dot{\bar{z}} \\ \dot{\bar{\phi}} \\ \dot{\bar{\theta}} \\ \dot{\overline{p_x}} \\ \dot{\overline{p_y}} \\ \dot{\overline{p_z}} \\ \dot{\overline{p_\phi}} \\ \dot{\overline{p_\theta}} \end{pmatrix} = \begin{pmatrix} 0 & 0 & 0 & 0 & 0 & \frac{1}{m} & 0 & 0 & 0 & 0 \\ 0 & 0 & 0 & 0 & 0 & 0 & \frac{1}{m} & 0 & 0 & 0 \\ 0 & 0 & 0 & 0 & 0 & 0 & 0 & \frac{1}{m} & 0 & 0 \\ 0 & 0 & 0 & 0 & -\frac{p_\psi}{I_X} & 0 & 0 & 0 & \frac{1}{I_X} & 0 \\ 0 & 0 & 0 & 0 & 0 & 0 & 0 & 0 & 0 & \frac{1}{I_X} \\ \frac{\mu B_0''(z_e)}{2} & 0 & 0 & 0 & \frac{\mu B_0'(z_e)}{2} & 0 & 0 & 0 & 0 & 0 \\ 0 & \frac{\mu B_0''(z_e)}{2} & 0 & \frac{-\mu B_0'(z_e)}{2} & 0 & 0 & 0 & 0 & 0 & 0 \\ 0 & 0 & -\mu B_0''(z_e) & 0 & 0 & 0 & 0 & 0 & 0 & 0 \\ 0 & \frac{-\mu B_0'(z_e)}{2} & 0 & \mu B_0(z_e) & 0 & 0 & 0 & 0 & 0 & 0 \\ \frac{\mu B_0'(z_e)}{2} & 0 & 0 & 0 & \left(\mu B_0(z_e) - \frac{p_\psi^2}{I_X}\right) & 0 & 0 & 0 & \frac{p_\psi}{I_X} & 0 \end{pmatrix} \begin{pmatrix} \bar{x} \\ \bar{y} \\ \bar{z} \\ \bar{\phi} \\ \bar{\theta} \\ \overline{p_x} \\ \overline{p_y} \\ \overline{p_z} \\ \overline{p_\phi} \\ \overline{p_\theta} \end{pmatrix} \tag{9.4}$$

In terms of the nondimensional variables, we have:

$$\begin{cases} \dot{\bar{x}} = \overline{p_x} \\ \dot{\bar{y}} = \overline{p_y} \\ \dot{\bar{z}} = \overline{p_z} \\ \dot{\bar{\phi}} = R\overline{p_\phi} - Rp_\psi\bar{\theta} \\ \dot{\bar{\theta}} = R\overline{p_\theta} \\ \dot{\overline{p_x}} = \dfrac{\beta B_0'(z_e)}{2}\bar{\theta} + \dfrac{\beta B_0''(z_e)}{2}\bar{x} \\ \dot{\overline{p_y}} = -\dfrac{\beta B_0'(z_e)}{2}\bar{\phi} + \dfrac{\beta B_0''(z_e)}{2}\bar{y} \\ \dot{\overline{p_z}} = -\beta B_0''(z_e)\bar{z} \\ \dot{\overline{p_\phi}} = -\dfrac{\beta B_0'(z_e)}{2}\bar{y} + \beta B_0(z_e)\bar{\phi} \\ \dot{\overline{p_\theta}} = \dfrac{\beta B_0'(z_e)}{2}\bar{x} + \left(\beta B_0(z_e) - Rp_\psi^2\right)\bar{\theta} + Rp_\psi\overline{p_\phi} \end{cases} \tag{9.5}$$

Using that $\beta B_0'(z_{eq}) = -1$, the system of equations can be simplified to:

$$\begin{pmatrix} \dot{\bar{x}} \\ \dot{\bar{y}} \\ \dot{\bar{z}} \\ \dot{\bar{\phi}} \\ \dot{\bar{\theta}} \\ \dot{\overline{p_x}} \\ \dot{\overline{p_y}} \\ \dot{\overline{p_z}} \\ \dot{\overline{p_\phi}} \\ \dot{\overline{p_\theta}} \end{pmatrix} = \begin{pmatrix} 0 & 0 & 0 & 0 & 0 & 1 & 0 & 0 & 0 & 0 \\ 0 & 0 & 0 & 0 & 0 & 0 & 1 & 0 & 0 & 0 \\ 0 & 0 & 0 & 0 & 0 & 0 & 0 & 1 & 0 & 0 \\ 0 & 0 & 0 & 0 & -Rp_\psi & 0 & 0 & 0 & R & 0 \\ 0 & 0 & 0 & 0 & 0 & 0 & 0 & 0 & 0 & R \\ \dfrac{\beta B_0''(z_e)}{2} & 0 & 0 & 0 & -\dfrac{1}{2} & 0 & 0 & 0 & 0 & 0 \\ 0 & \dfrac{\beta B_0''(z_e)}{2} & 0 & \dfrac{1}{2} & 0 & 0 & 0 & 0 & 0 & 0 \\ 0 & 0 & -\beta B_0''(z_e) & 0 & 0 & 0 & 0 & 0 & 0 & 0 \\ 0 & \dfrac{1}{2} & 0 & \beta B_0(z_e) & 0 & 0 & 0 & 0 & 0 & 0 \\ -\dfrac{1}{2} & 0 & 0 & 0 & \left(\beta B_0(z_e) - Rp_\psi^2\right) & 0 & 0 & 0 & Rp_\psi & 0 \end{pmatrix} \begin{pmatrix} \bar{x} \\ \bar{y} \\ \bar{z} \\ \bar{\phi} \\ \bar{\theta} \\ \overline{p_x} \\ \overline{p_y} \\ \overline{p_z} \\ \overline{p_\phi} \\ \overline{p_\theta} \end{pmatrix} \tag{9.6}$$

The solutions of the characteristic polynomial of the matrix $\boldsymbol{L}$ (its eigenvalues) provide the ten natural frequencies of the system:

$$|\boldsymbol{L} - \lambda \boldsymbol{I}| = 0 \tag{9.7}$$

Moreover, the solutions of the equation $\boldsymbol{L}\vec{\varphi}_i = \lambda_i\vec{\varphi}_i$ for each of the natural frequencies λ_i give the ten eigenvectors $\boldsymbol{\varphi_i}$, which represent the normal modes of the linear system. The analysis of these natural modes will be done at chapter 9.8.

From now on, the constants S and B are introduced to simplify the expressions:

$$S = \beta\frac{\mathrm{d}^2 B_0}{\mathrm{d}z^2}(z_e) = -\frac{B_0''}{B_0'}(z_e) \qquad\qquad B = \beta B_0(z_e) = -\frac{B_0}{B_0'}(z_e) \tag{9.8}$$

As all the coefficients of the system of equations are real, given a real initial condition the solution of the set will be real at any time.

From this point forward, linear coordinates $\bar{q}_i$ and conjugate momenta $\bar{p}_i$ are going to be written without the upper line in $\bar{\ }$ in order to ease notation.

9.3. Solution of the system: expression with real trigonometric functions

We can try to find a basis of real solutions which enables to express any other as a combination of them.

As we can see from equations (9.5) , vertical motion is uncoupled from the horizontal one, which involves the coordinates x, y and its respective conjugate momenta p_x, p_y; and the whirl one, given by the degrees of freedom ϕ, θ and its conjugate momenta p_ϕ, p_θ .

Therefore, on one hand we have

$$\begin{aligned} \dot{z} &= p_z \\ \dot{p}_z &= -Sz \end{aligned} \tag{9.9}$$

that results in a simple harmonic motion in vertical direction with natural frequency

$$S = \beta \frac{\mathrm{d}^2 B_0}{\mathrm{d}z^2}(z_e) \tag{9.10}$$

and on the other hand we have the rest of equations of the system.

As we are looking for periodic orbits, we start with a solution with the following form:

$$x(t) = x_0 \cos(\lambda t) \qquad y(t) = y_0 \sin(\lambda t)$$

(in principle, $y(t)$ might also have a cosine component, but we will see that it does not appear).

Here, if λ and y have the same sign, the orbit is traversed in the positive sense (counterclockwise) around the OZ_1axis, whereas opposite sign shows that the trajectory goes in the negative sense (clockwise).

Differentiating once, we obtain

$$p_x = -\lambda x_0 \sin(\lambda t) \qquad p_y = \lambda y_0 \cos(\lambda t)$$

and differentiating again and solving for $\theta(t)$, $\phi(t)$:

$$\theta(t) = (S + 2\lambda^2) x_0 \cos(\lambda t) \qquad \phi(t) = -(S + 2\lambda^2) y_0 \sin(\lambda t) \tag{9.11}$$

Note that, for each mode, the vector $\theta\vec{\imath}_1 - \phi\vec{\jmath}_1$ is proportional to $x\vec{\imath}_1 + y\vec{\jmath}_1$. This implies that the dipole precesses while it is spinning, moving on the surface of an imaginary cone. Furthermore, as the proportionality constant is positive (λ^2 is positive and S is also positive in the region of interest) the unit vector $\vec{k}_3$ always points outwards.

Conjugates momenta $p_\theta(t)$ and $p_\phi(t)$ are obtained differentiating the expressions of $\theta(t)$ and $\phi(t)$ and solving:

$$p_\theta(t) = -\frac{\lambda}{R}(S + 2\lambda^2) x_0 \sin(\lambda t) \tag{9.12}$$

$$p_\phi(t) = \left(p_\psi x_0 - \frac{\lambda}{R} y_0\right)(S + 2\lambda^2) \cos(\lambda t) \tag{9.13}$$

and leading these results to the last two equations of the set, we have:

$$-\lambda\left(p_\psi x_0 - \frac{\lambda}{R}y_0\right)(S+2\lambda^2) = y_0\left(\frac{1}{2} - B(S+2\lambda^2)\right) \tag{9.14}$$

$$-\frac{\lambda^2}{R}(S+2\lambda^2)x_0 = x_0\left(\left(B - R{p_\psi}^2\right)(S+2\lambda^2) - \frac{1}{2}\right) + Rp_\psi\left(p_\psi x_0 - \frac{\lambda}{R}y_0\right)(S+2\lambda^2) \tag{9.15}$$

Simplifying and rewriting (9.15) in order to have a similar expression as (9.14),

$$-\lambda\left(p_\psi x_0 - \frac{\lambda}{R}y_0\right)(S+2\lambda^2) = y_0\left(\frac{1}{2} - B(S+2\lambda^2)\right) \tag{9.16}$$

$$\lambda\left(p_\psi y_0 - \frac{\lambda}{R}x_0\right)(S+2\lambda^2) = x_0\left(B(S+2\lambda^2) - \frac{1}{2}\right) \tag{9.17}$$

and dividing both expressions, we finally get

$$\frac{p_\psi y_0 - \frac{\lambda}{R}x_0}{p_\psi x_0 - \frac{\lambda}{R}y_0} = \frac{x_0}{y_0} \rightarrow p_\psi y_0^2 - \frac{\lambda}{R}x_0 y_0 = p_\psi x_0^2 - \frac{\lambda}{R}x_0 y_0 \tag{9.18}$$

$$y_0 = \pm x_0$$

We can see that oscillations along x and y have the same amplitude, and therefore the normal modes correspond with circular orbits.

The same result can be obtained, as it could not be otherwise, considering the linear set of equations derived from the equations of vector mechanics. For the vertical motion, we have

$$\begin{aligned} \dot{z} &= v_z \\ \dot{v}_z &= -Sz \end{aligned} \tag{9.19}$$

and the horizontal and whirl motions are described by the following equations

$$\begin{cases} \dot{x} = v_x \\ \dot{y} = v_y \\ \dot{v}_x = -\frac{1}{2}\theta + \frac{S}{2}x \\ \dot{v}_y = \frac{1}{2}\phi + \frac{S}{2}y \\ \dot{\phi} = \omega_X \\ \dot{\theta} = \omega_Y \\ \dot{\omega}_X = -\sigma\omega\omega_Y + \frac{R}{2}y + RB\phi \\ \dot{\omega}_Y = \sigma\omega\omega_X - \frac{R}{2}x + RB\theta \end{cases} \tag{9.20}$$

By simple inspection, we can see that $v_x = p_x$, $v_y = p_y$ and $v_z = p_z$, so

$$v_x = -\lambda x_0 \sin(\lambda t) \qquad v_y = \lambda y_0 \cos(\lambda t) \tag{9.21}$$

Nevertheless, one can see that the equations for the whirl motion in the vector mechanics set are simpler than in the Hamiltonian formulation , and the expressions of ω_X and ω_Y are different to p_ϕ and p_θ:

$$\omega_Y = -\lambda(2\lambda^2 + S)x_0 \sin(\lambda t) \qquad \omega_X = -\lambda(2\lambda^2 + S)y_0 \cos(\lambda t) \tag{9.22}$$

Leading these results to the last two equations,

$$\begin{aligned} \left((\lambda^2 + RB)(2\lambda^2 + S) - \frac{R}{2}\right) y_0 &= \sigma\omega\lambda(2\lambda^2 + S)x_0 \\ \left((\lambda^2 + RB)(2\lambda^2 + S) - \frac{R}{2}\right) x_0 &= \sigma\omega\lambda(2\lambda^2 + S)y_0 \end{aligned} \tag{9.23}$$

And dividing both expressions, we get again the same relation between the amplitudes

$$\frac{y_0}{x_0} = \frac{x_0}{y_0} \quad \Rightarrow \quad y_0 = \pm x_0 \tag{9.24}$$

One can see that the yardstick to determine whether the orbit is counterclockwise or clockwise is given by the factor

$$\Delta = \left((\lambda^2 + RB)(2\lambda^2 + S) - \frac{R}{2}\right) \tag{9.25}$$

If $\Delta > 0$, y_0 and λ have the same sign and the orbit is counterclockwise, whereas a negative sign means clockwise sense.

Note that the sign of λ also plays a crucial role. We are assuming that λ is positive, so that when we refer to positive spin we actually mean that “the top spins in the same sense to the proper rotation” and negative means that “it spins in the opposite sense to the proper rotation”. If we took the proper rotation in the opposite sense, signs of $-\lambda$ would change.

Considering $y_0 = +x_0$, we have the characteristic equation

$$(\lambda^2 + RB)(2\lambda^2 + S) - \frac{R}{2} = \sigma\omega\lambda(2\lambda^2 + S) \tag{9.26}$$

that provides the four eigenvalues.

To complete the basis of solutions, for each solution of the form

$$x = x_0 \cos(\lambda t) \qquad y = x_0 \sin(\lambda t)$$

there is another

$$x = -x_0 \sin(\lambda t) \qquad y = x_0 \cos(\lambda t)$$

that fulfills the same equations.

The complete solution is a linear combination of the 8 functions

$$x = \sum_{i=1}^{4} (a_i \cos(\lambda_i t) - b_i \sin(\lambda_i t)) \tag{9.27}$$

and the corresponding for the rest of variables.

9.4. Expression with complex exponentials

The previous results can also be written in term of complex exponential functions. Using Euler's formula

$$\cos(\lambda t) = \frac{1}{2} e^{j\lambda t} + \frac{1}{2} e^{-j\lambda t} \qquad \sin(\lambda t) = -\frac{j}{2} e^{j\lambda t} + \frac{j}{2} e^{-j\lambda t} \tag{9.28}$$

the expression for x is

$$x = \sum_{i=1}^{4} \left(\frac{a_i + jb_i}{2} e^{j\lambda_i t} + \frac{a_i - jb_i}{2} e^{-j\lambda_i t} \right) \tag{9.29}$$

Introducing c_i

$$c_i = \frac{a_i + jb_i}{2} \qquad c_i^* = \frac{a_i - jb_i}{2}$$

we have

$$x = \sum_{i=1}^{4} \left(c_i e^{j\lambda_i t} + c_i^* e^{-j\lambda_i t} \right) \tag{9.30}$$

The same can be done for the rest of variables:

$$y = \sum_{i=1}^{4} \left(-jc_i e^{j\lambda_i t} + jc_i^* e^{-j\lambda_i t} \right) \tag{9.31}$$

$$\theta = (2\lambda^2 + S) \sum_{i=1}^{4} \left(c_i e^{j\lambda_i t} + c_i^* e^{-j\lambda_i t} \right) \tag{9.32}$$

etc. If we consider the solutions for λ and $-\lambda$ as independent modes, the following eigenvector corresponds

with the frequency λ

$$\begin{pmatrix} x_0 \\ y_0 \\ v_{x0} \\ v_{y0} \\ \phi_0 \\ \theta_0 \\ \omega_X \\ \omega_Y \end{pmatrix} = \begin{pmatrix} 1 \\ \mathrm{j} \\ \mathrm{j}\lambda \\ -\lambda \\ -\mathrm{j}(2\lambda^2 + S) \\ (2\lambda^2 + S) \\ \lambda(2\lambda^2 + S) \\ \mathrm{j}\lambda(2\lambda^2 + S) \end{pmatrix} \tag{9.33}$$

On the other hand, frequency $-\lambda$ will be associated with the conjugate complex eigenvector.

It should be emphasized that if $\vec{\varphi}_i$ is an eigenvector, $c\vec{\varphi}_i$ it is also. This means that one can always scale the eigenvector so that one of the components is the unity, scaling the rest of the components.

9.5. Expression with complex variables

The set of equations can be reduced using the complex variables:

$$\begin{aligned} \hat{r} &= x + \mathrm{j}y \\ \hat{v} &= v_x + \mathrm{j}v_y \\ \hat{\theta} &= \theta - \mathrm{j}\phi \\ \hat{\omega} &= \omega_X + \mathrm{j}\omega_Y \end{aligned} \tag{9.34}$$

The reason why the variable $\hat{\theta} = \bar{\theta} - j\bar{\phi}$ has been introduced is the expression of the unit vector $\vec{k}_3 = \vec{k}_4$ in the linear approximation. Expressing its components in the reference frame 1

$$\vec{k}_4 = \sin\theta\vec{\imath}_1 - \sin\phi\cos\theta\vec{\jmath}_1 + \cos\phi\cos\theta\,\vec{k}_1 \simeq \theta\vec{\imath}_1 - \phi\vec{\jmath}_1 + \vec{k}_1 \tag{9.35}$$

we can see that $\hat{\theta}$ is the projection of this unit vector in the complex plane.

Therefore, variables $\hat{r}$, $\hat{v}$, $\hat{\theta}$, $\hat{\omega}$ represent the position of the center of mass, its velocity, the projection of the unit vector $\vec{k}_3$ and the angular velocity in the complex plane.

With complex variables, a solution of the form

$$\hat{r} = \hat{r}_0 \mathrm{e}^{\mathrm{j}\lambda t}$$

is equivalent to a counterclockwise rotation if λ is positive and clockwise if λ is negative.

In figure 9-2 we can see the physical interpretation of variables $\hat{r}$ and $\hat{\theta}$, that correspond respectively with the red and green trajectories.

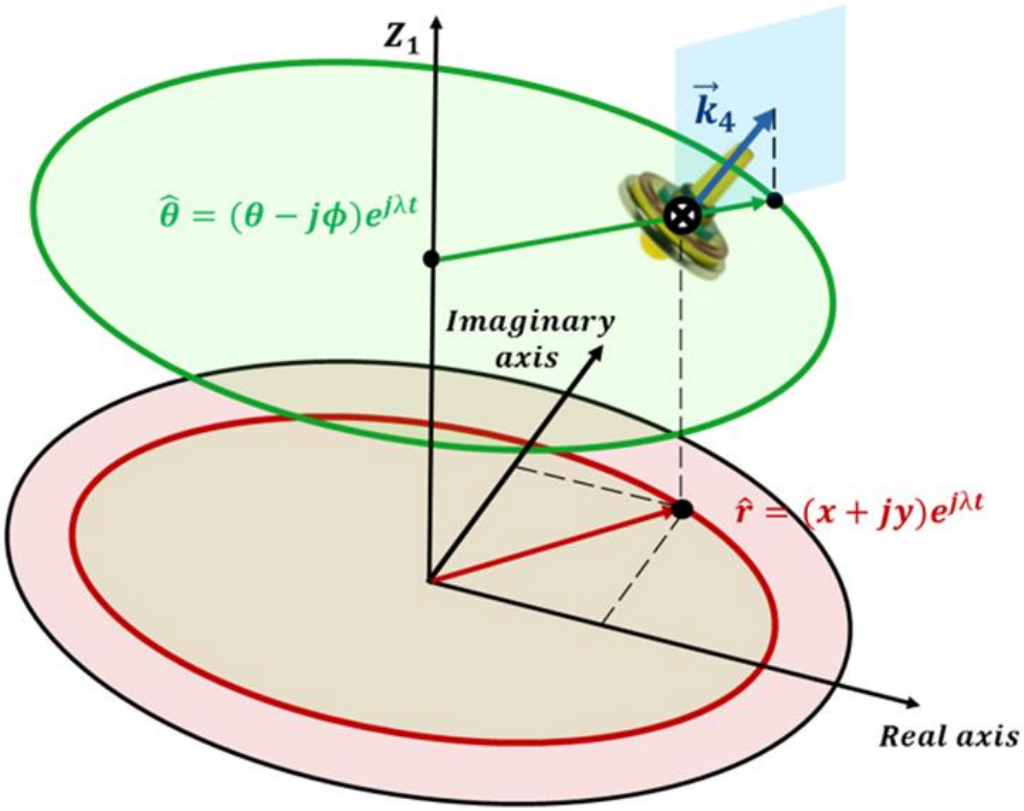

Figure 9-2: Interpretation of the complex variables.

The system is therefore reduced to

$$\begin{aligned}
\frac{\mathrm{d}\hat{r}}{\mathrm{d}t} &= \hat{v} \\
\frac{\mathrm{d}\hat{v}}{\mathrm{d}t} &= -\frac{1}{2}\hat{\theta} + \frac{S}{2}\hat{r} \\
\frac{\mathrm{d}\hat{\theta}}{\mathrm{d}t} &= -\mathrm{j}\hat{\omega} \\
\frac{\mathrm{d}\hat{\omega}}{\mathrm{d}t} &= \mathrm{j}\sigma\omega\hat{\omega} - \mathrm{j}\frac{R}{2}\hat{r} + \mathrm{j}RB\hat{\theta}
\end{aligned} \tag{9.36}$$

To analyse the linear problem, we start again with a solution

$$\hat{r} = \hat{r}_0 \mathrm{e}^{\mathrm{j}\lambda t}$$

obtaining the relation between amplitudes

$$\begin{aligned}
\mathrm{j}\lambda\hat{r}_0 &= \hat{v}_0 \\
\mathrm{j}\lambda\hat{v}_0 &= -\frac{1}{2}\hat{\theta}_0 + \frac{S}{2}\hat{r}_0 \\
\mathrm{j}\lambda\hat{\theta}_0 &= -\mathrm{j}\hat{\omega}_0 \\
\mathrm{j}\lambda\hat{\omega}_0 &= \mathrm{j}\sigma\omega\hat{\omega}_0 - \mathrm{j}\frac{R}{2}\hat{r}_0 + \mathrm{j}RB\hat{\theta}_0
\end{aligned} \tag{9.37}$$

where we get

$$\begin{aligned}\hat{v}_0 &= \mathrm{j}\lambda\hat{r}_0\\ \hat{\theta}_0 &= (2\lambda^2+S)\hat{r}_0\\ \hat{\omega}_0 &= -\lambda(2\lambda^2+S)\hat{r}_0\end{aligned} \tag{9.38}$$

Verifying the characteristic equation

$$\sigma\omega\lambda(2\lambda^2+S) = (\lambda^2+RB)(2\lambda^2+S) - \frac{R}{2} \tag{9.39}$$

which obviously is the same as that of the previous sections. The sign of the roots tell us again if the orbit is retrograde or not.

In this case, the eigenvectors have 4 complex components, and we can set one of them to be real

$$\begin{pmatrix}\hat{r}_0\\ \hat{v}_0\\ \hat{\theta}_0\\ \hat{\omega}_0\end{pmatrix} = \begin{pmatrix}1\\ \mathrm{j}\lambda\\ (2\lambda^2+S)\\ -\lambda(2\lambda^2+S)\end{pmatrix} \tag{9.40}$$

Real solutions can be obtained form the complex ones considering the following relations

$$x = \mathrm{Re}(\hat{r}) = \frac{\hat{r}+\hat{r}^*}{2} \qquad y = \mathrm{Im}(\hat{r}) = \frac{\hat{r}-\hat{r}^*}{2\mathrm{j}}$$

and therefore

$$\hat{r} = \sum_{i=1}^{4} \mathrm{c}_i \mathrm{e}^{\mathrm{j}w_i t} \tag{9.41}$$

the same result is achieved

$$x = \frac{1}{2}\sum_{i=1}^{4}\left(\mathrm{c}_i\mathrm{e}^{\mathrm{j}\lambda_i t} + \mathrm{c}_i^*\mathrm{e}^{-\mathrm{j}\lambda_i t}\right) \qquad y = \frac{1}{2}\sum_{i=1}^{4}\left(-\mathrm{j}\mathrm{c}_i\mathrm{e}^{\mathrm{j}\lambda_i t} + \mathrm{j}\mathrm{c}_i^*\mathrm{e}^{-\mathrm{j}\lambda_i t}\right) \tag{9.42}$$

It would be the same for the rest of the variables.

9.6. Linearization of Lagrange's equations: obtainment of mass, stiffness and gyroscopic matrixes using complex variables

In the previous sections we have reduced the system of equations from a 12x12 to a 4x4 set. Introducing p_ψ as a parameter and ignoring the trivial equation for ψ, the system became 10x10; then, the uncoupling between vertical and horizontal-whirl motion allowed to study a 8x8 set and, finally, the use of the complex led to a 4x4 system.

Moreover, we obtained the time evolution of the generalized coordinates and conjugate momenta as a function

of the basis of solutions determined.

Nevertheless, we can take a final step by converting the set in a 2x2 homogeneous system of equations. For that, we are going to take advantage of Lagrange's equations obtained at chapter 7.1

The linearization of the equations of motion about the known equilibrium configuration

$$\{x = y = 0;\ z = z_e;\ \phi = \theta = 0\}$$

provides

$$\begin{cases} m\ddot{\bar{x}} = \dfrac{\mu B_0''(z_e)}{2}\bar{x} + \dfrac{\mu B_0'(z_e)}{2}\bar{\theta} \\ m\ddot{\bar{y}} = \dfrac{\mu B_0''(z_e)}{2}\bar{y} - \dfrac{\mu B_0'(z_e)}{2}\bar{\phi} = 0 \\ \ddot{\bar{z}} = -\dfrac{\mu B_0''(z_e)}{m}z \\ I_X\ddot{\bar{\phi}} = \mu B_0(z_e)\bar{\phi} - I_Z\omega\dot{\bar{\theta}} - \dfrac{\mu B_0'(z_e)}{2}\bar{y} \\ I_X\ddot{\bar{\theta}} = \mu B_0(z_q)\bar{\theta} + I_Z\omega\dot{\bar{\phi}} + \dfrac{\mu B_0'(z_e)}{2}\bar{x} \\ \ddot{\bar{\psi}} = 0 \end{cases} \tag{9.43}$$

A simple analysis of the set of equations (9.43) allows to predict two important key aspects of the linearized model:

- The constancy of the spin velocity $\dot{\bar{\psi}} = \omega$, as well as that of the angular momentum.
- The uncoupling of the vertical motion with the horizontal one, which involves the x and y coordinates, and the whirl one, given by the degrees of freedom ϕ and θ (this was already known from the hamiltonian system).

Therefore, we can remove equations and in order to focus on the coupling between the horizontal and whirl behavior:

$$\begin{cases} m\ddot{\bar{x}} = \dfrac{\mu B_0''(z_e)}{2}\bar{x} + \dfrac{\mu B_0'(z_e)}{2}\bar{\theta} \\ m\ddot{\bar{y}} = \dfrac{\mu B_0''(z_e)}{2}\bar{y} - \dfrac{\mu B_0'(z_e)}{2}\bar{\phi} = 0 \\ I_X\ddot{\bar{\phi}} = \mu B_0(z_e)\bar{\phi} - I_Z\omega\dot{\bar{\theta}} - \dfrac{\mu B_0'(z_e)}{2}\bar{y} \\ I_X\ddot{\bar{\theta}} = \mu B_0(z_e)\bar{\theta} + I_Z\omega\dot{\bar{\phi}} + \dfrac{\mu B_0'(z_e)}{2}\bar{x} \end{cases} \tag{9.44}$$

At this point, we are going to combine the expressions for the displacement degrees of freedom and the whirl ones, using again complex variables:

$$(9.44.1) + (9.44.2)j$$

$$(9.44.4) - (9.44.3)j$$

This results in

$$\begin{cases} m(\ddot{\bar{x}} + j\ddot{\bar{y}}) = \dfrac{\mu B_0''(z_e)}{2}(\bar{x} + j\bar{y}) + \dfrac{\mu B_0'(z_e)}{2}(\bar{\theta} - j\bar{\phi}) \\ I_X\left(\ddot{\bar{\theta}} - j\ddot{\bar{\phi}}\right) = \mu B_0(\bar{\theta} - j\bar{\phi}) + I_Z\omega\left(\dot{\bar{\phi}} + j\dot{\bar{\theta}}\right) + \dfrac{\mu B_0'(z_e)}{2}(\bar{x} + j\bar{y}) \end{cases} \tag{9.45}$$

The term $\dot{\bar{\phi}} + j\dot{\bar{\theta}}$ can be rewritten as $j\left(\dot{\bar{\theta}} - j\dot{\bar{\phi}}\right)$, so that both expressions depend on $\bar{x} + j\bar{y}$, $\bar{\theta} - j\bar{\phi}$ and its derivatives:

$$\begin{cases} m(\ddot{\bar{x}} + j\ddot{\bar{y}}) = \dfrac{\mu B_0''(z_e)}{2}(\bar{x} + j\bar{y}) + \dfrac{\mu B_0'(z_e)}{2}(\bar{\theta} - j\bar{\phi}) \\ I_X\left(\ddot{\bar{\theta}} - j\ddot{\bar{\phi}}\right) = \mu B_0(\bar{\theta} - j\bar{\phi}) + I_Z\omega j\left(\dot{\bar{\theta}} - j\dot{\bar{\phi}}\right) + \dfrac{\mu B_0'(z_e)}{2}(\bar{x} + j\bar{y}) \end{cases} \tag{9.46}$$

Using the complex displacement $\hat{r} = \bar{x} + j\bar{y}$ and the complex rotation $\hat{\theta} = \bar{\theta} - j\bar{\phi}$ defined in section 9.5, equations (9.45) become

$$\begin{cases} m\ddot{\hat{r}} - \dfrac{\mu B_0''(z_e)}{2}\hat{r} - \dfrac{\mu B_0'(z_e)}{2}\hat{\theta} = 0 \\ I_X\ddot{\hat{\theta}} - I_Z\omega j\dot{\hat{\theta}} - \mu B_0\hat{\theta} - \dfrac{\mu B_0'(z_e)}{2}\hat{r} = 0 \end{cases} \tag{9.47}$$

The previous four equations set has been reduced to two complex equations. By defining the complex vector

$$\hat{\boldsymbol{\xi}} = \begin{pmatrix} \hat{r} \\ \hat{\theta} \end{pmatrix}$$

we can rewrite it in matrix format

$$\begin{pmatrix} m & 0 \\ 0 & I_X \end{pmatrix}\begin{pmatrix} \ddot{\hat{r}} \\ \ddot{\hat{\theta}} \end{pmatrix} - j\omega\begin{pmatrix} 0 & 0 \\ 0 & I_z \end{pmatrix}\begin{pmatrix} \dot{\hat{r}} \\ \dot{\hat{\theta}} \end{pmatrix} + \begin{pmatrix} -\dfrac{\mu B_0''(z_e)}{2} & -\dfrac{\mu B_0'(z_e)}{2} \\ -\dfrac{\mu B_0'(z_e)}{2} & -\mu B_0 \end{pmatrix}\begin{pmatrix} \hat{r} \\ \hat{\theta} \end{pmatrix} = \begin{pmatrix} 0 \\ 0 \end{pmatrix} \tag{9.48}$$

$$\boldsymbol{M}\ddot{\hat{\boldsymbol{\xi}}} + \boldsymbol{G}\dot{\hat{\boldsymbol{\xi}}} + \boldsymbol{K}\hat{\boldsymbol{\xi}} = \boldsymbol{0}$$

where it has been used the usual notation in rotordynamics, in generalized matrix format, for an axially symmetric rotor rotating at a constant speed. Hence,

$\boldsymbol{M} = \begin{pmatrix} m & 0 \\ 0 & I_X \end{pmatrix}$ is the symmetric mass matrix

$\boldsymbol{K} = \begin{pmatrix} -\frac{\mu B_0''(z_e)}{2} & -\frac{\mu B_0'(z_e)}{2} \\ -\frac{\mu B_0'(z_e)}{2} & -\mu B_0 \end{pmatrix}$ is the symmetric stiffness matrix

$\boldsymbol{G} = -j\omega\begin{pmatrix} 0 & 0 \\ 0 & I_Z \end{pmatrix}$ is a skew-symmetric gyroscopic matrix, which is proportional to the spin speed ω

The analysis of the stability can be studied by substituting the following solution in the matrix equation:

$$\hat{\boldsymbol{\xi}} = \begin{pmatrix} \hat{r} \\ \hat{\theta} \end{pmatrix} = \begin{pmatrix} \hat{r}_0 \\ \hat{\theta}_0 \end{pmatrix} e^{j\lambda t} \tag{9.49}$$

Computing the first and second derivative of $\hat{\boldsymbol{\xi}}$ with respect to time

$$\dot{\hat{\boldsymbol{\xi}}} = j\lambda\hat{\boldsymbol{\xi}}$$
$$\ddot{\hat{\boldsymbol{\xi}}} = -\lambda^2\hat{\boldsymbol{\xi}}$$

and substituting in eq. (9.48) , we have

$$\left[\begin{pmatrix} -\frac{\mu B_0''(z_e)}{2} & -\frac{\mu B_0'(z_e)}{2} \\ -\frac{\mu B_0'(z_e)}{2} & -\mu B_0 \end{pmatrix} - \lambda^2 \begin{pmatrix} m & 0 \\ 0 & I_x \end{pmatrix} + j\omega \begin{pmatrix} 0 & 0 \\ 0 & I_z \end{pmatrix}\right]\hat{\boldsymbol{\xi}} = \mathbf{0} \tag{9.50}$$

Therefore, we get a homogeneous system which depends on the eigenvalues λ and the constant rotational speed ω:

$$\begin{pmatrix} -m\lambda^2 - \frac{\mu B_0''(z_e)}{2} & -\frac{\mu B_0'(z_e)}{2} \\ -\frac{\mu B_0'(z_e)}{2} & -I_X\lambda^2 + I_Z\omega\lambda - \mu B_0 \end{pmatrix} \begin{pmatrix} \hat{r} \\ \hat{\theta} \end{pmatrix} = \begin{pmatrix} 0 \\ 0 \end{pmatrix} \tag{9.51}$$

For a nontrivial solution to exist, the determinant of the matrix must vanish:

$$det = \left(m\lambda^2 + \frac{\mu B_0''(z_e)}{2}\right)(I_X\lambda^2 - I_Z\omega\lambda + \mu B_0) - \left(\frac{\mu B_0'(z_e)}{2}\right)^2 = 0 \tag{9.52}$$

If we want the solutions $\begin{pmatrix} \hat{r} \\ \hat{\theta} \end{pmatrix} = \begin{pmatrix} \hat{r}_0 \\ \hat{\theta}_0 \end{pmatrix} e^{j\lambda t}$ to be stable for all times, it is necessary that the four roots λ_i to be real. Since the coefficients of the characteristic polynomial depend on the spin velocity ω, one can find a range of values between ω_{min} and ω_{max} in which the stability of motion is assured.

In terms of the nondimensional parameters, and using that $\beta B_0'(z_e) = -1$, eq. (9.51) becomes

$$\begin{pmatrix} -\lambda^2 - \frac{\beta B_0''(z_e)}{2} & -\frac{\beta}{2}B_0'(z_e) \\ -\frac{R\beta}{2}B_0'(z_e) & -\lambda^2 + \sigma\omega\lambda - R\beta B_0(z_e) \end{pmatrix} \begin{pmatrix} \hat{r} \\ \hat{\theta} \end{pmatrix} = \begin{pmatrix} 0 \\ 0 \end{pmatrix} \tag{9.53}$$

being its determinant

$$det = \lambda^4 - \sigma\omega\lambda^3 - \left(\frac{\beta B_0''(z_e)}{2} + \beta R B_0(z_e)\right)\lambda^2 - \sigma\omega\beta B_0''(z_e)\lambda + \left(R\beta^2 B_0(z_e)B_0''(z_e) - \frac{R}{4}\right) = 0 \tag{9.54}$$

9.7. Stability region

In eq. (9.54) the values of the parameters σ and R were given in chapter 8.1. Moreover, as β is related with the height of levitation z_e by means of eq. (5.15), we can look for the range $\omega_{min} \leq \omega \leq \omega_{max}$ that provides a stable solution (four real roots λ_i) for each z_e. Also, in chapter 5.3 we determined the minimum value of z_e for which levitation is possible (remember that below $z_e = 2.9235$ the spinning top cannot hover), so the region starts in this value.

The physical reason for the existence of the lower limit ω_{min} is obvious. Since the effect on stability due to the gyroscopic effect is proportional to the spin velocity, if the top is spun too slowly then it becomes unstable against rotation and tips over.

On the other hand, if the top is spun too fast, its axis becomes too stiff and cannot respond quickly enough to the changing direction of the magnetic field. Then the magnetic dipole moment, which has the same direction of the axis of the top, can be considered as fixed in space and, according to Earnshaw's theorem, becomes unstable against translations. This explains the existence of the upper limit ω_{max}.

The stability region has the following form

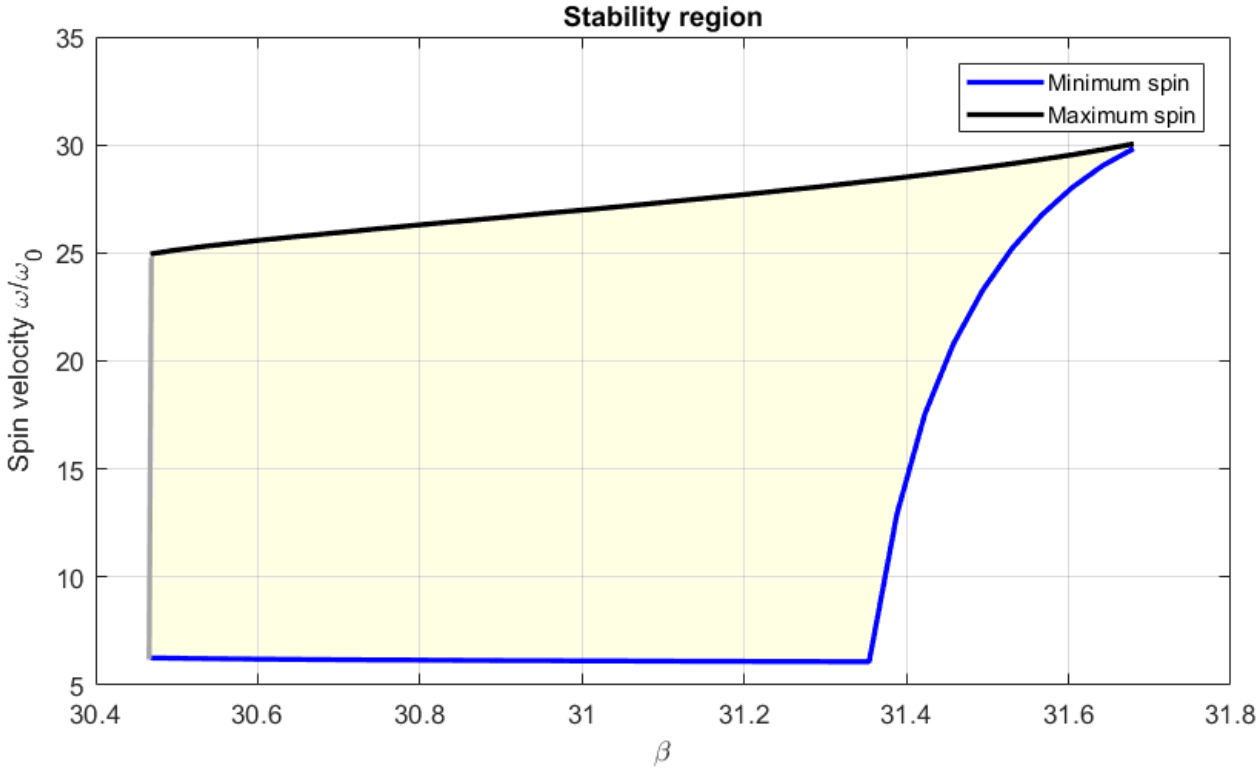

Figure 9-3: Stability region.

In terms of the β parameter, linear stability is possible within the range

$$30.43 \leq \beta \leq 31.68$$

This corresponds with a stable range of z_e

$$2.9235 \leq z_e \leq 3.22$$

or, in dimensional variables

$$7.31\ cm \leq z_e \leq 8.05\ cm$$

Genta et al. [4] provide an analytical approximation of the expressions for the lower and upper stability limits. The lower bound takes its origin from the coupling between the two rotational modes. To analytically compute the value, it is sufficient to study the stability of the rotational motion (described by the ϕ and θ degrees of freedom), considered as uncoupled with the vibrational one. Using the complex variable $\hat{\theta}$, the equation of the whirl motion becomes

$$I_X\ddot{\hat{\theta}} - j\omega I_Z\dot{\hat{\theta}} - \mu B_0\hat{\theta} = 0 \tag{9.55}$$

A solution $\hat{\theta} = \hat{\theta}_0 e^{j\lambda t}$ provides

$$I_X\lambda^2 - I_Z\omega\lambda + \mu B_0(z_e) = 0 \rightarrow \lambda = \frac{I_Z\omega \pm \sqrt{(I_Z\omega)^2 - 4I_X\mu B_0(z_e)}}{2I_X} \tag{9.56}$$

For the roots λ_i to be real, the discriminant of the quadratic equation must be positive. This condition provides the lower limit of ω to have a stable solution:

$$\omega_{min} = 2\sqrt{\mu B_0(z_e)\frac{I_X}{I_Z^2}} \tag{9.57}$$

To obtain the upper limit, one can use the fast top condition. Doing $I_X = 0$, equations become:

$$\begin{cases} m\ddot{\hat{r}} - \dfrac{\mu B_0''(z_e)}{2}\hat{r} - \dfrac{\mu B_0'(z_e)}{2}\hat{\theta} = 0 \\ I_X\ddot{\hat{\theta}} - I_Z\omega j\dot{\hat{\theta}} - \mu B_0(z_e)\hat{\theta} - \dfrac{\mu B_0'(z_e)}{2}\hat{r} = 0 \end{cases} \tag{9.58}$$

The characteristic equation of the previous set is the following cubic function:

$$4mI_z\omega\lambda^3 - 4m\mu B_0(z_e)\lambda^2 + 2\mu B_0''(z_e)I_z\omega\lambda + m^2g^2 - 2\mu^2 B_0''(z_e)B_0(z_e) = 0 \tag{9.59}$$

Using that the discriminant of a cubic equation with the form

$$a_3z^3 + a_2z^2 + a_1z + a_0 = 0$$

is given by

$$D_3 = a_1^2a_2^2 - 4a_0a_2^3 - 4a_1^3a_3 + 18a_0a_1a_2a_3 - 27a_0^2a_3^2$$

and introducing the variables

$$\zeta = \frac{B_0'(z_e)^2}{2B_0(z_e)B_0''(z_e)} - 1$$

$$f(\zeta) = 1 - 18\zeta - 27\zeta^2$$

$$\gamma_{max} = \sqrt{\frac{1+\zeta}{2}\left[f(\zeta) + \sqrt{f(\zeta)^2 + 64\zeta}\right]}$$

One gets the expression for the maximum rotational speed is

$$\omega_{max} = \frac{\gamma_{max}}{gI_Z}\sqrt{\frac{\mu^3 B_0(z_e)^3}{m}} \tag{9.60}$$

Based on figure 9-3 and the definition of β in (5.11), we can define the dimensionless variable m_0

$$m_0 = \frac{\mu B_0}{ga}$$

and plot the nondimensional variable $\frac{m}{m_0}$ against the rotational speed.

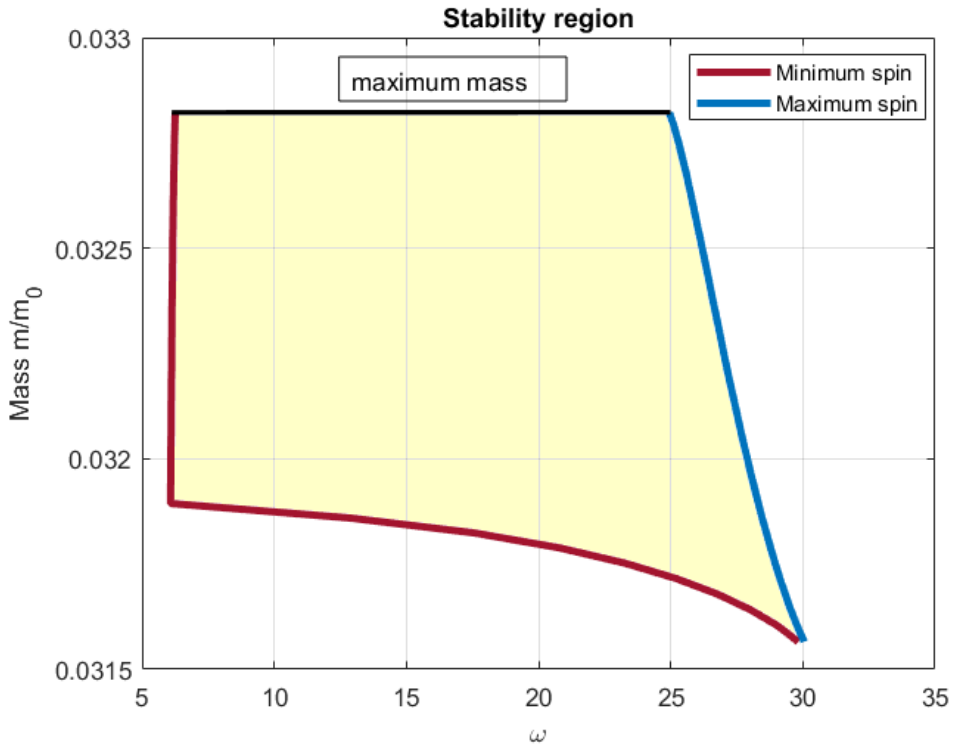

Figure 9-4: Stability region in terms of the mass and rotational speed.

Therefore, figure 9-4 provides the mass tolerance of the toy

$$\frac{\Delta m}{m} = 100\frac{m_{max} - m_{min}}{m_{max}} \simeq 3.8\ \%$$

Following Gov et al. [6], experimentally the tolerance is only about 1%. Note, however, that the lower mass region is difficult to access.

Two numerical examples are given to clarify all the ideas presented:

Example 9.7.1 *Evolution of the natural frequencies for a centered value of z_e in the stability region: $z_e = 3.1$*

The centered value $z_e = 3.1$ (that equals to a dimensional height of 7.75 cm) corresponds with

$$\beta = 30.9078$$

For this z_e, the range of ω that provides linear stability is given by

$$\omega_{min} = 6.13 \equiv 1159\ rpm$$
$$\omega_{max} = 26.67 \equiv 5045\ rpm$$

The evolution of the four natural frequencies of the system for that height of levitation as a function of ω (with ω moving in the previous range) is depicted in the following Campbell diagram:

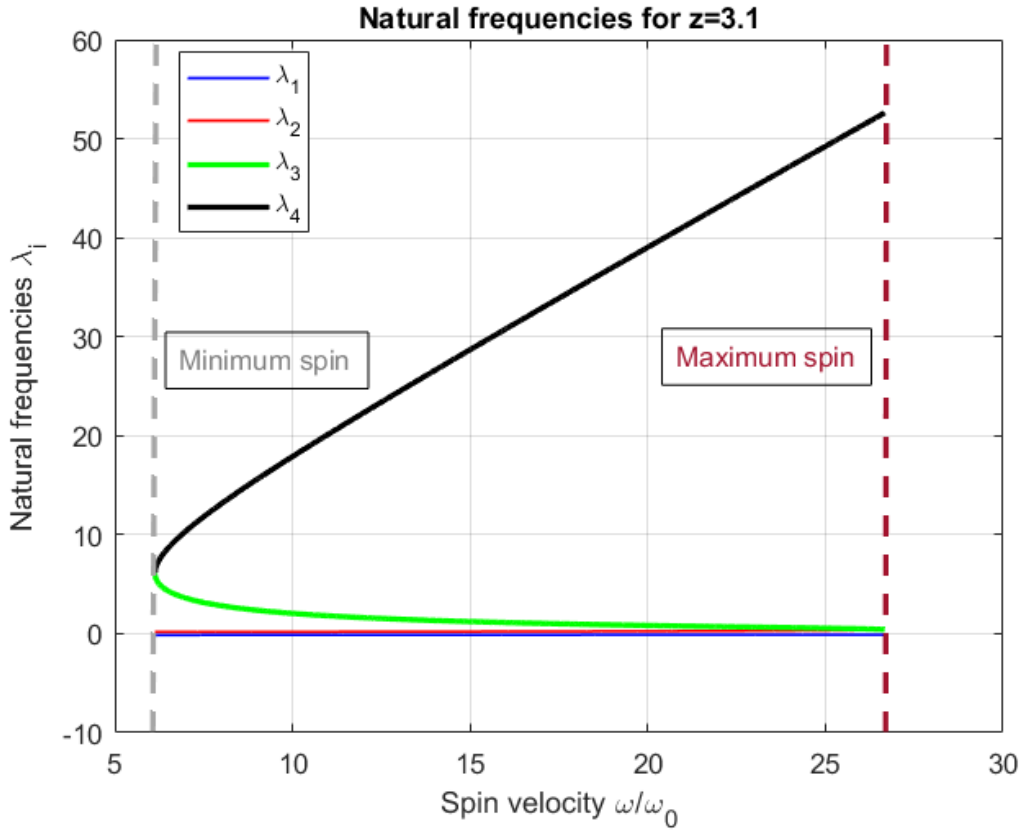

Figure 9-5: Campbell diagram for $z_e = 3.1$

We can compute these natural frequencies for a particular value of ω within the stable range. Therefore, for $\omega = 20$ (for which we are situated in the middle of the stability region)

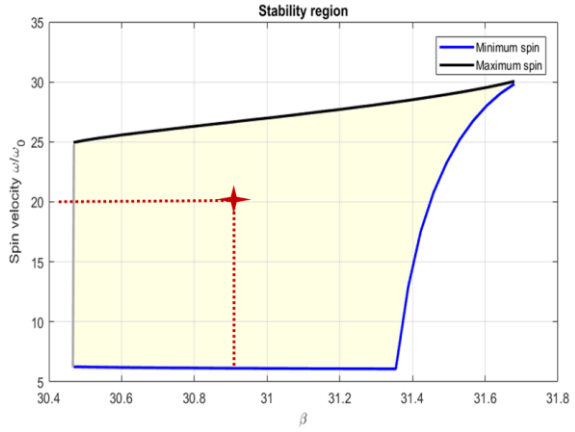

Figure 9-6: Centered point in the stability region.

the natural frequencies λ_i are

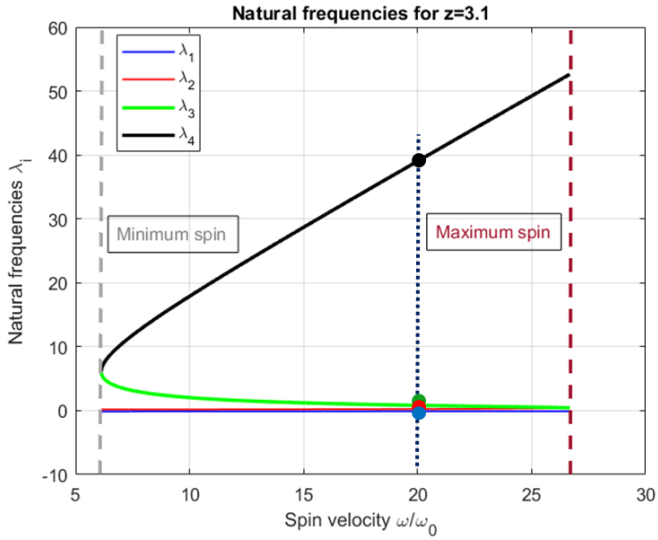

Figure 9-7: Natural frequencies for a centered value in the stability region.

$$\lambda_1 = -0.1122$$
$$\lambda_2 = 0.2481$$
$$\lambda_3 = 0.8294$$
$$\lambda_4 = 39.0347$$

Note that the natural frequency λ_1 corresponds with the slowest and retrograde mode (because of the minus sign).

Example 9.7.2 *Evolution of the natural frequencies for a noncentered value of* z_e *in the stability region:*

$$z_e = 3.19$$

The noncentered value $z_e = 3.19$ (that equals to a dimensional height of 7.98 cm) corresponds with

$$\beta = 31.4581$$

For this z_e, the range of ω that provides linear stability is given by

$$\omega_{min} = 20.80 \equiv 3935\ rpm$$
$$\omega_{max} = 28.78 \equiv 5444\ rpm$$

The evolution of the four natural frequencies of the system for that height of levitation as a function of ω (with ω moving in the previous range) is given in the following Campbell diagram:

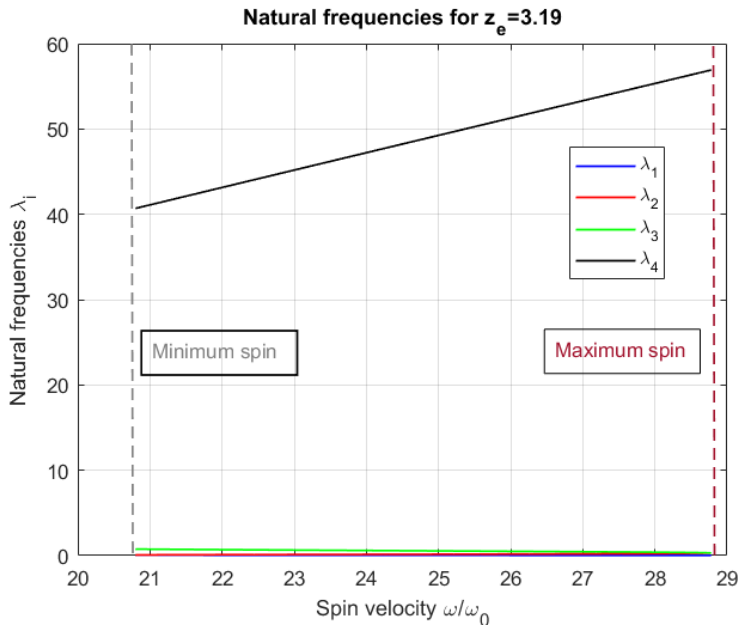

Figure 9-8: Diagram Campbell for $z_e = 3.19$.

As λ_4 (the natural frequency corresponding with the fast mode) is much larger than the others, we show the evolution of $\lambda_1, \lambda_2, \lambda_3$ separately from the previous one.

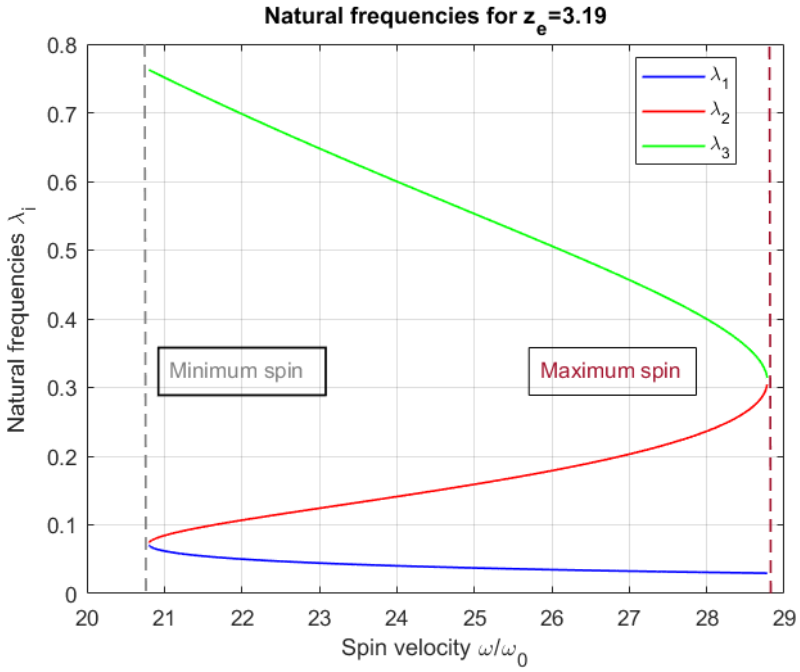

Figure 9-9: Evolution of λ_1, λ_2 and λ_3 for $z_e = 3.19$

Computing these natural frequencies for $\omega = 24.79$ (in the middle of ω_{min} and ω_{max}), we are situated in

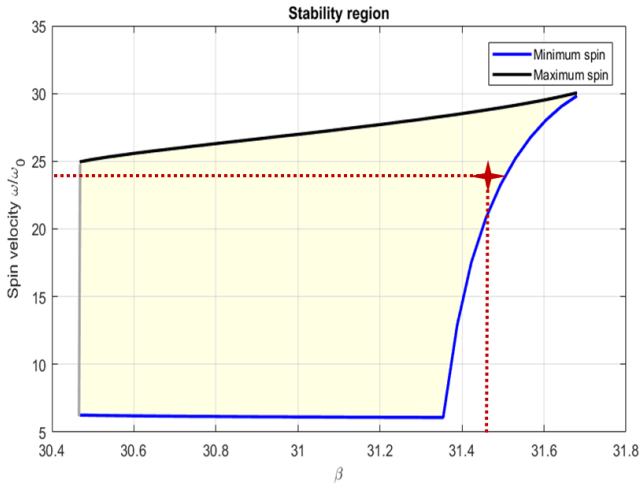

Figure 9-10: Noncentered point in the stability region.

and the natural frequencies are

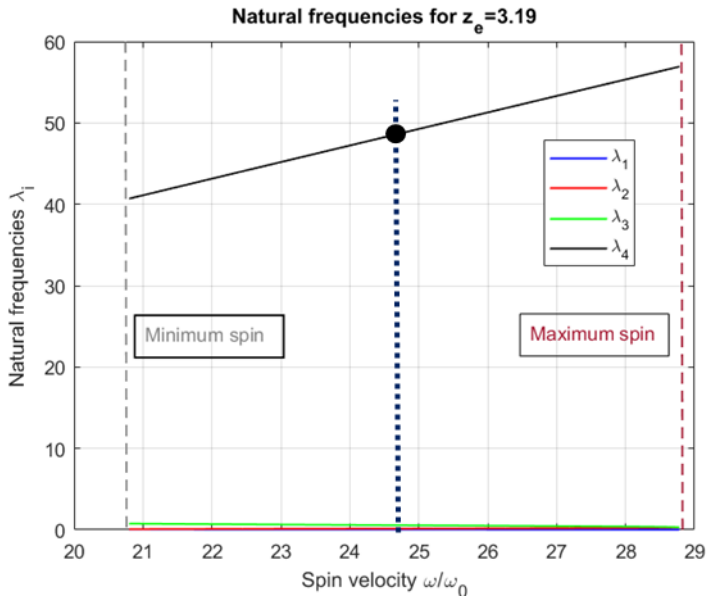

Figure 9-11: Natural frequencies for a noncentered point in the stability region.

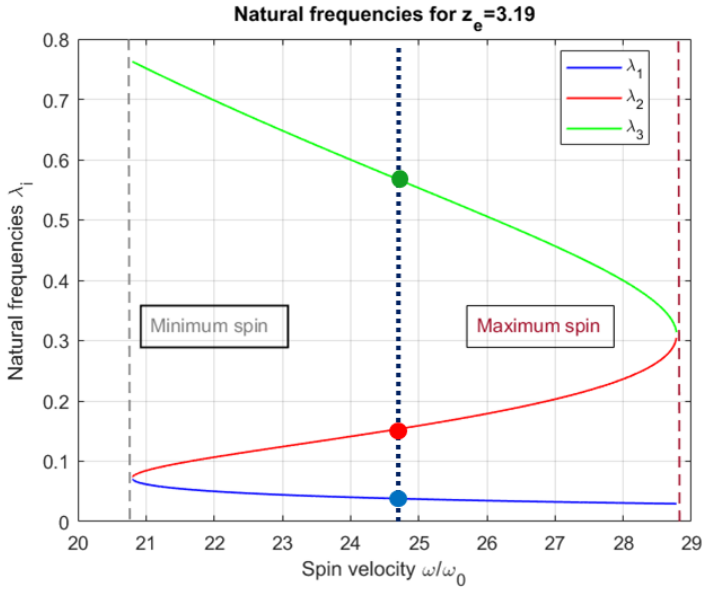

Figure 9-12: Natural frequencies for a noncentered point in the stability region.

$$\lambda_1 = 0.0444$$
$$\lambda_2 = 0.1242$$
$$\lambda_3 = 0.6481$$
$$\lambda_4 = 45.1834$$

9.8. Analysis of the normal modes

As we said in 9.2, solving the characteristic equation

$$|\boldsymbol{L} - \lambda \boldsymbol{I}| = 0, \text{ where L is the 10x10 linear matrix}$$

in the stability region previously bounded, we obtain 5 pairs of conjugate imaginary frequencies. Moreover, each of the frequencies λ_i have its corresponding eigenvector $\vec{\varphi}_i$, and these eigenvectors correspond with the normal modes.

Nevertheless, as we have complex eigenvectors, an immediate identification with real motions is not possible. Taking into account the linearity of the equations, we can combine the corresponding $+\lambda$ and $-\lambda$ solutions so that we still get oscillating solutions with the same frequencies. In practice, this is the same as analyzing real and imaginary parts separately and study their associated motions. These ideas are clarified in the following example:

Example 9.8.2 *Identification of the motions given two complex conjugate eigenvectors*

We can numerically compute the eigenvalues and eigenvectors of matrix L. To continue with example 9.7.1, that corresponds with a centered value of the stability region, we choose

$$z_e = 3.1 \equiv 7.75 \text{ cm}$$

$$\omega = 20 \equiv 3783 \text{ rpm}$$

and particularize matrix L for this values.

The identification of the motions is going to be explained considering two of the ten complex cojugate eigenvectors.

Naming them $\hat{\varphi}_1$and $\hat{\varphi}_2$, we have

$$\hat{\varphi}_1 = \begin{pmatrix} 0 \\ -0.0001 \\ 0 \\ 0.3545 \\ 0 \\ 0.0045 \\ 0 \\ 0 \\ 0 \\ 0.8649 \end{pmatrix} + j \begin{pmatrix} -0.0001 \\ 0 \\ 0 \\ 0 \\ -0.3545 \\ 0 \\ -0.0045 \\ 0 \\ -0.0214 \\ 0 \end{pmatrix} \qquad \hat{\varphi}_2 = \begin{pmatrix} 0 \\ -0.0001 \\ 0 \\ 0.3545 \\ 0 \\ 0.0045 \\ 0 \\ 0 \\ 0 \\ 0.8649 \end{pmatrix} + j \begin{pmatrix} 0.0001 \\ 0 \\ 0 \\ 0 \\ 0.3545 \\ 0 \\ 0.0045 \\ 0 \\ 0.0214 \\ 0 \end{pmatrix}$$

As it was said before, we take the real and imaginary parts separately of one of the complex eigenvectors and study their associate motions. Therefore, taking into accout that the components of the real or imaginary parts correspond with

$$\vec{\varphi}_i = \begin{pmatrix} x_0 \\ y_0 \\ z_0 \\ \phi_0 \\ \theta_0 \\ v_{x0} \\ v_{y0} \\ v_{z0} \\ \omega_{X0} \\ \omega_{Y0} \end{pmatrix}$$

we consider $\hat{\varphi}_1$ (it would be the same for $\hat{\varphi}_2$). Its real part provides

$$y_0 = -0.0001 \text{ and } v_{x0} = 0.0045$$

so we start in the negative part of the Y-axis (as we have $y_0 < 0$) with a positive velocity in the X-direction (as $v_{x0} > 0$). Therefore, the trajectory corresponds with a counterclockwise circumference (see figure 9-13, left).

Similarly, the imaginary part provides

$$x_0 = -0.0001 \text{ and } v_{y0} = -0.0045$$

and we start in the negative part of the X-axis with a negative velocity in the Y-direction (figure 9-13, right). Note that, as in the case mentioned above, we have a counterclockwise circumference and the interpretation of the real and imaginary parts results in the same trajectory.

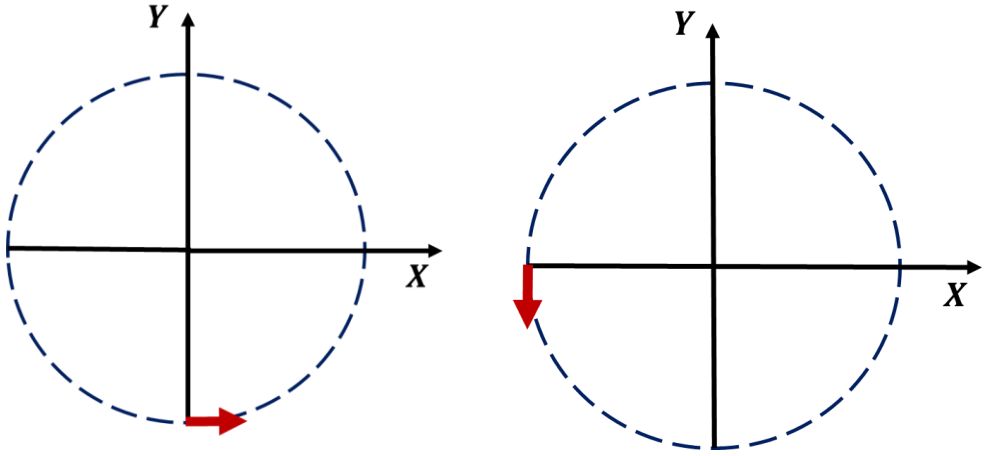

Figure 9-13: Identification of the motions using real and imaginary parts

Therefore, the five independent normal modes of the Hamiltonian system for

$$z_e = 3.1 \equiv 7.75 \text{ cm}$$

$$\omega = 20 \equiv 3783 \text{ rpm}$$

scaled to $\theta_0 = 1° = \frac{\pi}{180}$ rad, are

$$\vec{\varphi}_1 = \begin{pmatrix} 0.0920 \\ 0 \\ 0 \\ 0 \\ 0.0175 \\ 0 \\ -0.0103 \\ 0 \\ 0.0438 \\ 0 \end{pmatrix} \quad \vec{\varphi}_2 = \begin{pmatrix} 0.0607 \\ 0 \\ 0 \\ 0 \\ 0.0175 \\ 0 \\ 0.0151 \\ 0 \\ 0.0434 \\ 0 \end{pmatrix} \quad \vec{\varphi}_3 = \begin{pmatrix} 0.0113 \\ 0 \\ 0 \\ 0 \\ 0.0175 \\ 0 \\ 0.0094 \\ 0 \\ 0.0427 \\ 0 \end{pmatrix} \quad \vec{\varphi}_4 = \begin{pmatrix} 5.7 \cdot 10^{-6} \\ 0 \\ 0 \\ 0 \\ 0.0175 \\ 0 \\ 2.2 \cdot 10^{-4} \\ 0 \\ 0.0011 \\ 0 \end{pmatrix} \quad \vec{\varphi}_5 = \begin{pmatrix} 0 \\ 0 \\ z_0 \\ 0 \\ 0 \\ 0 \\ 0 \\ 0 \\ 0 \\ 0 \end{pmatrix}$$

where we have continued with the color pattern used to compute the evolution of the natural frequencies in examples 9.7.1 and 9.7.2. Thus, $\vec{\varphi}_1$ corresponds with the slow, retrograde mode and $\vec{\varphi}_4$ is the fast mode. Also note that $\vec{\varphi}_5$ only has as nonzero component z_0, as it corresponds with the vertical motion (remember that it is uncoupled with the horizontal and whirl motions).

Arrived to this point, we numerically solve the linear Hamiltonian system introducing the previous eigenvectors as initial conditions. Following eq. (9.18), the trajectories correspond with four circumferences:

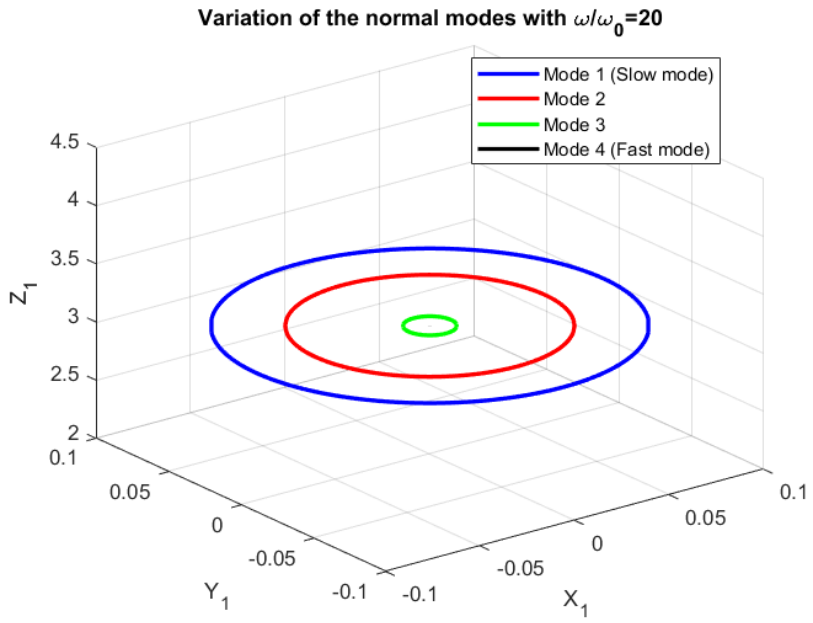

Figure 9-14: Circular trajectories of the normal modes.

The radius of these circumferences, according to the normal modes scaled to $\theta = 1°$, are

$$x_{01} = 0.0920$$

$$x_{02} = 0.0607$$

$$x_{03} = 0.0113$$

$$x_{04} = 5.7 \cdot 10^{-6}$$

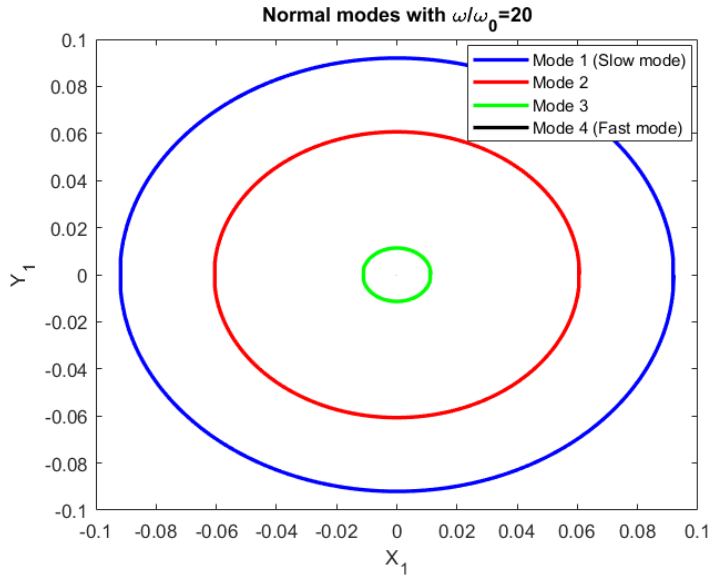

Figure 9-15: Circumferences of the four normal modes.

The smallest circumference, which corresponds with the fast mode, cannot be seen in figure 9-16 as the radius x_{04} is much smaller than the others. It can be seen in figure 9-17.

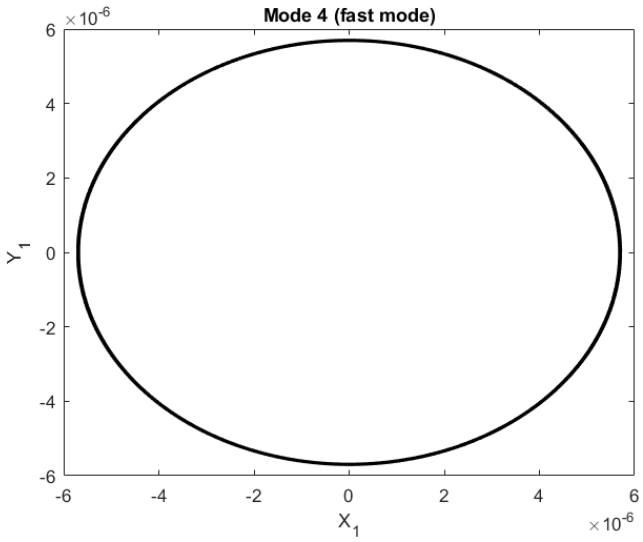

Figure 9-16: Circumference corresponding with the fast mode.

On the other hand, choosing $\vec{\varphi}_5$ as initial condition, we get vertical oscillations around the stable height of levitaton $z_e = 3.1$. Therefore, considering $z_0 = 3.05$, the oscillatory behaviour of the system around z_e can be seen in figures 9-18 and 9-19 (left). It is also shown the time evolution of the conjugate momenta $p_z(t)$.

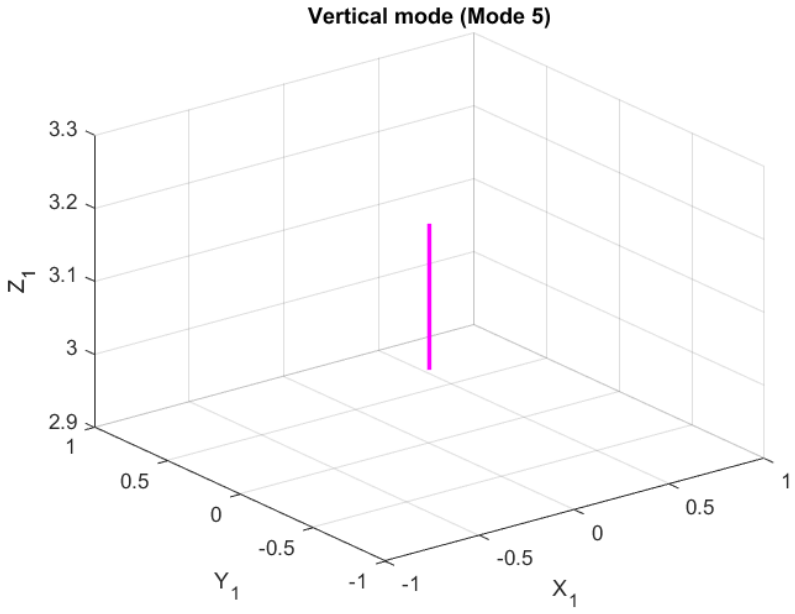

Figure 9-17: Vertical mode

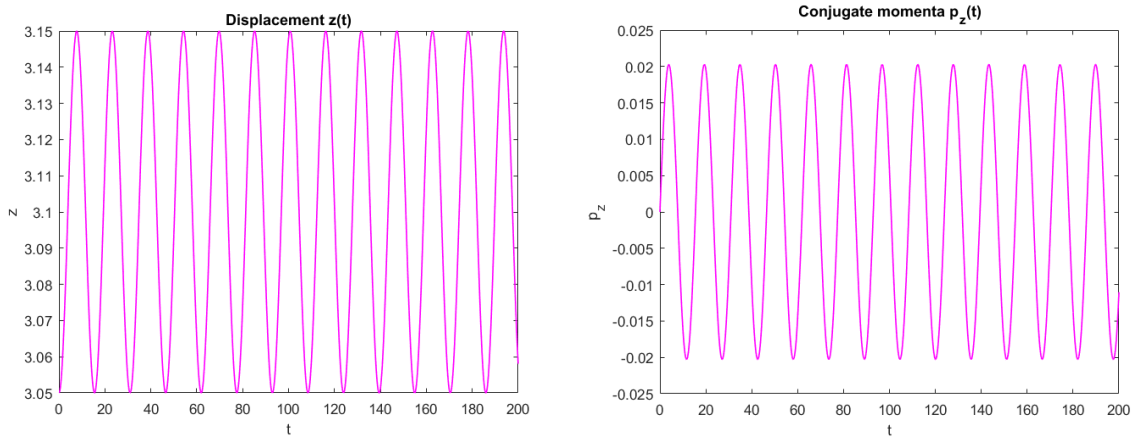

Figure 9-18: Time evolution of $z(t)$ and $p_z(t)$.

We can also verify that the combination of the vertical mode with the others has no effect on the horizontal projection of normal modes $\vec{\varphi}_1, \vec{\varphi}_2, \vec{\varphi}_3, \vec{\varphi}_4$, so that we continue having circumferences in the X_1Y_1 plane. The three-dimensional trajectories of these modes can be seen in figure 9-20.

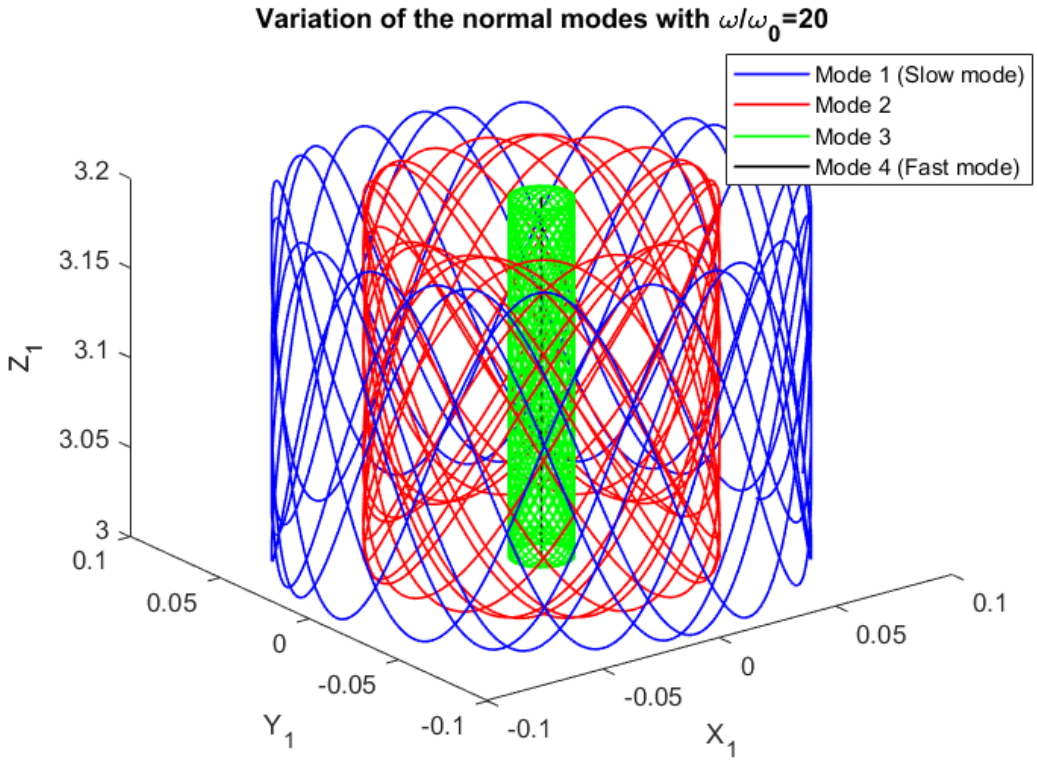

Figure 9-19: Three-dimensional trajectories of the normal modes, adding a vertical perturbation.

As we have different simple harmonic motions along the $X_1$and Z_1, the projection of the three-dimensional trajectories in the X_1Z_1 plane (it would be the same for the Y_1Z_1 plane) provides Lissajous curves, that can be seen in figure 9-21.

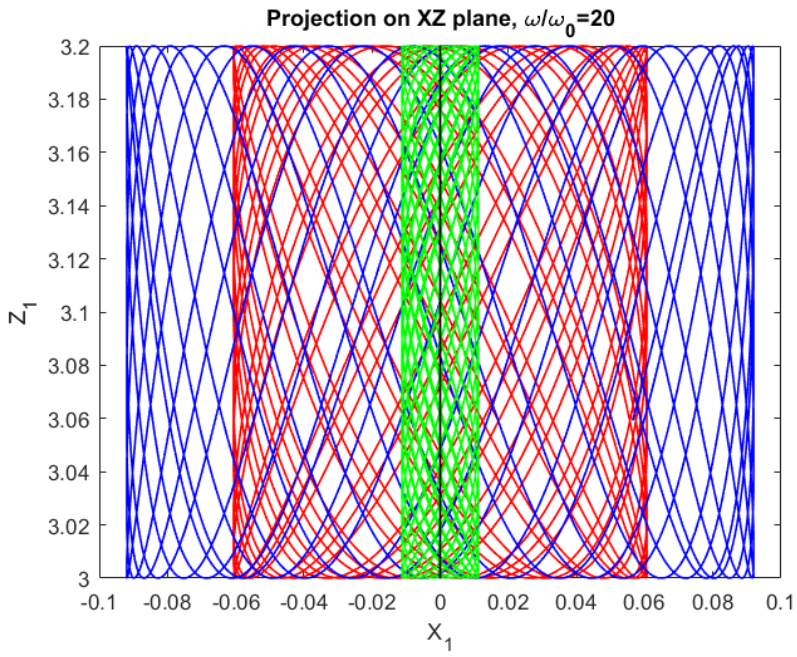

Figure 9-20: Projection of the trajectories in the X_1Z_1 plane: Lissajous curves.

In figure 9-22 we can see the time evolution of the x and y degrees of freedom and its corresponding conjugate momenta $p_x(t)$ and $p_y(t)$ for the different modes:

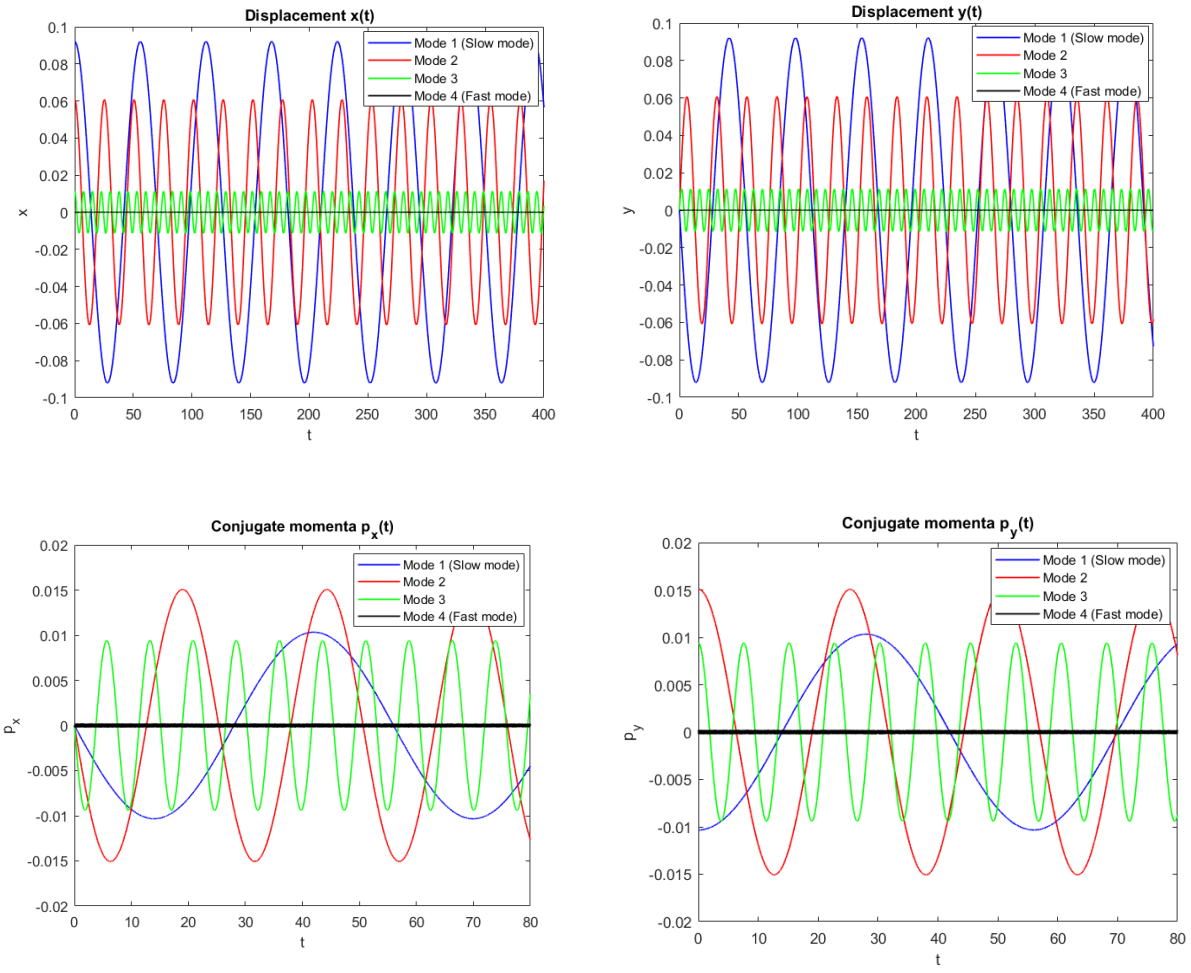

Figure 9-21: Time evolution of x, y, p_x, p_y

We also show in figure 9-23 the time evolution of the rotational degrees of freedon ϕ, θ. Note that, as we scaled the eigenvectors to $\theta_0 = 1°$, the amplitude is the same for the four modes. Fast mode is plotted separately in order to have a better visualization:

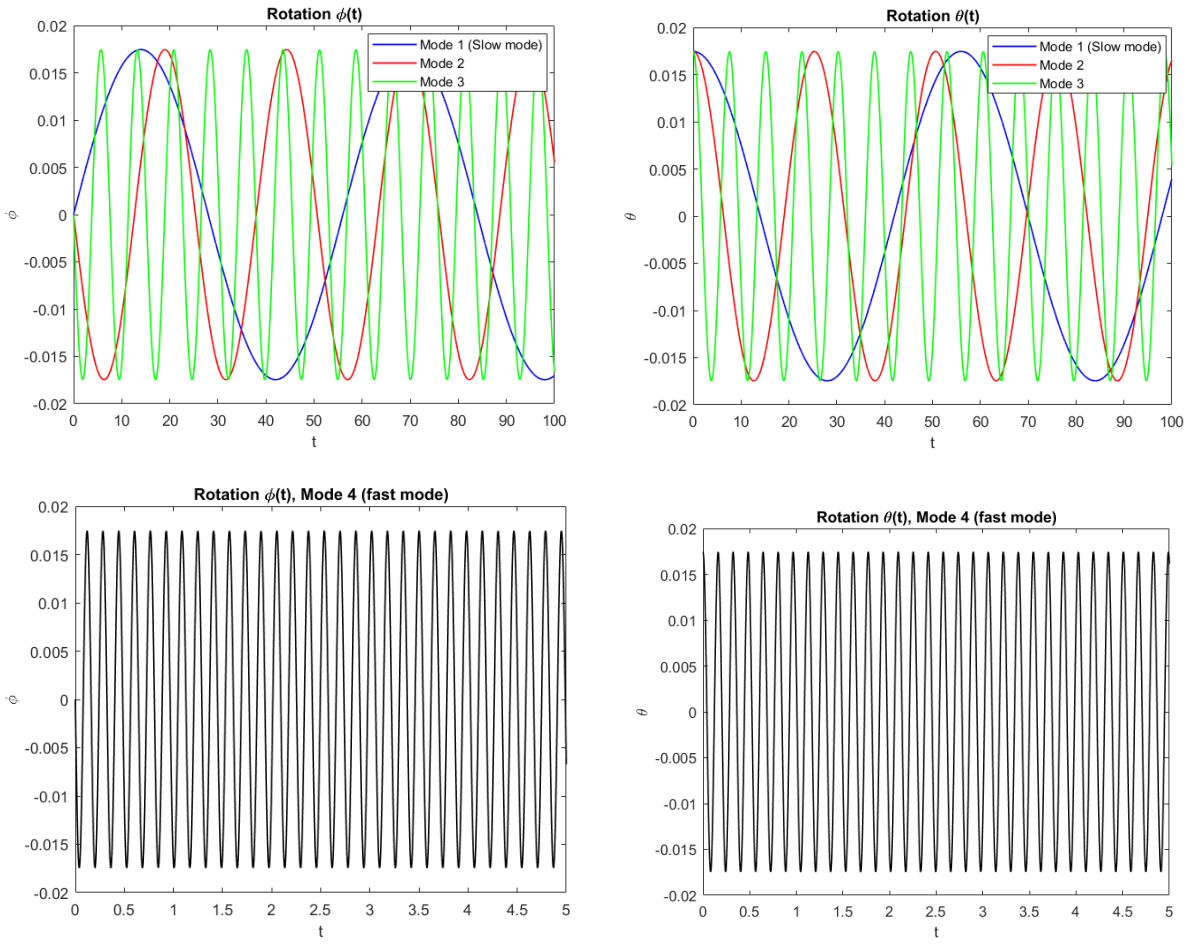

Figure 9-22: Time evolution of ϕ, θ

Ending with the analysis of the normal modes, we show in figure 9-24 the evolution of the radius of the circular paths as a function of the rotational speed for $z_e = 3.1$. Note that the circumference of the fast mode is much smaller than the others in all the range and the radius corresponding with Modes 2 and 3 tend to the same value for larger rotational speeds. Finally, the radius of the slow, retrograde mode grows in all the range.

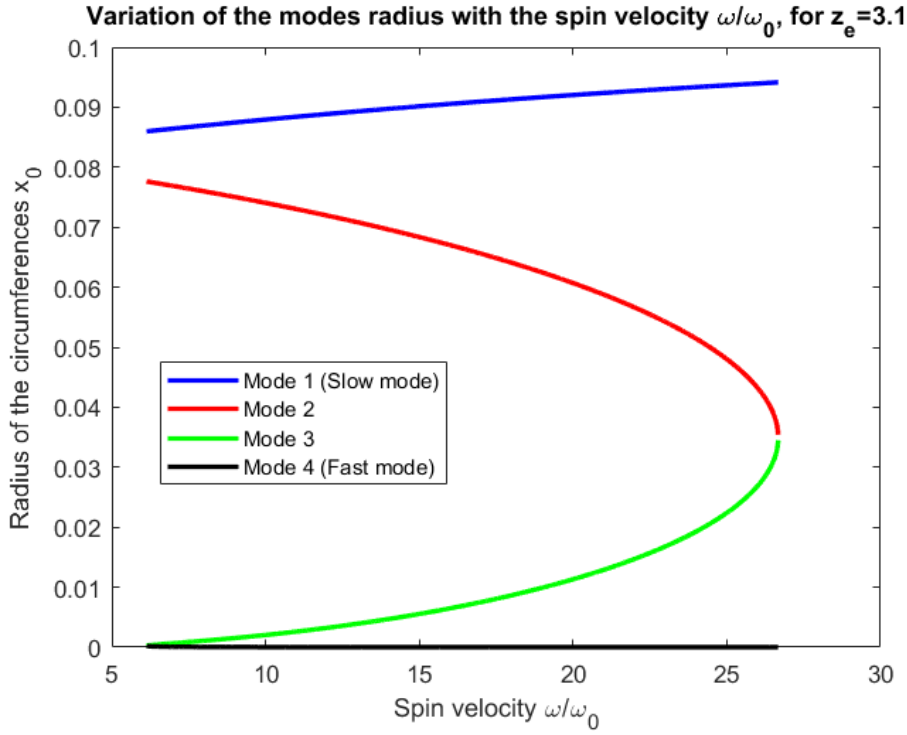

Figure 9-23: Variation of the normal modes radius with the spin velocity

9.9. Behaviour of the system in interesting situations

In this section, two interesting situations are going to be studied. We also validate the rotational speed range that provides stable hovering for $z_e = 3.1$, that was given in example 9.7.1.

For that, we are going to numerically simulate the linear system with different initial conditions and plot the trajectory of the top.

9.9.1. Trajectory of the top considering a horizontal perturbation

As we are not interested in the vertical motion, we make $z_0 = z_e = 3.1$, so that the trajectory is contained in the X_1Y_1 plane. The initial condition is given by $\boldsymbol{q_0}$ and figure 9-25 shows the initial position of the top.

$$\boldsymbol{q_0} = \begin{pmatrix} x_0 \\ y_0 \\ z_0 \\ \phi_0 \\ \theta_0 \\ p_{x0} \\ p_{y0} \\ p_{z0} \\ p_{\phi 0} \\ p_{\theta 0} \end{pmatrix} = \begin{pmatrix} 0 \\ 0.02 \\ 3.1 \\ 0 \\ 0 \\ 0 \\ 0 \\ 0 \\ 0 \\ 0 \end{pmatrix}$$

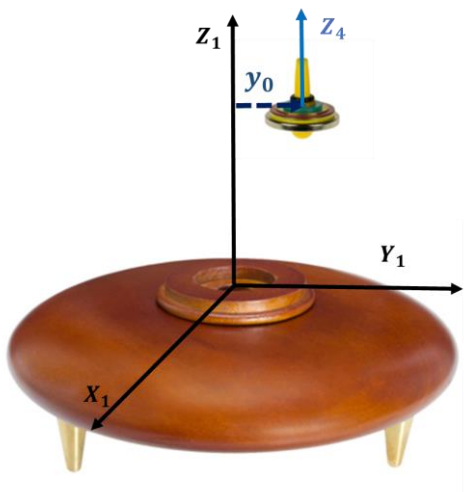

Figure 9-24: Horizontal perturbation of the top.

In figure 9-26 we can see the trajectories of the spinning top for three different values of rotational speed within the range of 9.7.1:

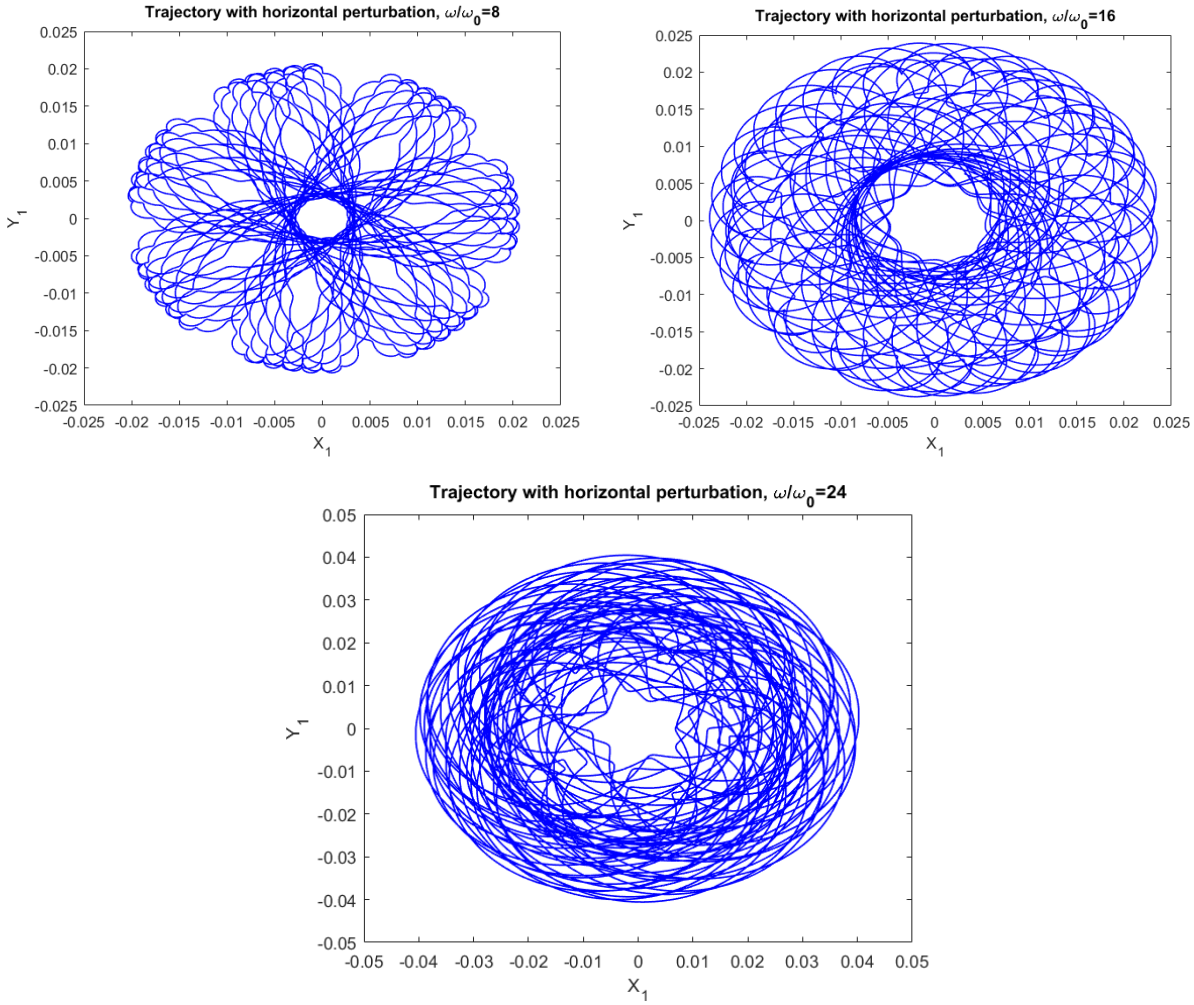

Figure 9-25: Trajectories of the linear system for horizontal perturbations

9.9.2. Trajectory of the top considering a pitch perturbation

We next consider a pitch perturbation. This corresponds with the initial condition $\boldsymbol{q_0}$ and figure 9-27.

$$q_0 = \begin{pmatrix} x_0 \\ y_0 \\ z_0 \\ \phi_0 \\ \theta_0 \\ p_{x0} \\ p_{y0} \\ p_{z0} \\ p_{\phi 0} \\ p_{\theta 0} \end{pmatrix} = \begin{pmatrix} 0 \\ 0 \\ 3.1 \\ 0 \\ 0.035 \\ 0 \\ 0 \\ 0 \\ 0 \\ 0 \end{pmatrix}$$

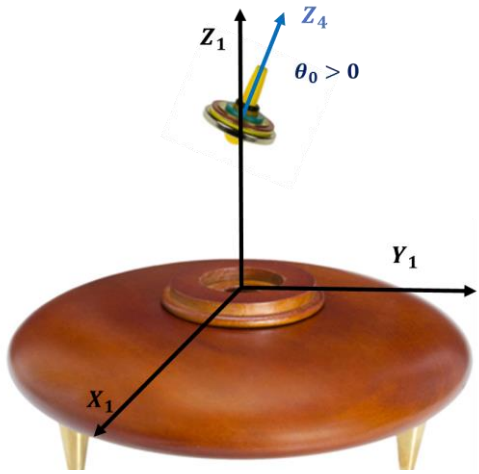

Figure 9-26: Pitch perturbation of the top

The trajectory is shown in figure 9-28. We note that, despite the top starts in the OZ_1 axis, the perturbation in θ_0 causes small displacements, moving the top away from the origin (remember that, in the linear system, translational and whirl motions continue being coupled).

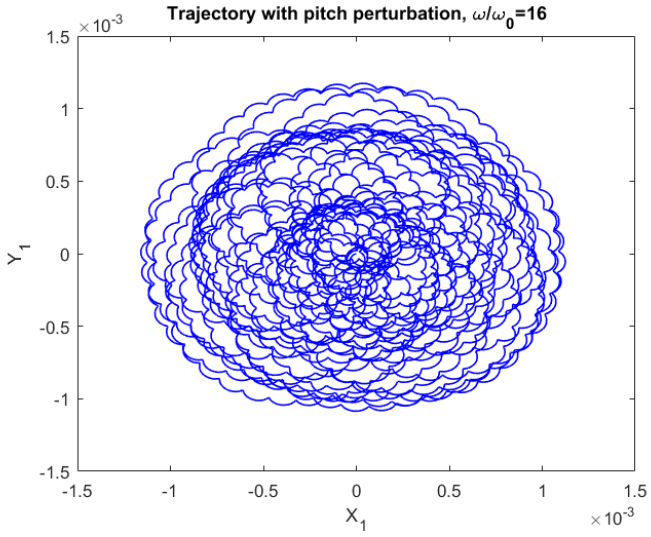

Figure 9-27: Trajectory of the linear system with pitch perturbation

It should be mentioned that the representation of the horizontal and pitch perturbations shown in figures 9-25 and 9-27 has been exagerated in order to provide a better understanding.

In the real toy, these two situations can be matched with the influence of weak air streams or a bad use of the starter, placing it off-centered or not vertically in the lifter plate.

9.9.3. Validation of the rotational speed range

For $z_e = 3.1$, we saw that

$$\omega_{min} = 6.13 \equiv 1159\, rpm$$
$$\omega_{max} = 26.67 \equiv 5045\, rpm$$

are the lower and upper rotational speed bounds in order to have stability. Considering a more general initial condition $\boldsymbol{q_0}$, adding vertical, horizontal and rotational perturbations and also nonzero initial values of the conjugate momenta, we are going to check this range, showing the shape of the trajectories for different values of ω.

$$\boldsymbol{q_0} = \begin{pmatrix} x_0 \\ y_0 \\ z_0 \\ \phi_0 \\ \theta_0 \\ p_{x0} \\ p_{y0} \\ p_{z0} \\ p_{\phi 0} \\ p_{\theta 0} \end{pmatrix} = \begin{pmatrix} 0.02 \\ 0 \\ 3 \\ 0.01 \\ 0.02 \\ -0.01 \\ 0.04 \\ 0.01 \\ 0.03 \\ -0.01 \end{pmatrix}$$

In figure 9-29, the trajectories for a rotational speed under ω_{min} and for this limit are shown. In the first situation, stable levitation is not possible and the top moves away from the OZ_1 axis, whereas for $\omega = \omega_{min}$ we see that hovering becomes stable.

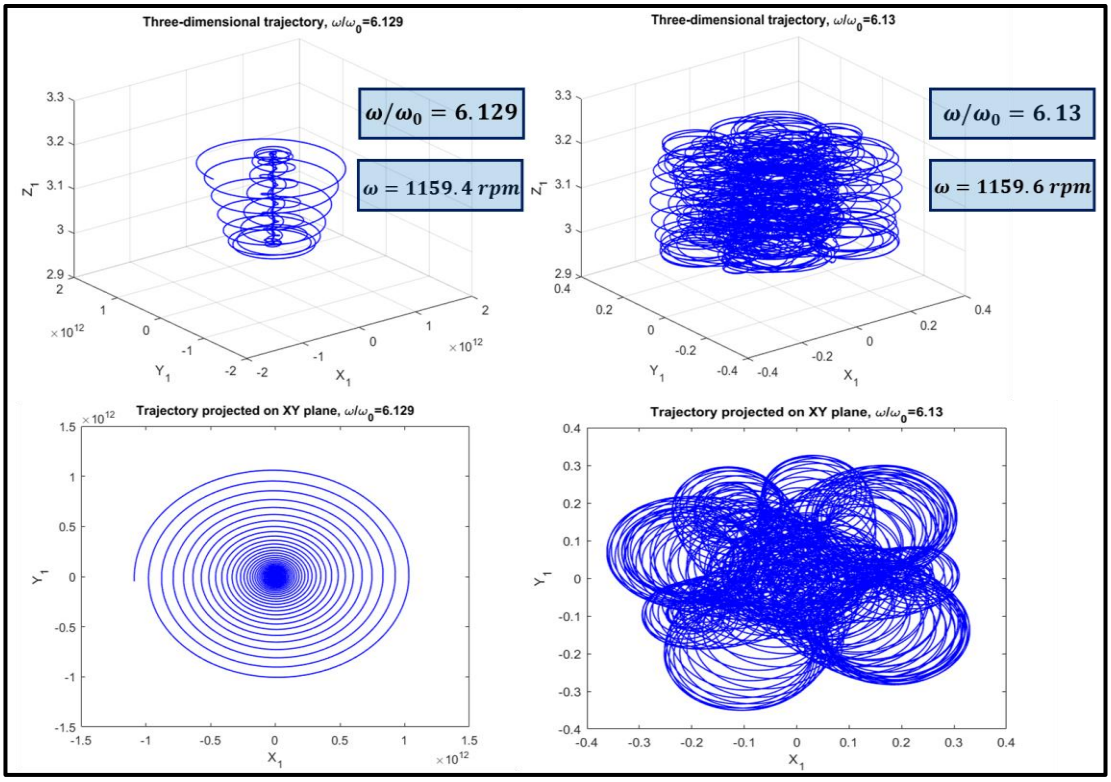

Figure 9-28: Trajectories for $\omega < \omega_{min}$ and $\omega = \omega_{min}$

In figures 9-30 and 9-31, we show the stable trajectories for values of ω within the stability range:

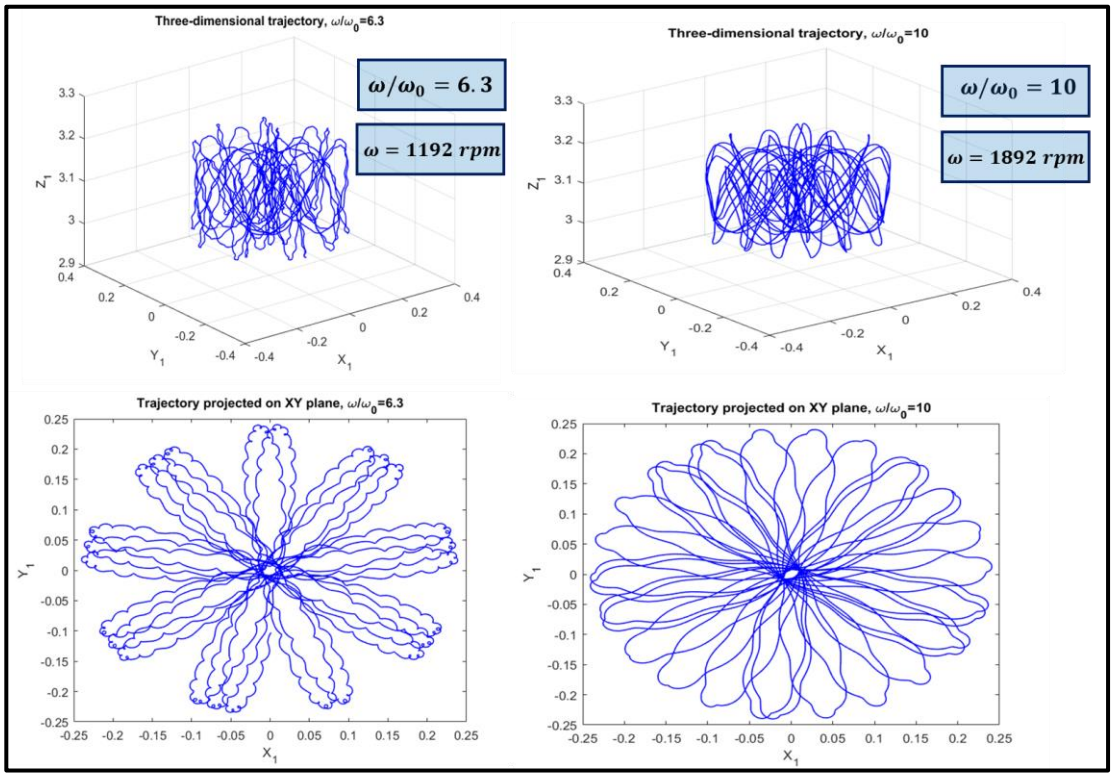

Figure 9-29: Trajectories within the stable rotational speed range

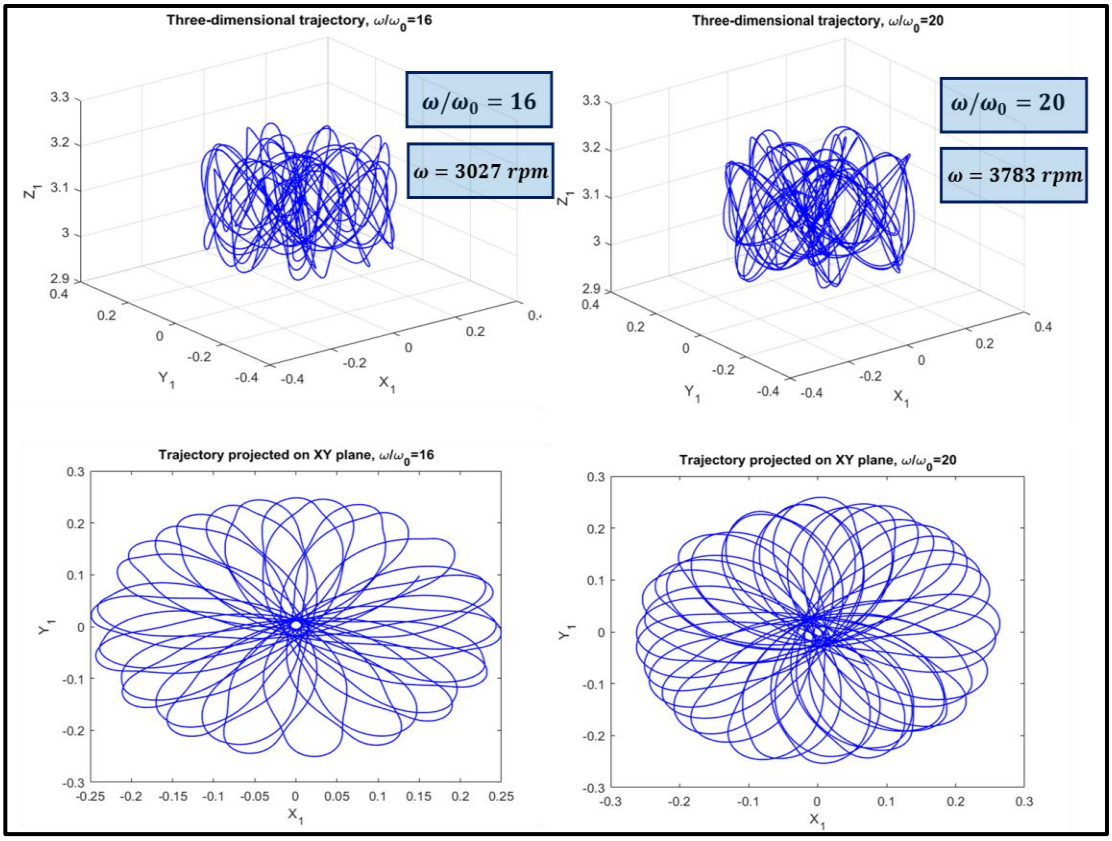

Figure 9-30: Trajectories within the stable rotational speed range

Finally, in figure 9-32 we arrive to the upper bound ω_{max}. In the first situation, which corresponds with this limit, we still have a stable motion, but for larger rotational speed we see that hovering is not possible.

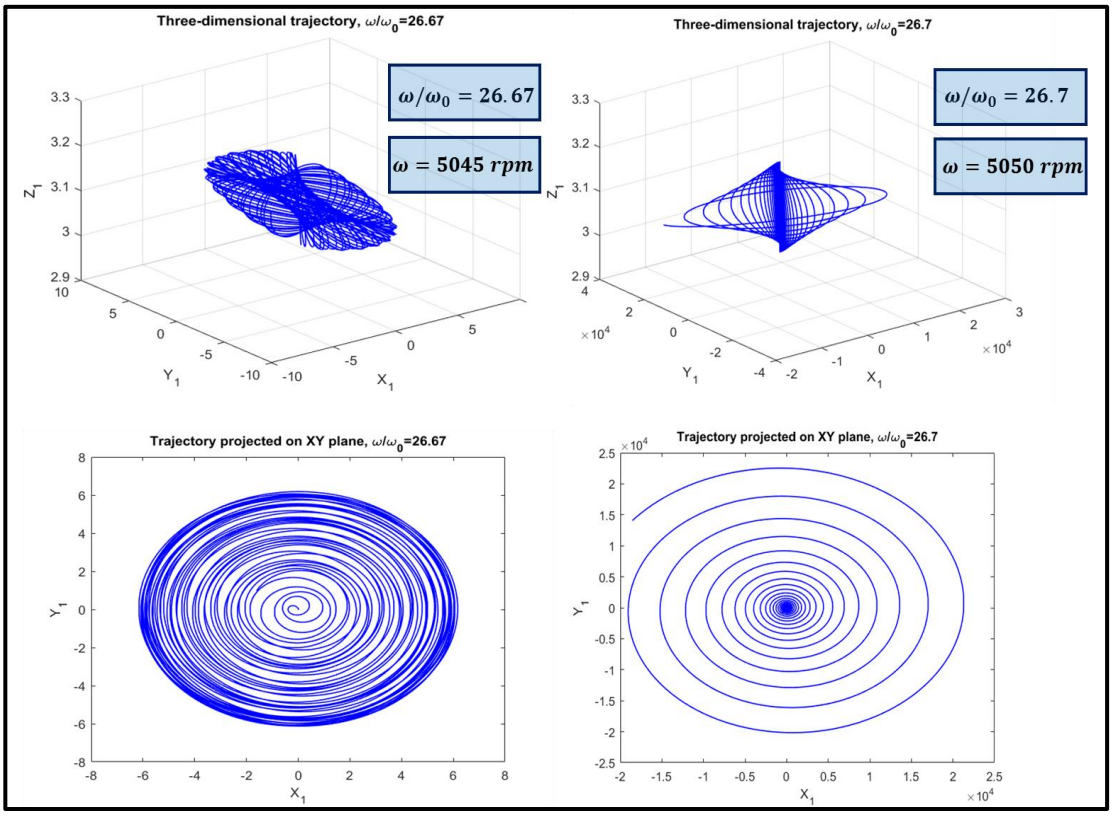

Figure 9-31: Trajectories for $\omega = \omega_{max}$ and $\omega > \omega_{max}$

10 STUDY OF THE NONLINEAR SYSTEM

At chapter 9.8, we gave the expression of the five independent normal modes. The analytical and numerical study showed that these modes correspond with circular orbits.

In this chapter, we numerically solve the nonlinear system with initial conditions proportional to these eigenvectors and study the structural stability of the system.

In this way, we are going to start with the study of the linear coupling, continue with the nonlinear coupling and finally see the behavior of the system in interesting situations.

10.1. Study of the linear coupling

To study the linear coupling, we numerically solve the nonlinear system choosing as initial condition the expression for the normal modes given in chapter 9.8 and see if the expected circular orbits take place.

In figure 10-1 we can see that these circular orbits are well reproduced. In particular, the smaller the circumference is, the better the circumference is replayed.

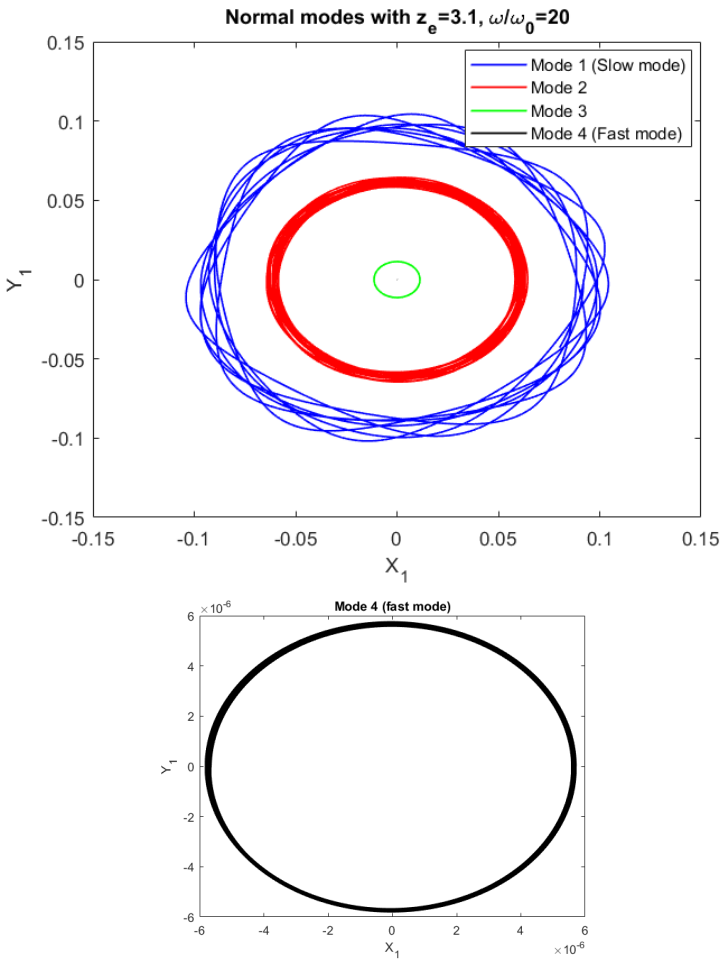

Figure 10-1: Circumferences in the nonlinear system.

As happened in 9.8, the circumference corresponding with the fast mode cannot be seen with the others, so we plot it separetly.

We also show the time evolution of the x and y degrees of freedom for the different modes. In figure 10-2 we can see the oscillations of these modes, obtaining similar results as those of figure 9-22.

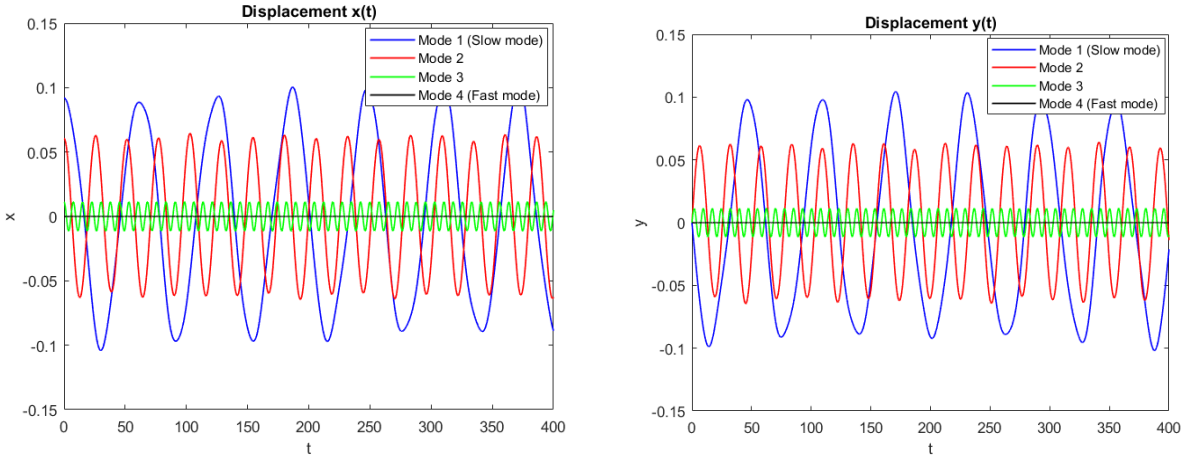

Figure 10-2: Linear coupling: time evoluton of x, y.

10.2. Study of the nonlinear coupling

After the study of the linear coupling, we can verify if the qualitative behavior of the trajectories is unaffected by small perturbations, in order to verify its structural stability. Therefore, we are going to raise the amplitudes of the previous initial conditions and see when the circular orbits stop being reproduced. As we scaled the normal modes making $\theta_0 = 1°$, this is equivalent to find the maximum pitch angle $\varepsilon_i \theta_0 = \varepsilon_i°$ for which we still have circumferences. For these values ε_i, the linear approximation $\sin(\theta) \simeq \theta$ is not true, as the other terms of the Taylor expansion become important.

We therefore obtain, for the different modes

$$\varepsilon_1 = 2.6°$$
$$\varepsilon_2 = 1.9°$$
$$\varepsilon_3 = 9.4°$$
$$\varepsilon_4 = 5°$$

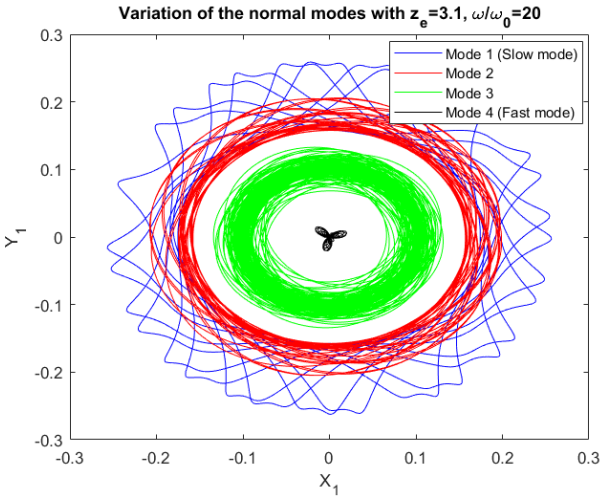

Figure 10-3: Nonlinear coupling

10.3. Behaviour of the system in interesting situations

10.3.1. Base not levelled with gravity

When one plays with the device, in all likelihood the spinning top will fly off to a side at some time. If this happens multiple times, it means that the base is not leveled with gravity.

Thus, one of the things that we can study is the maximum percentaje of misalignment between the base and gravity that allows stable hovering. It can be done adding a constant ε in the equations of motion for eather x or y degrees of freedom and testing different values in order to find the maximum

$$\dot{p_x^*} = -\beta\left(-\frac{1}{2}\frac{dB_0^*}{dz}\sin(\theta^*) - \frac{x^*}{2}\frac{d^2B_0^*}{dz^2}\cos(\phi^*)\cos(\theta^*)\right) + \varepsilon \tag{10.1}$$

$$\dot{p_y^*} = -\beta\left(\frac{1}{2}\frac{dB_0^*}{dz}\sin(\phi^*)\cos(\theta^*) - \frac{y^*}{2}\frac{d^2B_0^*}{dz^2}\cos(\phi^*)\cos(\theta^*)\right) \tag{10.2}$$

The numerical simulations provide a maximum $\varepsilon = 0.0018$. This corresponds with a percentage of misalignment of 0.18 % , which is equivalent to an inclination along this axis of 0.12 °. Therefore, we have numerically verified the great importance of having a levelled base, as it is usually the first problem that one faces with when plays with the toy.

10.3.2. Trajectory of the top considering a horizontal perturbation

In the study of the linear system, we obtained the trajectories simulating the influence of weak air streams or a bad use of the starter, placing it off-centered in the lifter plate, by means of a horizontal perturbatioin. The same can be done with the nonlinear system.

The initial condition is given by $\boldsymbol{q_0}$ and figure 10-4 shows the initial position of the top.

$$\boldsymbol{q_0} = \begin{pmatrix} x_0 \\ y_0 \\ z_0 \\ \phi_0 \\ \theta_0 \\ p_{x0} \\ p_{y0} \\ p_{z0} \\ p_{\phi 0} \\ p_{\theta 0} \end{pmatrix} = \begin{pmatrix} 0 \\ 0.02 \\ 3.1 \\ 0 \\ 0 \\ 0 \\ 0 \\ 0 \\ 0 \\ 0 \end{pmatrix}$$

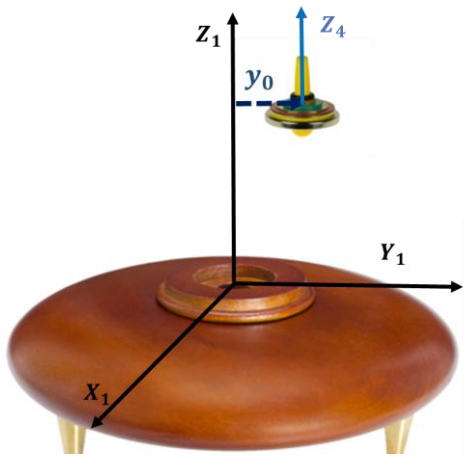

Figure 10-4: Horizontal perturbation.

The results, for two different rotational speeds, are shown in figure 10-5. The trajectories are similar to those obtained for the linear system (figure 9-26).

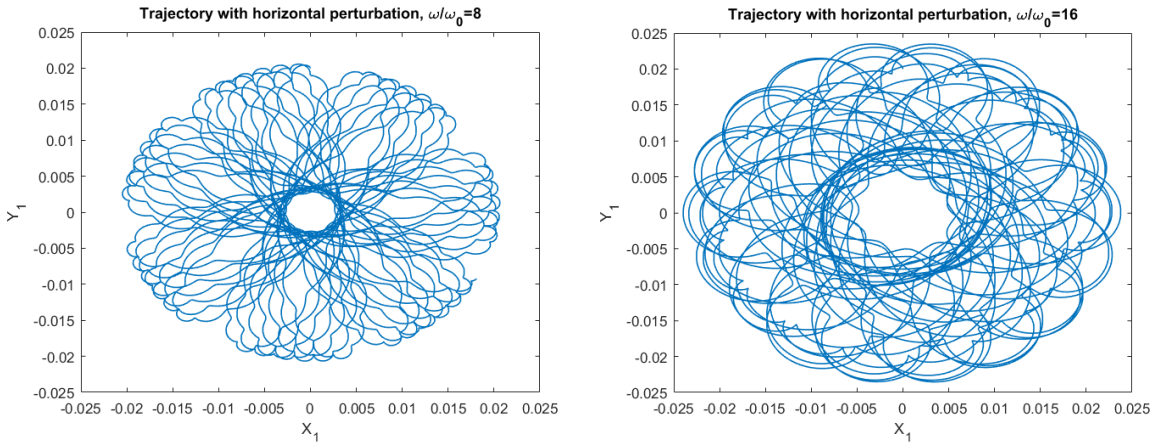

Figure 10-5: Trajectories of the nonlinear system with horizontal perturbation.

10.3.3. Trajectory of the top considering a pitch perturbation

We can also see how the nonlinear system responds to a pitch perturbation. Considering the initial condition given by $\boldsymbol{q_0}$, the trajectory can be seen in figure 10-7.

$$q_0 = \begin{pmatrix} x_0 \\ y_0 \\ z_0 \\ \phi_0 \\ \theta_0 \\ p_{x0} \\ p_{y0} \\ p_{z0} \\ p_{\phi 0} \\ p_{\theta 0} \end{pmatrix} = \begin{pmatrix} 0 \\ 0 \\ 3.1 \\ 0 \\ 0.035 \\ 0 \\ 0 \\ 0 \\ 0 \\ 0 \end{pmatrix}$$

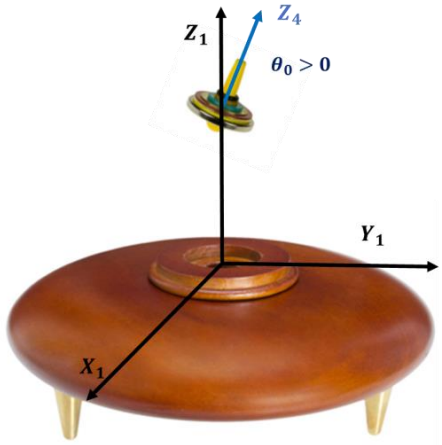

Figure 10-6: Pitch perturbation

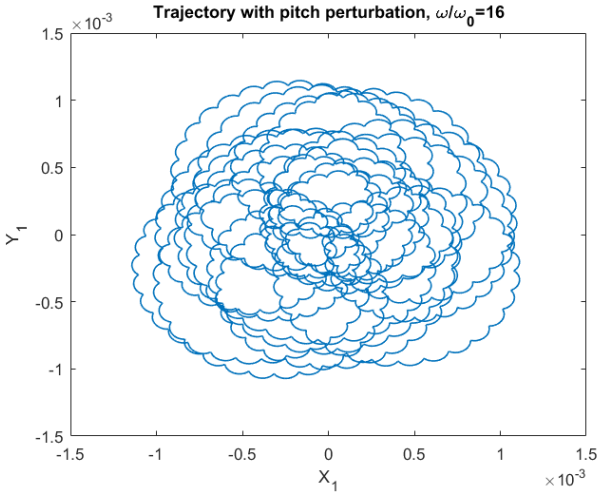

Figure 10-7: Trajectory of the nonlinear system with pitch perturbation

As happened in 9.9.2, we can see that θ_0 causes small displacements, moving the top away from the origin.

10.3.4. Influence of the initial height in the trajectory

Another aspect that can be analyzed is how the trajectories change depending on the initial condition z_0. In the nonlinear model, vertical motion is coupled with horizontal and whirl motion, so that different values of z_0 provide different trajectories. The change of z_0 corresponds in the real toy with placing the lifter plate at different heights.

We consider again an equilibrium height $z_e = 3 \equiv 7.75\ cm$.

In figure 10-8, we can see that values of $z_0 = 3$ and $z_0 = 3.02$ provide a flower-shape trajectory in the X_1Y_1 plane.

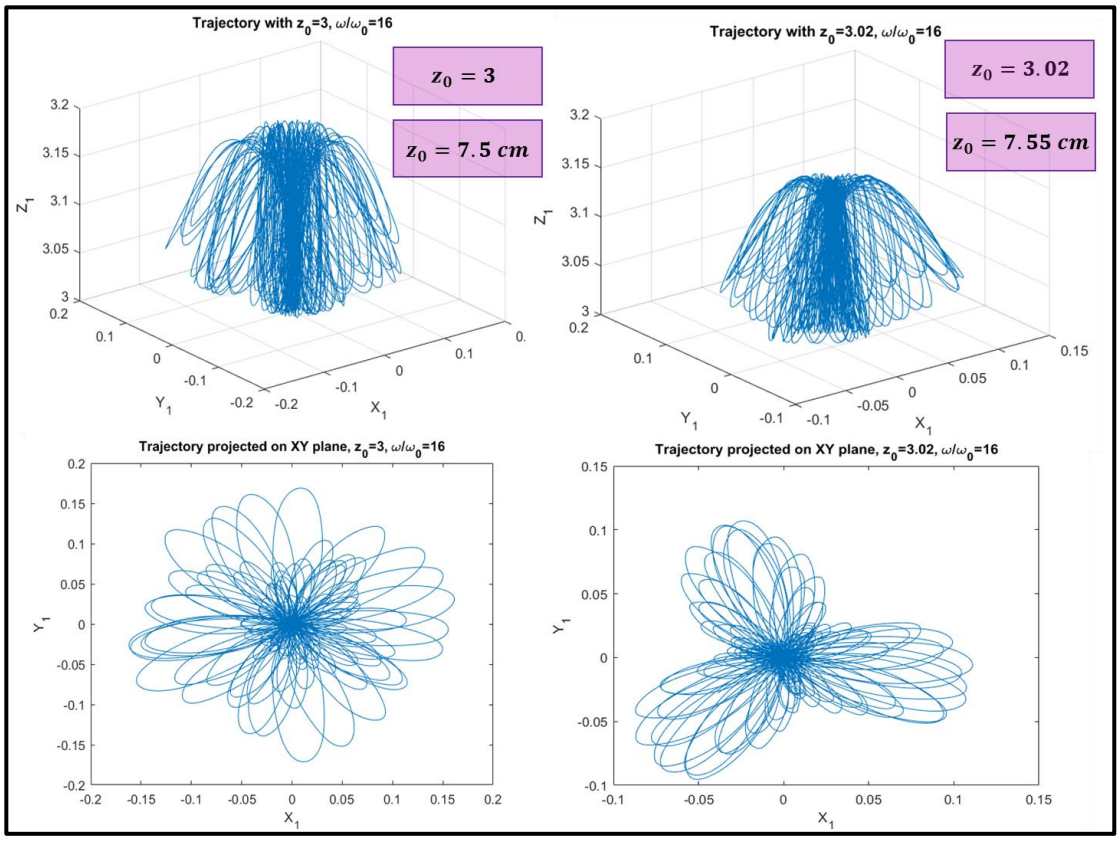

Figure 10-8: Flower-shape trajectories.

Nevertheless, as z_0 tends to z_e, one can see that the three-dimensional trajectories and their projections on the X_1Y_1 change, losing the flower shape and approaching to the characteristic form of the linear trajectories (see figures 9-31 and 9-31). These changes can be seen in figures 10-9 and 10-10.

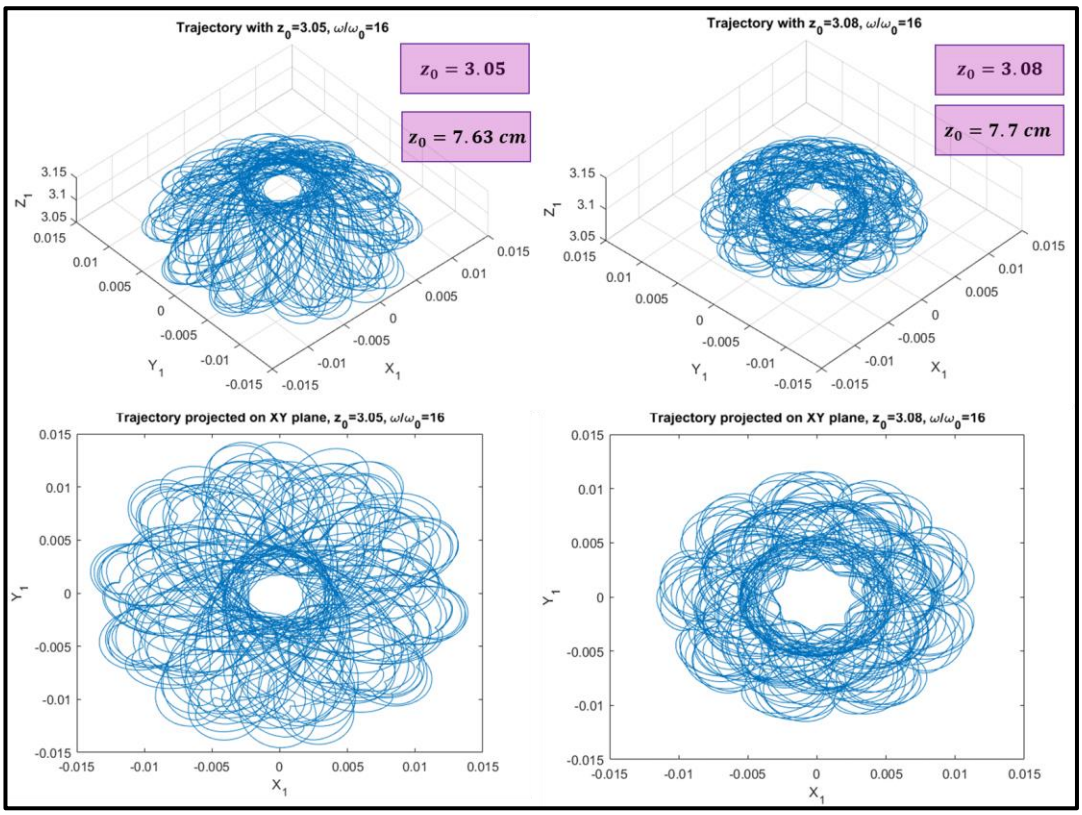

Figure 10-9: Nonlinear trajectories near the equilibrium height.

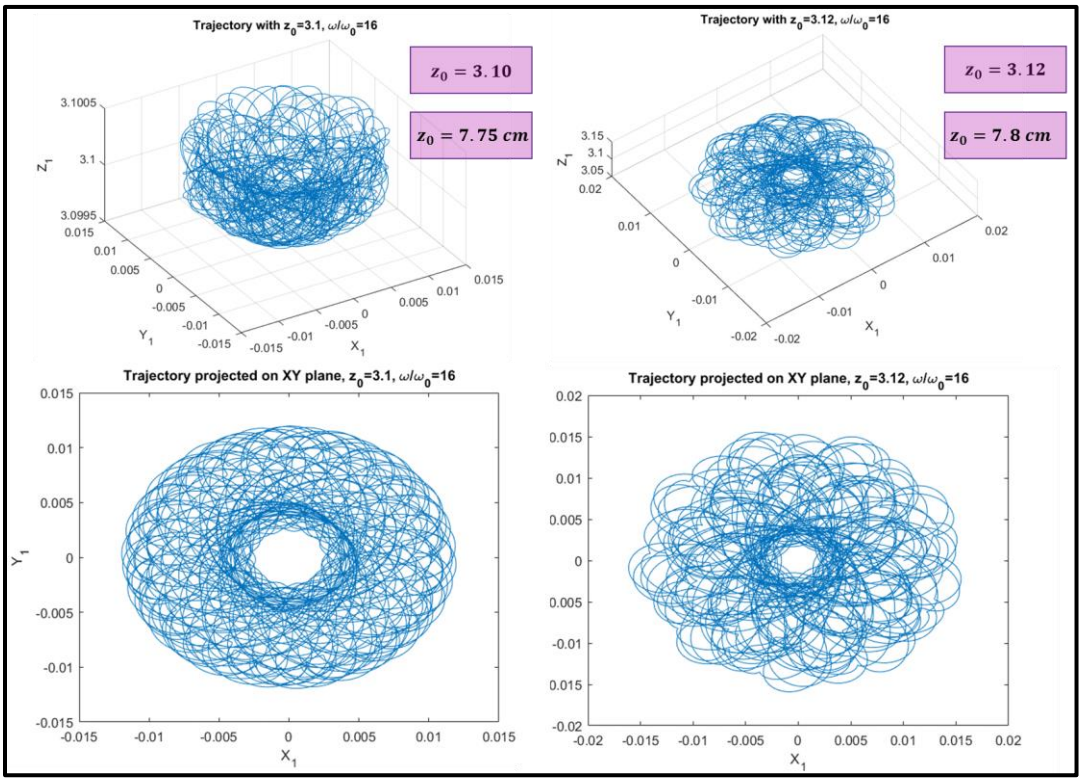

Figure 10-10: Nonlinear trajectories near the equilibrium height.

Finally, if we exceed z_e and move away from its value, the flower shape is recovered. This can be seen in figure 10-11.

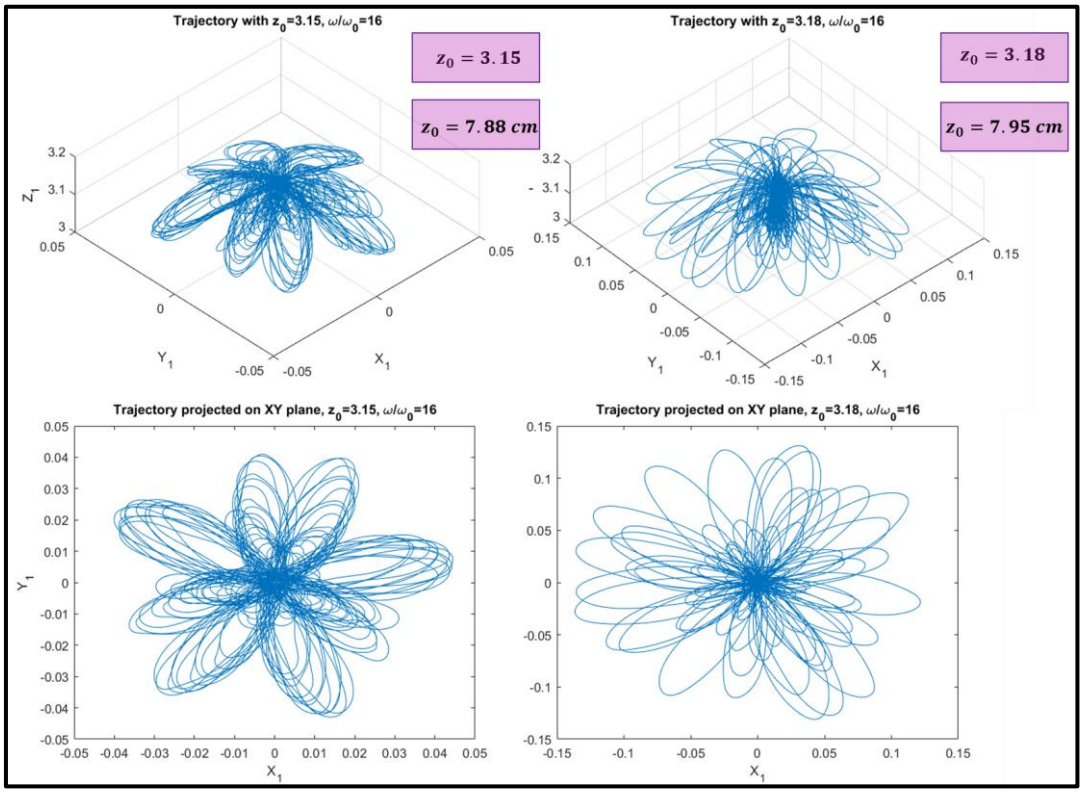

Figure 10-11: Flower shape trajectories.

It is also interesting to analyze the time evolution of the different degrees of freedom and its respective conjugate momenta depending on z_0.

As we have just seen, when z_0 is far from z_e, the projection of the three-dimensional path corresponds with a flower shape trajectory. In this case, the time evolution of the variables reach different peaks that correspond with the petals of the trajectory.

On the other hand, for values of z_0 close to z_e, the time evolution is much more uniform and these peaks dissapear.

Considering $z_0 = 3$ and $z_0 = 3.08$, this can be seen in figures 10-12 to 10-18.

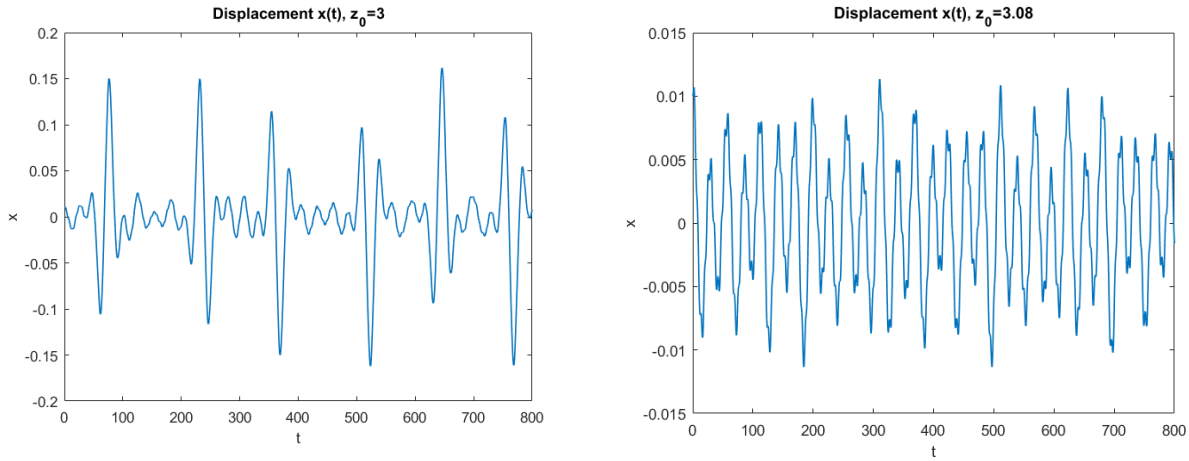

Figure 10-12: Time evolution of x for $z_0 = 3$ and $z_0 = 3.08$

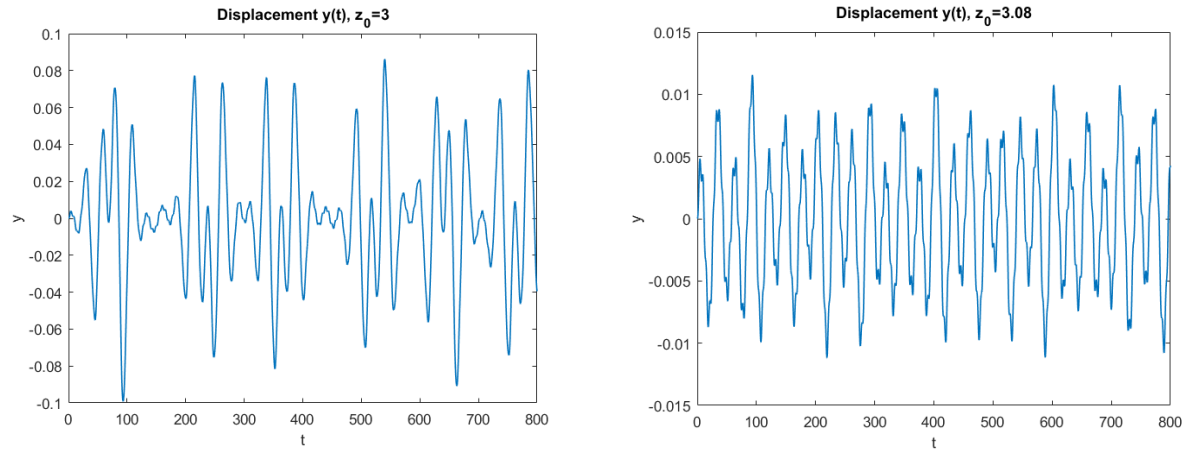

Figure 10-13: Time evolution of y for $z_0 = 3$ and $z_0 = 3.08$

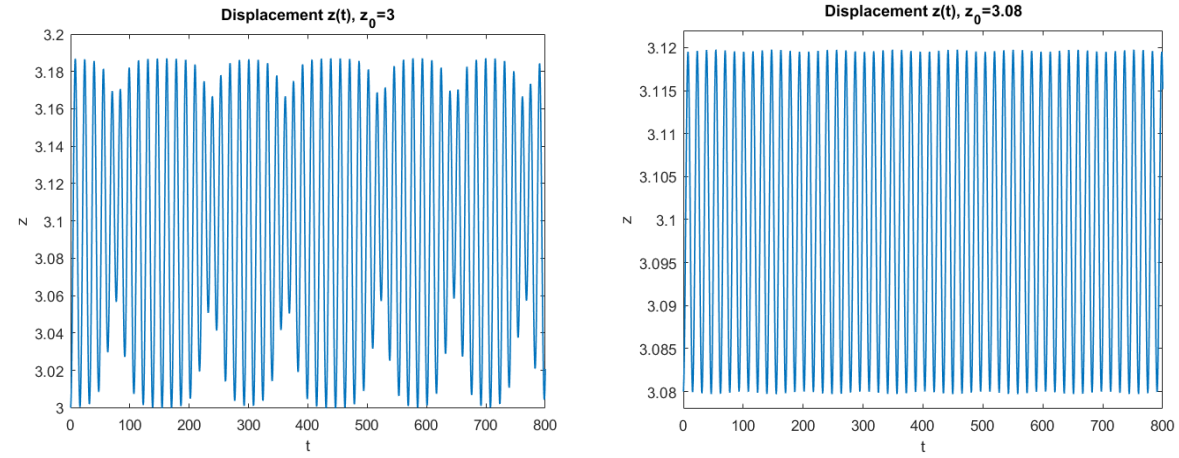

Figure 10-14: Time evolution of z for $z_0 = 3$ and $z_0 = 3.08$

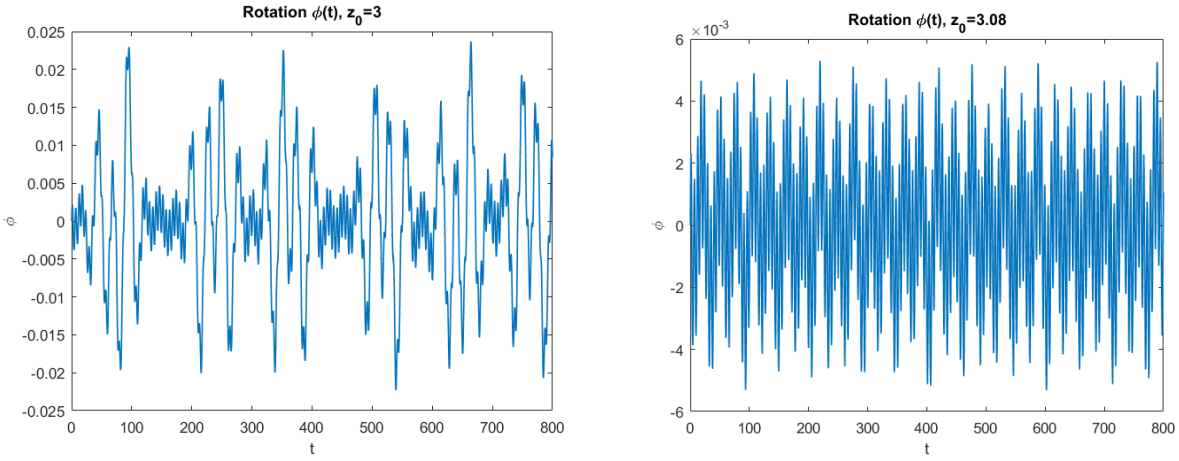

Figure 10-15: Time evolution of ϕ for $z_0 = 3$ and $z_0 = 3.08$

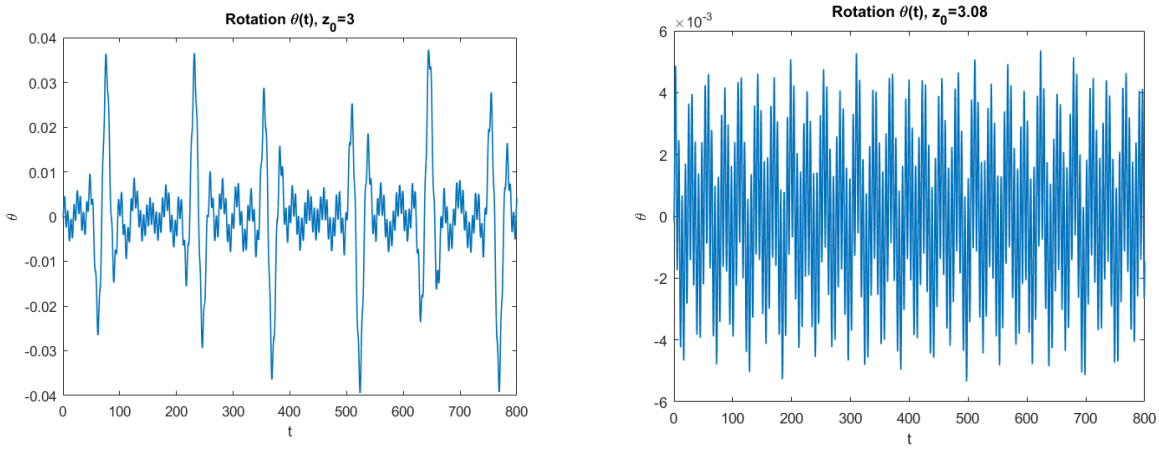

Figure 10-16: Time evolution of θ for $z_0 = 3$ and $z_0 = 3.08$

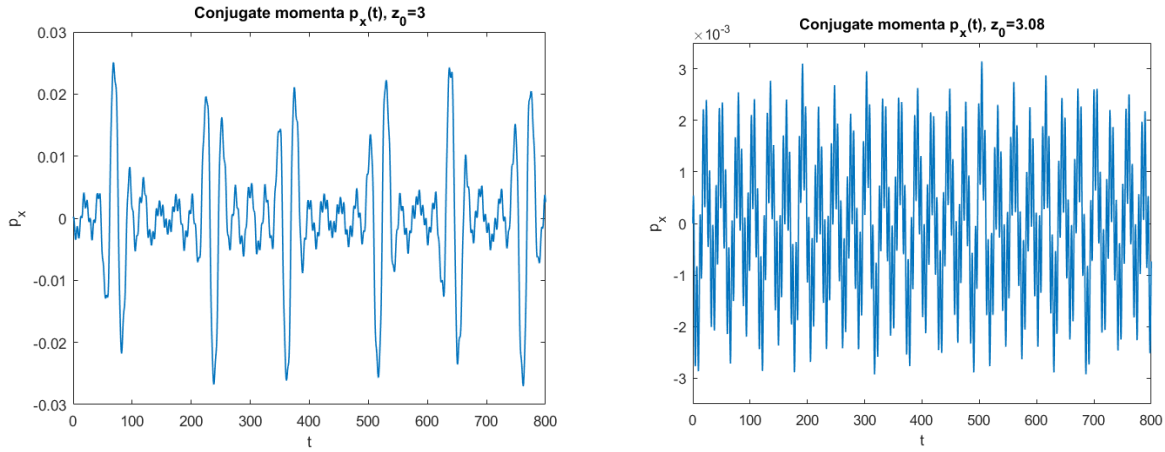

Figure 10-17: Time evolution of p_x for $z_0 = 3$ and $z_0 = 3.08$

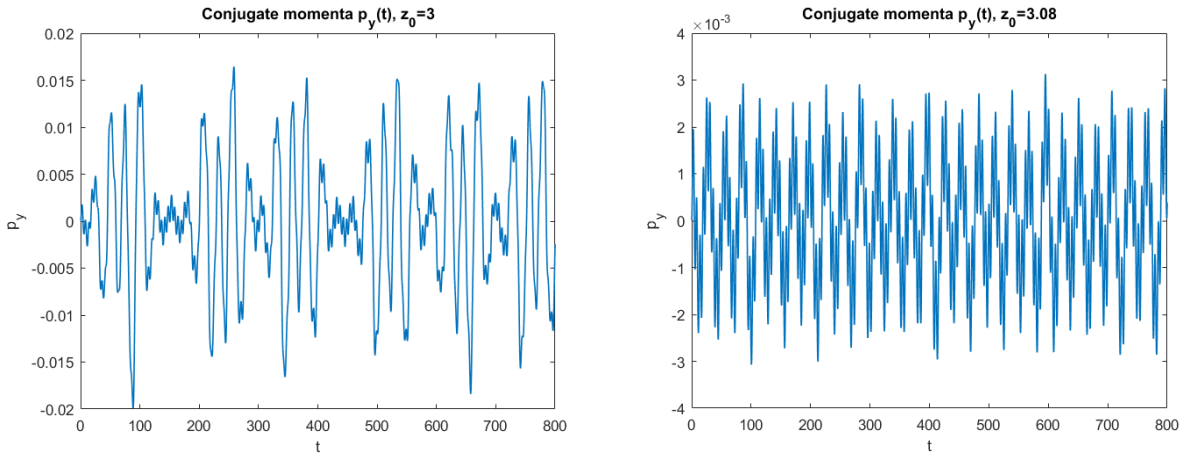

Figure 10-18: Time evolution of p_y for $z_0 = 3$ and $z_0 = 3.08$

10.3.5. Validation of the rotational speed range

To finish with the numerical analysis, we can see if the rotational speed range for $z_e = 3.1$ obtained in the linear system is reproduced in the nonlinear model. In the real toy, different rotational speeds would correspond with hand spinning method (not all the toys have a spin starter, that provides a constant rotational speed).

This range was limited by the lower and upper bounds

$$\omega_{min} = 6.13 \equiv 1159\ rpm$$
$$\omega_{max} = 26.67 \equiv 5045\ rpm$$

Considering an initial condition corresponding with a horizontal, vertical and pitch perturbation:

$$\boldsymbol{q_0} = \begin{pmatrix} x_0 \\ y_0 \\ z_0 \\ \phi_0 \\ \theta_0 \\ p_{x0} \\ p_{y0} \\ p_{z0} \\ p_{\phi 0} \\ p_{\theta 0} \end{pmatrix} = \begin{pmatrix} 0.02 \\ 0 \\ 3 \\ 0 \\ 0.0175 \\ 0 \\ 0 \\ 0 \\ 0 \\ 0 \end{pmatrix}$$

We are going to numerically simulate different trajectories for

$$\omega_{min} \leq \omega \leq \omega_{max}$$

In figures 10-19 to 10-21 we can see that, for the given initial condition, the limits of the nonlinear stable range do not exactly correspond with the bounds of the linear model, obtaining

$$\omega'_{min} = 6.27 \equiv\ 1186\ rpm$$
$$\omega'_{max} = 26 \equiv 4918\ rpm$$

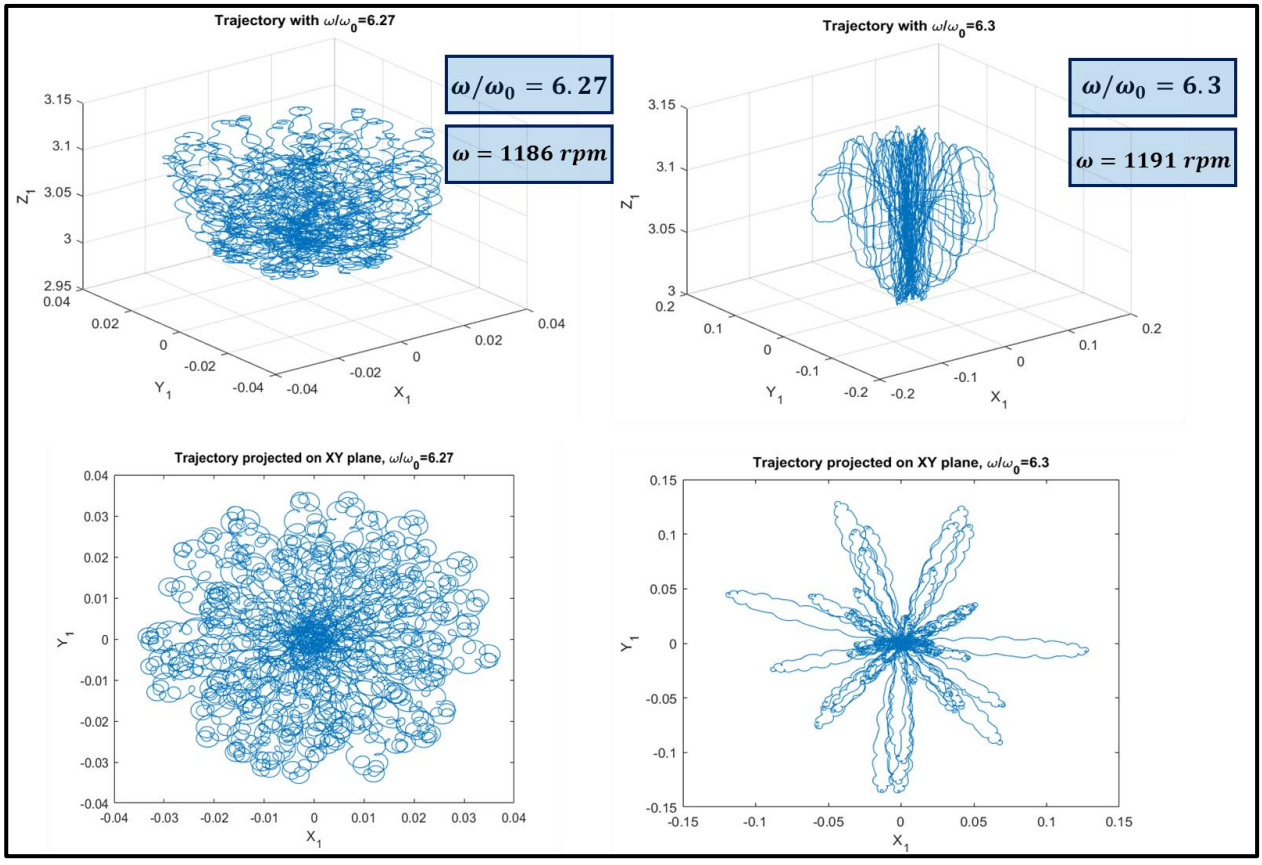

Figure 10-19: Lower limit and stable trajectory of the nonlinear system.

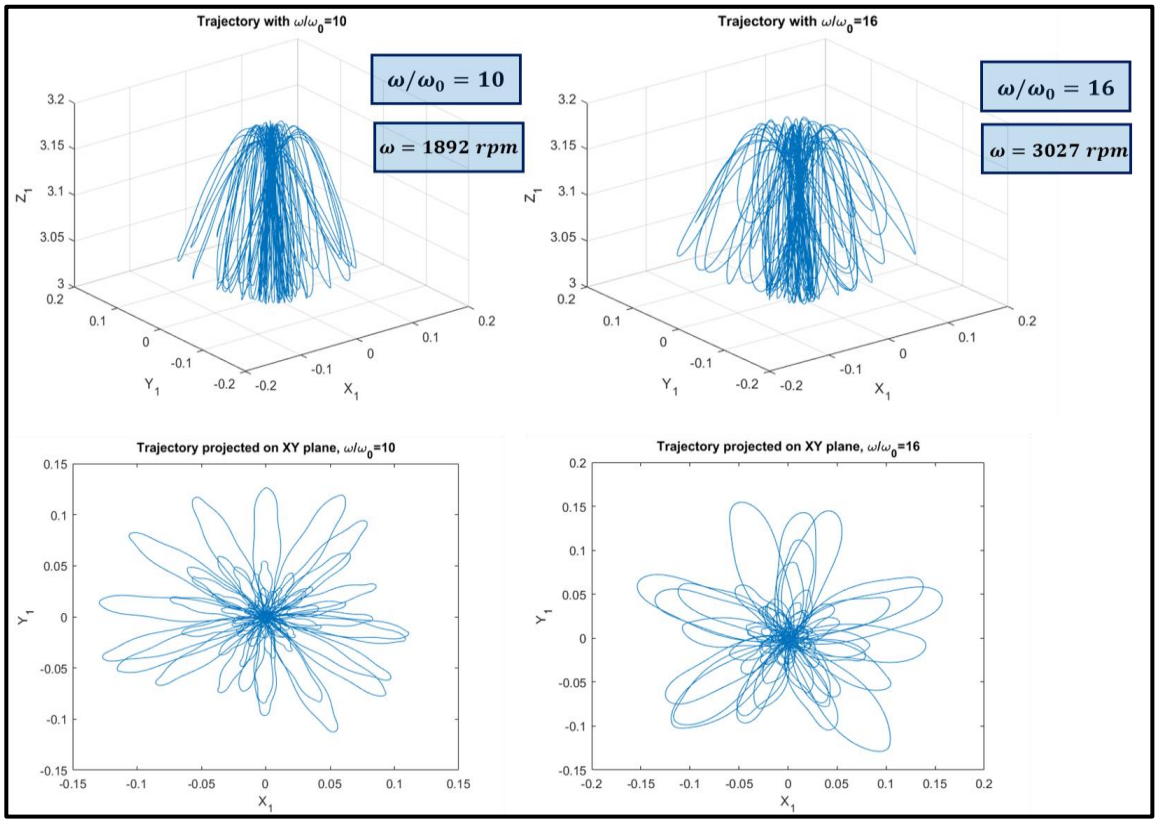

Figure 10-20: Stable trajectories of the nonlinear model. Flower shape trajectories.

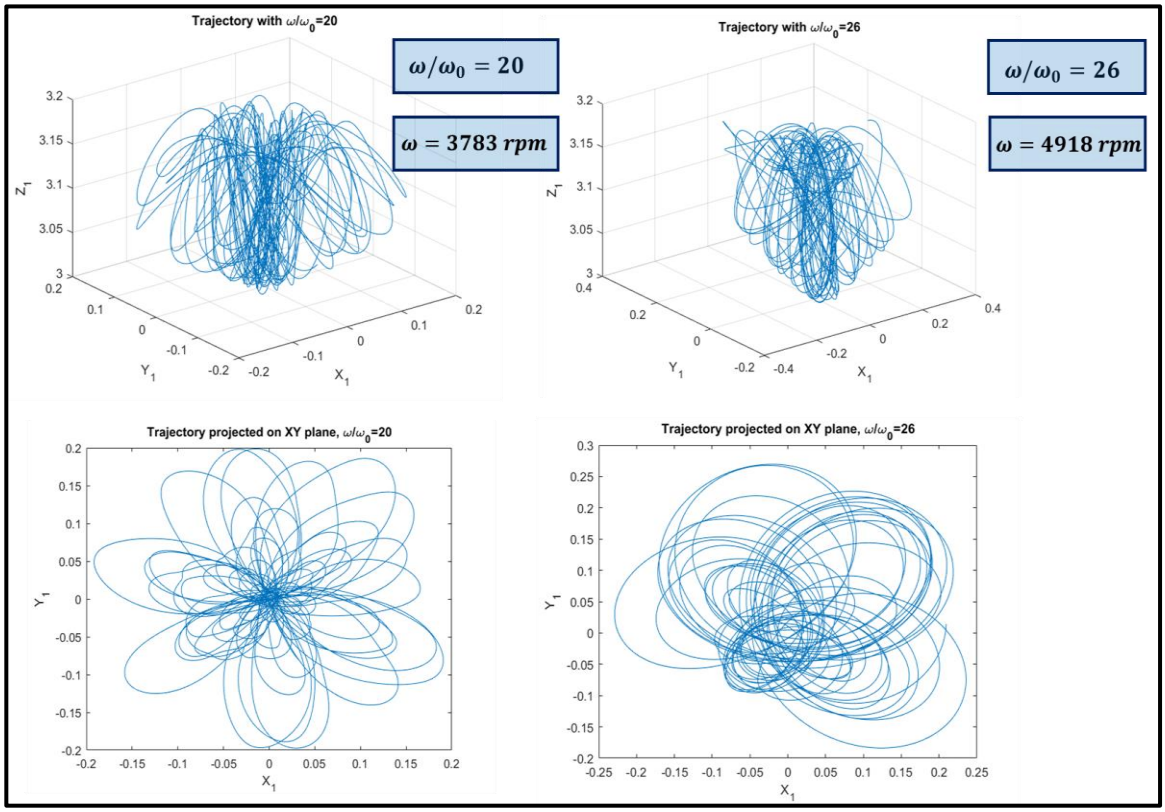

Figure 10-21: Stable trajectory and upper limit of the nonlinear model.

11 INTEGRALS OF THE MOTION

In this chapter we show the constants of motion (quantities that are conserved throughout the trajectory of the dipole) and demonstrate their constancy.

11.1. Conservation of mechanical energy E

The constancy of the mechanical energy of the system E is justified by the fact that the gravitational force is a conservative force and the magnetic force does not work. Therefore, E is a constant of motion.

Moreover, the Levitron toy is an example of system submitted to ideal links, independent coordinates, conservative active forces and the Lagrangian is explicitly time-independent and quadratic velocity dependant. Therefore, the Hamiltonian is a conserved quantity and it coincides with the total energy of the system:

$$\mathcal{H} = E = T + U \tag{11.1}$$

This constancy can be numerically verified for the example considered in previous chapters.

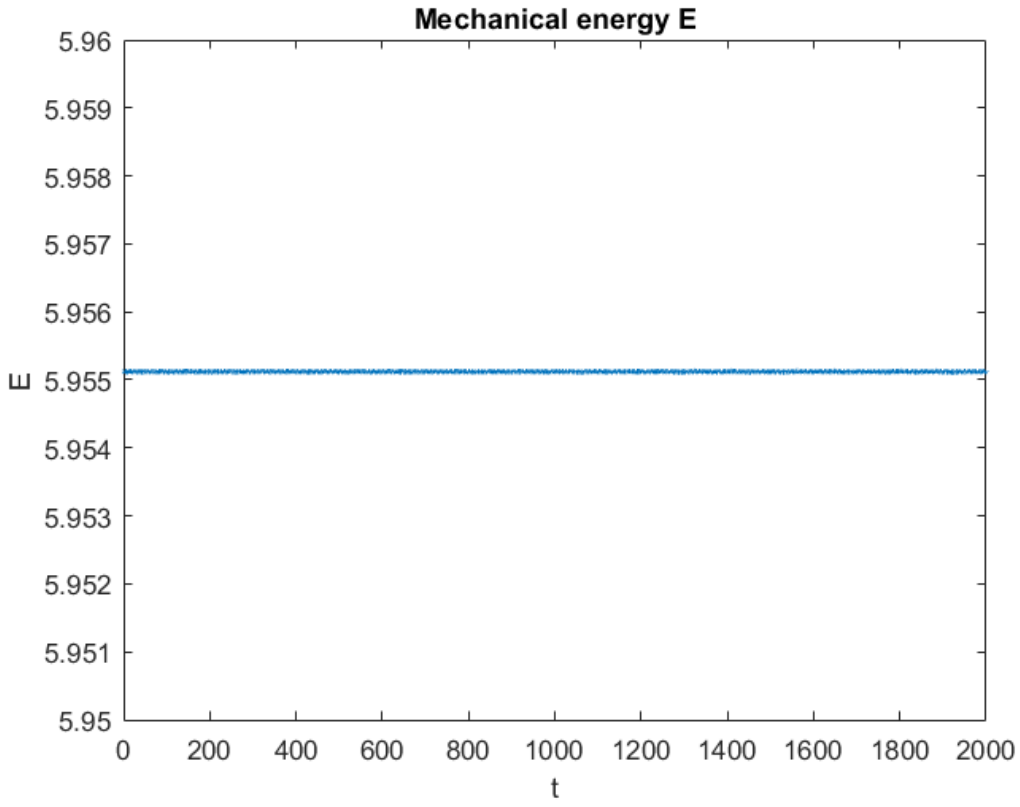

Figure 11-1: Mechanical energy of the system.

11.2. Conservation of L_{0Z_1}

We next demonstrate that the Z-component of the angular momentum with respect to the origin of coordinates L_{0Z_1} is a constant of the motion, provided that we have cylindrical symmetry. The latter condition implies that

$$\frac{B_x}{x} = \frac{B_y}{y} \tag{11.2}$$

We start from the angular momentum theorem

$$\left.\frac{\mathrm{d}\vec{L}_0}{\mathrm{d}t}\right|_1 = \vec{M}_G + \vec{r} \times \vec{F} \tag{11.3}$$

Using Newton's Second law

$$\vec{F} = m\vec{g} + \nabla\left(\vec{\mu} \cdot \vec{B}\right) = m\vec{a}_G \tag{11.4}$$

Expressing $\vec{\mu}$ in frame '1'

$$\vec{\mu} = -\mu\vec{k}_3 = -\mu \begin{pmatrix} \sin(\theta) \\ -\sin\phi\cos\theta \\ \cos\phi\cos\theta \end{pmatrix} \tag{11.5}$$

and computing the cross products $\vec{\mu} \times \vec{B}$ and $\vec{r} \times m\vec{a}_G$ in the fixed frame, we have

$$\vec{\mu} \times \vec{B}\big|_1 = -\mu \begin{vmatrix} \vec{i}_1 & \vec{j}_1 & \vec{k}_1 \\ \sin(\theta) & -\sin\phi\cos\theta & \cos\phi\cos\theta \\ B_x & B_y & B_z \end{vmatrix} = \begin{pmatrix} \mu\left(B_y\cos(\phi)\cos(\theta) + B_z\sin(\phi)\cos(\theta)\right) \\ \mu(B_z\sin(\theta) - B_x\cos(\phi)\cos(\theta)) \\ -\mu\left(B_y\sin(\theta) + B_x\sin(\phi)\cos(\theta)\right) \end{pmatrix} \tag{11.6}$$

$$\vec{r} \times \left(m\vec{g} + \nabla\left(\vec{\mu} \cdot \vec{B}\right)\right)\Big|_1 = \vec{r} \times m\vec{a}_G|_1 = m \begin{vmatrix} \vec{i}_1 & \vec{j}_1 & \vec{k}_1 \\ x & y & \mathrm{z} \\ \ddot{x} & \ddot{y} & \ddot{z} \end{vmatrix} = m \begin{pmatrix} y\ddot{z} - \ddot{y}z \\ \ddot{x}z - x\ddot{z} \\ x\ddot{y} - \ddot{x}y \end{pmatrix} \tag{11.7}$$

Substituting in the expression of the angular momentum theorem

$$\left.\frac{\mathrm{d}\vec{L}_0}{\mathrm{d}t}\right|_1 = \begin{pmatrix} \mu\left(B_y\cos(\phi)\cos(\theta) + B_z\sin(\phi)\cos(\theta)\right) + m(y\ddot{z} - \ddot{y}z) \\ \mu(B_z\sin(\theta) - B_x\cos(\phi)\cos(\theta)) + m(\ddot{x}z - x\ddot{z}) \\ -\mu\left(B_y\sin(\theta) + B_x\sin(\phi)\cos(\theta)\right) + m(x\ddot{y} - \ddot{x}y) \end{pmatrix} \tag{11.8}$$

To show the constancy of L_{0Z_1}, we substitute the following relations

$$\begin{aligned} m\ddot{x} &= -\mu\left(\frac{\partial B_x}{\partial x}\sin(\theta) + \frac{\partial B_z}{\partial x}\cos(\phi)\cos(\theta)\right) \\ m\ddot{y} &= -\mu\left(-\frac{\partial B_y}{\partial y}\sin(\phi)\cos(\theta) + \frac{\partial B_z}{\partial y}\cos(\phi)\cos(\theta)\right) \end{aligned} \tag{11.9}$$

in the third component of $\left.\frac{\mathrm{d}\vec{L}_0}{\mathrm{d}t}\right|_1$

$$\frac{\mathrm{d}L_{0Z_1}}{\mathrm{d}t} = -\mu\big(B_y\sin(\theta) + B_x\sin(\phi)\cos(\theta)\big) + \mu x\frac{\partial B_y}{\partial y}\sin(\phi)\cos(\theta) - \mu x\frac{\partial B_z}{\partial y}\cos(\phi)\cos(\theta) + \mu y\frac{\partial B_x}{\partial x}\sin(\theta) + \mu y\frac{\partial B_z}{\partial x}\cos(\phi)\cos(\theta) \tag{11.10}$$

The components of the magnetic field, differentiating eq. with respect x and y, verify:

$$y\frac{\partial B_x}{\partial x} = B_y + x\frac{\partial B_y}{\partial x}$$
$$x\frac{\partial B_y}{\partial y} = B_x + y\frac{\partial B_x}{\partial y}$$

Therefore

$$\frac{\mathrm{d}L_{0Z_1}}{\mathrm{d}t} = -\mu\big(B_y\sin(\theta) + B_x\sin(\phi)\cos(\theta)\big) + \mu B_x\sin(\phi)\cos(\theta) + \mu y\frac{\partial B_x}{\partial y}\sin(\phi)\cos(\theta) - \mu x\frac{\partial B_z}{\partial y}\cos(\phi)\cos(\theta) + \mu B_y\sin(\theta) + \mu x\frac{\partial B_y}{\partial x}\sin(\theta) + \mu y\frac{\partial B_z}{\partial x}\cos(\phi)\cos(\theta) \tag{11.11}$$

Differentiating with respect to z the relation provided by the cylindrical symmetry in eq. (11.2) and taking into account the properties of the partial derivatives,

$$\begin{aligned} x\frac{\partial B_y}{\partial z} &= y\frac{\partial B_x}{\partial z} \\ \frac{\partial B_x}{\partial y} &= \frac{\partial B_y}{\partial x} \\ \frac{\partial B_x}{\partial z} &= \frac{\partial B_z}{\partial x} \\ \frac{\partial B_z}{\partial y} &= \frac{\partial B_y}{\partial z} \end{aligned} \tag{11.12}$$

we arrive to

$$\frac{\mathrm{d}L_{0Z_1}}{\mathrm{d}t} = 0 \qquad \text{QED} \tag{11.13}$$

Note that this constant of motion had not been obtained using the equations of motion in any of the previous formulations studied.

11.3. Conservation of L_{GZ_3}

The constancy of L_{GZ_3} can be easily deduced seeing that the gravitational force is parallel to $GZ_3 = GZ_4$, and the magnetic force cuts this axis. Moreover, as $\vec{\mu} = -\mu\vec{k}_3$, the magnetic torque $\vec{M}_G = \vec{\mu}\times\vec{B}$ is perpendicular

to the axis.

In contrast to L_{0Z_1}, this constant of motion has been obtained in the vectorial mechanics and hamiltonian formulations:

$$\frac{d}{dt}\Big(I_z\big(\dot{\psi}+\dot{\phi}\sin(\theta)\big)\Big)=0 \Rightarrow L_{GZ_3}=I_z\big(\dot{\psi}+\dot{\phi}\sin(\theta)\big)=constant \tag{11.14}$$

12 ANALYSIS INCLUDING FRICTION

Once the top is hovering over the base, air friction causes the loss of energy of the spinning top. If spin velocity decreases under the lower bound of stability (remember the stability region in figure 9-3), hovering ends and the top falls.

We could not finish this study without creating a model taking into account the effects of the air. These effects are going to be considered computing a drag force, a drag torque and Magnus force and introducing them in the Hamiltonian system as a generalized force.

$$\begin{aligned} \frac{dq_i}{dt} &= \frac{\partial \mathcal{H}}{\partial p_i} \\ \frac{dp_i}{dt} &= -\frac{\partial \mathcal{H}}{\partial q_i} + Q_i \end{aligned} \tag{12.1}$$

where Q_i is the generalized force associated with the generalized coordinate q_i.

The expressions of these forces were stabilished by Rubinow et al. in [10] for a sphere moving in a viscous fluid. In short, the results are the Stokes force, which is proportional to velocity

$$\vec{F}_D = -k\vec{v} \tag{12.2}$$

a force which depends on the cross product, known as Magnus force

$$\vec{F}_M = A\,\vec{\omega} \times \vec{v} \tag{12.3}$$

and a torque against the spinning

$$\vec{M}_D = -B\vec{\omega} \tag{12.4}$$

Note that there is no torque caused by $\vec{v}$.

In these results, constants k, A and B have known values for a sphere and it has been assummed low Reynolds number. To study the effect of friction on our spinning top, we have to consider the motion in air, so that these expressions can be modelled as quadratic functions. For this case, Luckerchenko et al. in [11] provide the expressions of drag force, Magnus force and drag torque.

Generalized forces can be obtained from the computation of the virtual work δW of the applied forces.

12.1. Drag force

The expression of this force is

$$\vec{F}_D = -\frac{3}{4}\rho\frac{C_d}{d}|\vec{v}|\vec{v} = -k|\vec{v}|\vec{v} \tag{12.5}$$

where ρ is the air density, d is the diameter of the sphere and C_d is a drag coefficient, dependant of the traslational Reynolds number. All these constants are going to be grouped in the constant C_{drag}. Therefore, this force can be written as

$$\vec{F}_D = -C_{drag}\sqrt{p_x^2 + p_y^2 + p_z^2}\begin{pmatrix} p_x \\ p_y \\ p_z \end{pmatrix} \tag{12.6}$$

Computing its virtual work

$$\delta W = \vec{F}_D \cdot \delta\vec{r} = Q_D \cdot \delta q \tag{12.7}$$

we get

$$Q_D = \begin{pmatrix} Q_{DX} \\ Q_{DY} \\ Q_{DZ} \end{pmatrix} = -C_{drag}\sqrt{p_x^2 + p_y^2 + p_z^2}\begin{pmatrix} p_x \\ p_y \\ p_z \end{pmatrix} \tag{12.8}$$

12.2. Magnus force

The usual explanation of this phenomenon is that the rotating body produces a swirl of fluid around it, modifying the uniform flow of fluid. As a result, the pressure is diminished on one side of the body and increased on the other side, giving a side thrust.

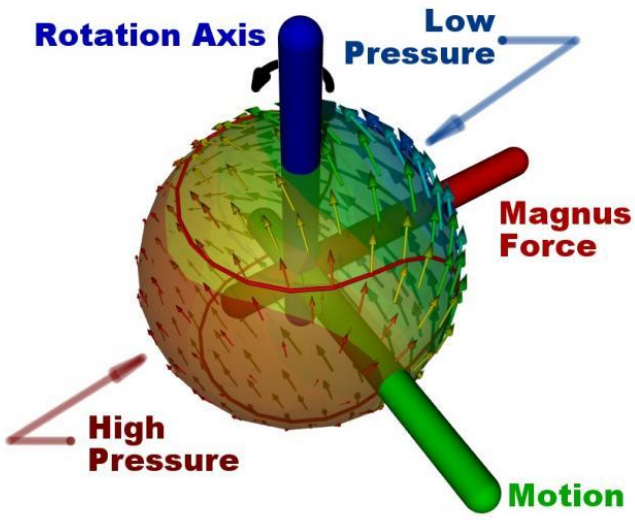

Figure 12-1: Magnus Force on a rotating sphere.

Following Lukerchenko et al. [11], the lateral Magnus force per unit volume is

$$\vec{F}_M = C_m \rho \vec{\omega} \times \vec{v} \tag{12.9}$$

where C_m is a Magnus coefficient, whose expression can be found in [15]. Grouping again all the constants in C_{mag}, we have

$$\vec{F}_M = C_{mag}\vec{\omega} \times \vec{v} = C_{mag}\begin{vmatrix} \vec{\imath}_1 & \vec{\jmath}_1 & \vec{k}_1 \\ \omega_X & \omega_Y & \omega_Z \\ v_X & v_Y & v_Z \end{vmatrix} = C_{mag}\begin{pmatrix} \omega_Y v_Z - \omega_Z v_Y \\ \omega_Z v_X - \omega_X v_Z \\ \omega_X v_Y - \omega_Y v_X \end{pmatrix} \tag{12.10}$$

To compute the expression of the force, we express the angular velocity in frame '1'

$$\vec{\omega}|_1 = \begin{pmatrix} \dot{\phi} + \dot{\psi}\sin(\theta) \\ \dot{\theta}\cos(\phi) - \dot{\psi}\sin(\phi)\cos(\theta) \\ \dot{\theta}\sin(\phi) + \dot{\psi}\cos(\phi)\cos(\theta) \end{pmatrix} \tag{12.11}$$

and rewriting $\dot{\phi}$, $\dot{\theta}$ and $\dot{\psi}$ in terms of the conjugate momenta

$$\begin{cases} \dot{\phi} = \dfrac{p_\phi - p_\psi \sin(\theta)}{I_x \cos^2(\theta)} \\ \dot{\theta} = \dfrac{p_\theta}{I_X} \\ \dot{\psi} = \dfrac{p_\psi}{I_z} - \dfrac{p_\phi - p_\psi \sin(\theta)}{I_x \cos^2(\theta)}\sin(\theta) \end{cases} \tag{12.12}$$

the components of $\vec{\omega}|_1$ are

$$\begin{cases} \omega_X = \dfrac{p_\phi}{I_x} + \left(\dfrac{1}{I_Z} - \dfrac{1}{I_X}\right) p_\psi \sin(\theta) \\ \omega_Y = \dfrac{p_\theta}{I_X}\cos(\phi) + \dfrac{p_\phi}{I_x}\sin(\phi)\tan(\theta) - \left(\dfrac{\cos(\theta)}{I_Z} + \dfrac{\sin(\theta)\tan(\theta)}{I_X}\right) p_\psi \sin(\phi) \\ \omega_Z = \dfrac{p_\theta}{I_X}\sin(\phi) - \dfrac{p_\phi}{I_x}\cos(\phi)\tan(\theta) + \left(\dfrac{\cos(\theta)}{I_Z} + \dfrac{\sin(\theta)\tan(\theta)}{I_X}\right) p_\psi \cos(\phi) \end{cases} \tag{12.13}$$

Computing its virtual work

$$\delta W = \vec{F}_M \cdot \delta\vec{r} = Q_m \cdot \delta q \tag{12.14}$$

The generalized force corresponding with the Magnus Force is therefore

$$Q_m = C_{mag}\begin{pmatrix} \omega_Y p_Z - \omega_Z p_Y \\ \omega_Z p_X - \omega_X p_Z \\ \omega_X p_Y - \omega_Y p_X \end{pmatrix} \tag{12.15}$$

12.3. Drag Torque

The expression provided again by [11] for the drag torque is

$$\vec{M}_D = -C_\omega \frac{\rho}{2} r^5 |\vec{\omega}|\vec{\omega} = -C_{torque}|\vec{\omega}|\vec{\omega} \tag{12.16}$$

where we have grouped in C_{torque} the constants C_ω (dependant of the rotational Reynolds number), ρ and the radius of the sphere r.

The virtual work of the torque is given by

$$\delta W = \vec{M}_D \cdot \delta\vec{\varphi} = \vec{M}_D\big|_3 \vec{\omega}|_3 \cdot dt = Q_M \cdot \delta q \tag{12.17}$$

where $\vec{\omega}|_3 \cdot dt$ is

$$\vec{\omega}|_3\, dt = \left(\dot{\phi}\cos(\theta)\,\vec{\imath}_3 + \dot{\theta}\vec{\jmath}_3 + \left(\dot{\psi} + \dot{\phi}\sin(\theta)\right)\vec{k}_3\right)dt \tag{12.18}$$

Note that in the computation of δW vectors have been expressed in frame '3' to take advantage, once again, of the rotational symmetry of the top.

Using the relations $\{\delta\phi = \dot{\phi}dt;\ \delta\theta = \dot{\theta}dt;\ \delta\psi = \dot{\psi}dt\}$ we have

$$\vec{\omega}|_3\, dt = \delta\phi\cos(\theta)\,\vec{\imath}_3 + \delta\theta\vec{\jmath}_3 + (\delta\psi + \delta\phi\sin(\theta))\vec{k}_3 \tag{12.19}$$

Therefore, virtual work is

$$\begin{aligned}\delta W &= -C_{torque}|\vec{\omega}|\left(\left(\dot{\phi} + \dot{\psi}\sin(\theta)\right)\delta\phi + \dot{\theta}\delta\theta + \left(\dot{\psi} + \dot{\phi}\sin(\theta)\right)\delta\psi\right)\\ &= Q_{M\phi}\delta\phi + Q_{M\theta}\delta\theta + Q_{M\psi}\delta\psi\end{aligned} \tag{12.20}$$

and the components of the generalized torque are

$$\begin{cases} Q_{M\phi} = -C_{torque}|\vec{\omega}|\left(\dot{\phi} + \dot{\psi}\sin(\theta)\right) \\ Q_{M\theta} = -C_{torque}|\vec{\omega}|\dot{\theta} \\ Q_{M\psi} = -C_{torque}|\vec{\omega}|\left(\dot{\psi} + \dot{\phi}\sin(\theta)\right) \end{cases} \tag{12.21}$$

In terms of the conjugate momenta, the generalized torque results in:

$$\begin{cases} Q_{M\phi} = -C_{torque}|\vec{\omega}|\left(\dfrac{p_\phi}{I_x} + \left(\dfrac{1}{I_Z} - \dfrac{1}{I_X}\right)p_\psi\sin(\theta)\right) \\ Q_{M\theta} = -C_{torque}|\vec{\omega}|\dfrac{p_\theta}{I_x} \\ Q_{M\psi} = -C_{torque}|\vec{\omega}|\dfrac{p_\psi}{I_x} \end{cases} \tag{12.22}$$

12.4. Set of equations considering air friction

The Hamiltonian system, including the generalized forces computed in the previous sections, is

$$
\begin{aligned}
\dot{x}^* &= p_x^* \\
\dot{y}^* &= p_y^* \\
\dot{z}^* &= p_z^* \\
\dot{\phi}^* &= R\frac{p_\phi^* - p_\psi^*\sin(\theta^*)}{\cos^2(\theta^*)} \\
\dot{\theta}^* &= Rp_\theta^* \\
\dot{\psi}^* &= \frac{R}{\sigma}p_\psi^* - R\frac{\sin(\theta^*)}{\cos^2(\theta^*)}\left(p_\phi^* - p_\psi^*\sin(\theta^*)\right) \\
\dot{p_x^*} &= -\beta\left(-\frac{1}{2}\frac{dB_0^*}{dz^*}\sin(\theta^*) - \frac{x^*}{2}\frac{d^2B_0^*}{dz^{*2}}\cos(\phi^*)\cos(\theta^*)\right) - C_{drag}p_x^*\sqrt{p_x^{*2}+p_y^{*2}+p_z^{*2}} \\
&\quad + C_{mag}(\omega_Y^*p_z^* - \omega_Z^*p_y^*) \\
\dot{p_y^*} &= -\beta\left(\frac{1}{2}\frac{dB_0^*}{dz^*}\sin(\phi^*)\cos(\theta^*) - \frac{y^*}{2}\frac{d^2B_0^*}{dz^{*2}}\cos(\phi^*)\cos(\theta^*)\right) - C_{drag}p_y^*\sqrt{p_x^{*2}+p_y^{*2}+p_z^{*2}} \\
&\quad + C_{mag}(\omega_Z^*p_x^* - \omega_X^*p_z^*) \\
\dot{p_y^*} &= -\beta\left(\frac{1}{2}\frac{dB_0^*}{dz^*}\sin(\phi^*)\cos(\theta^*) - \frac{y^*}{2}\frac{d^2B_0^*}{dz^{*2}}\cos(\phi^*)\cos(\theta^*)\right) - C_{drag}p_y^*\sqrt{p_x^{*2}+p_y^{*2}+p_z^{*2}} \\
&\quad + C_{mag}(\omega_Z^*p_x^* - \omega_X^*p_z^*) \\
\dot{p_z^*} &= -1 - \beta\left(-\frac{1}{2}x^*\frac{d^2B_0^*}{dz^{*2}}\sin(\theta^*)\right. \\
&\quad + \frac{1}{2}y^*\frac{d^2B_0^*}{dz^{*2}}\sin(\phi^*)\cos(\theta^*) \\
&\quad \left. + \frac{dB_0^*}{dz^*}\cos(\phi^*)\cos(\theta^*) - \frac{x^{*2}+y^{*2}}{4}\frac{d^3B_0^*}{dz^{*3}}\cos(\phi^*)\cos(\theta^*)\right) \\
&\quad - C_{drag}p_z^*\sqrt{p_x^{*2}+p_y^{*2}+p_z^{*2}} + C_{mag}(\omega_X^*p_y^* - \omega_Y^*p_x^*) \\
\dot{p_\phi^*} &= -\beta\left(\frac{1}{2}y^*\frac{dB_0^*}{dz^*}\cos(\phi^*)\cos(\theta^*) - B_0^*\sin(\phi^*)\cos(\theta^*)\right. \\
&\quad \left. + \frac{x^{*2}+y^{*2}}{4}\frac{d^2B_0^*}{dz^{*2}}\sin(\phi^*)\cos(\theta^*)\right) \\
&\quad - C_{torque}|\vec{\omega}|\left(Rp_\phi^* + R\left(\frac{1}{\sigma}-1\right)p_\psi^*\sin(\theta^*)\right) \\
\dot{p_\theta^*} &= \frac{R}{\cos^3(\theta^*)}\left(p_\psi^*\sin(\theta^*) - p_\phi^*\right)\left(p_\phi^*\sin(\theta^*) - p_\psi^*\right) \\
&\quad - \beta\left(-\frac{1}{2}x^*\frac{dB_0^*}{dz^*}\cos(\theta^*) - \frac{1}{2}y^*\frac{dB_0^*}{dz^*}\sin(\phi^*)\sin(\theta^*) - B_0^*\cos(\phi^*)\sin(\theta^*)\right. \\
&\quad \left. + \frac{x^{*2}+y^{*2}}{4}\frac{d^2B_0^*}{dz^{*2}}\cos(\phi^*)\sin(\theta^*)\right) - C_{torque}|\vec{\omega}|Rp_\theta^* \\
\dot{p_\psi^*} &= -C_{torque}|\vec{\omega}|Rp_\psi^*
\end{aligned}
\tag{12.23}
$$

The derivatives of $B_0^*(z^*)$ with respect to $z^*$are the same as those of the previous chapters, and the nondimensional components of the angular velocity, expressed in frame '1', are

$$\begin{cases} \omega_X^* = Rp_\phi^* + R\left(\frac{1}{\sigma} - 1\right)p_\psi^* \sin(\theta^*) \\ \omega_Y^* = Rp_\theta^* \cos(\phi^*) + Rp_\phi^* \sin(\phi^*)\tan(\theta^*) - R\left(\frac{\cos(\theta^*)}{\sigma} + \sin(\theta^*)\tan(\theta^*)\right)p_\psi^* \sin(\phi^*) \\ \omega_Z^* = Rp_\theta^* \sin(\phi^*) - Rp_\phi^* \cos(\phi^*)\tan(\theta^*) + R\left(\frac{\cos(\theta^*)}{\sigma} + \sin(\theta^*)\tan(\theta^*)\right)p_\psi^* \cos(\phi^*) \end{cases} \quad (12.24)$$

12.5. Values of the coefficients C_{drag}, C_{mag} and C_{torque}

Once the set of equations has been obtained, we have tested different values for the coefficients C_{drag}, C_{mag} and C_{torque} in order to achieve a simulation time that corresponds with the hovering time of the real toy.

Following the examples of the linear and nonlinear stability (where we numerically solved the problem for $z_e = 3.1$), we have considered an initial condition consisting on a little horizontal and vertical perturbation.

Moreover, in the linear and nonlinear models, we chose a rotational speed that was constant throughout the trajectory of the spinning top. In the friction model, this speed is not constant due to the loss of energy caused by air friction, and we only introduce an initial rotational speed by means of the initial value of the conjugate momenta $p_{\psi 0}$.

For $z_e = 3.1$, the centered value of rotational speed is

$$\frac{\omega}{\omega_0} = 16 \Rightarrow \omega = 3026\, rpm$$

that corresponds, in the hamiltonian formulation, with

$$p_{\psi 0} = \frac{\sigma}{R}\frac{\omega}{\omega_0} = 2$$

Therefore, the initial condition to perform the numerical integration is

$$\boldsymbol{q_0} = \begin{pmatrix} x_0 \\ y_0 \\ z_0 \\ \phi_0 \\ \theta_0 \\ p_{x0} \\ p_{y0} \\ p_{z0} \\ p_{\phi 0} \\ p_{\theta 0} \\ p_{\psi 0} \end{pmatrix} = \begin{pmatrix} 0.02 \\ 0 \\ 3.08 \\ 0 \\ 0 \\ 0 \\ 0 \\ 0 \\ 0 \\ 0 \\ 2 \end{pmatrix}$$

The following values of C_{drag}, C_{mag} and C_{torque}

$$\begin{cases} C_{drag} = 0.0002 \\ C_{mag} = 0.0002 \\ C_{torque} = 0.00001 \end{cases}$$

provide a stable simulation time of about 1250 unit of time, which corresponds with a hovering time of one minute. In the following figures, we can see the trajectories provided by the linear, nonlinear and friction model for 1200 unit of time.

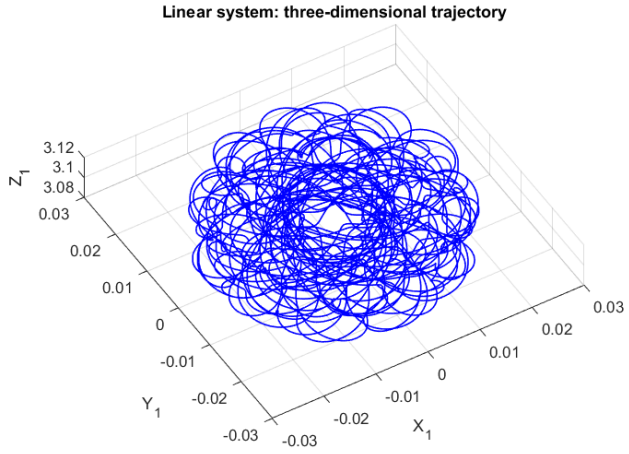

Figure 12-2: Trajectory of the linear system.

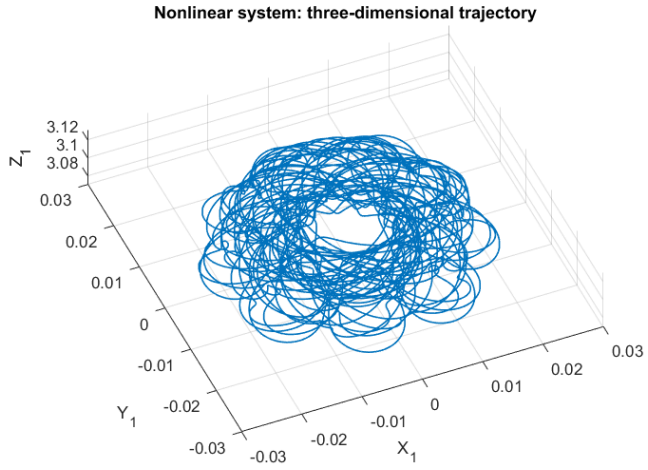

Figure 12-3: Trajectory of the nonlinear system.

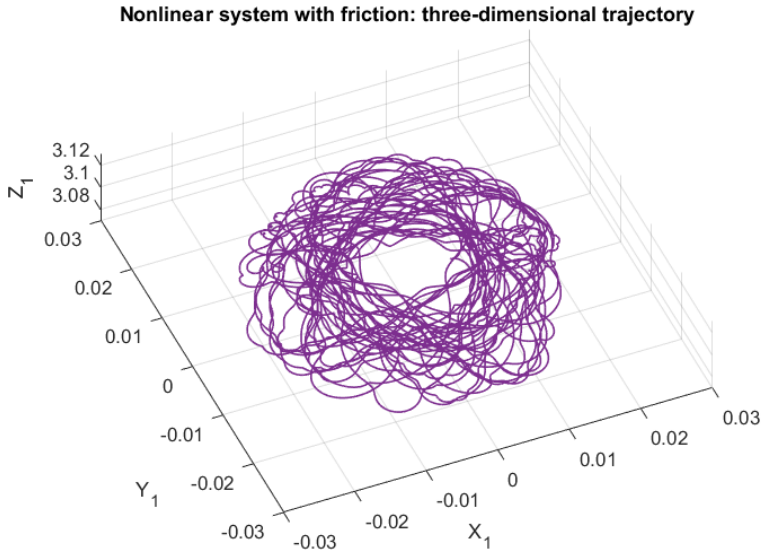

Figure 12-4: Trajectory considering air friction.

The simulation of the linear and nonlinear models can continue as long as we want. Nevertheless, in the friction model there comes a moment when the rotational speed is not large enough to provide the neccesary gyroscopic effect (we reach the lower speed bound) and the spinning top starts falling. We can see this in figure 12-5, that corresponds with a numerical integration of 1250 unit of times.

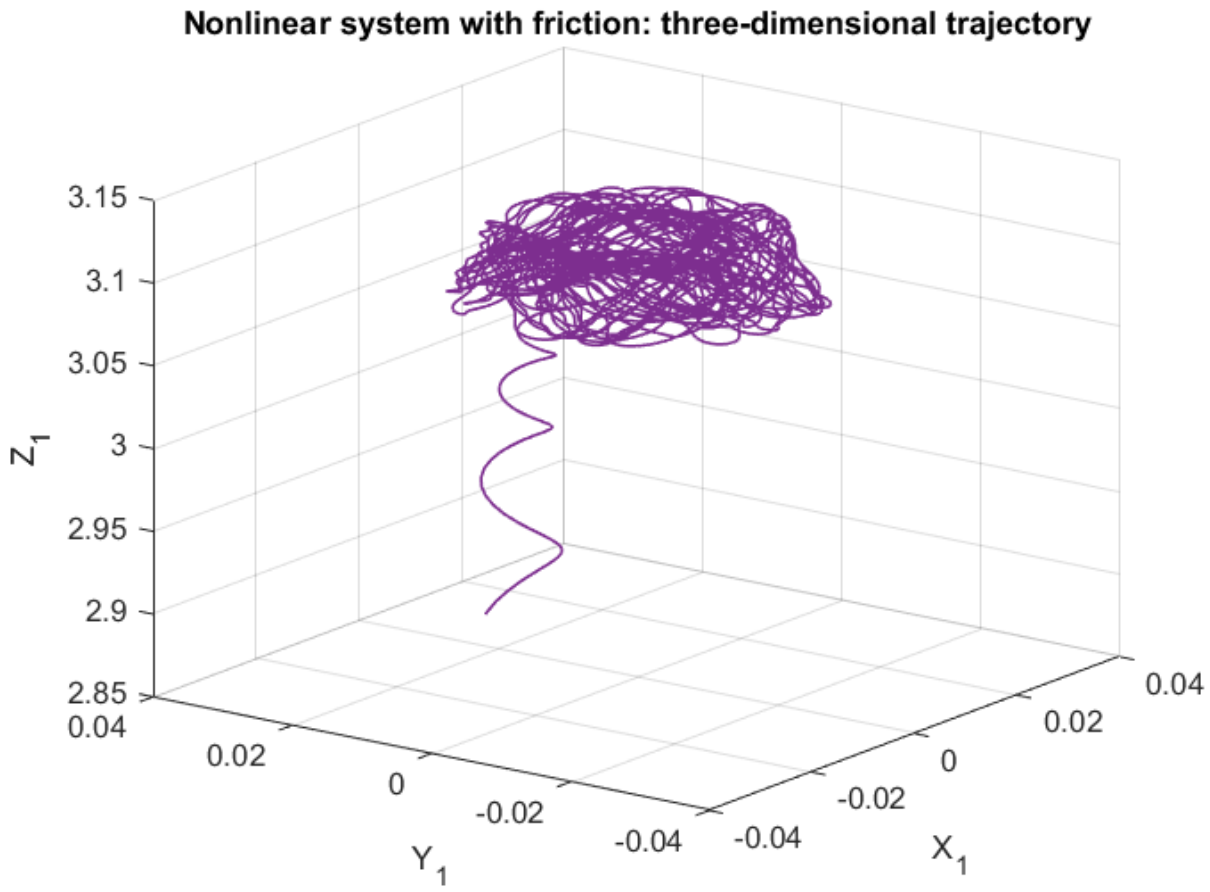

Figure 12-5: Trajectory and fall of the spinning top due to air friction.

13 LET'S PLAY!

After all the analysis carried out through all these pages, one should not forget that this is a toy! Therefore, it is time to play. Nevertheless, the complexity of the hovering magnetic top cannot be narrowed down to theory: using it properly is a big challenge.

The Levitron can be a very difficult toy to use. It can take quite a long time to get both the base level and the top properly weighted such that the top can hover in equilibrium. A set of instructions following [12] has been compiled in 13.1 in order to use the toy properly. Moreover, we have prepared a flowchart in 13.2 to clarify all the ideas and connect the failure modes of the toy with the study carried out in the previous chapters.

13.1. Instructions

When the base magnet of the Levitron is not level with gravity, the top will fly off to a side. If the top flies off to the same side multiple times, this means that the base is not level. If the top flies to one side immediately, the best option is raise the peg on that side at least two turns. If the peg is as high as it goes, we can lower the pegs on the other two sides.

The adjustment of the pegs should continue until:
1. The top flies off to different sides each time, or
2. The top hovers for a little bit and then flies off to the same side, or
3. The top hovers and does not fly off.

If (1) is reached, it is time to proceed to choosing weight for the Levitron by means of the washers.
If we are in situation (2), it is recommendable to adjust the height of the pegs very slightly rather than two turns.
If (3) is reached, we will have mastered our Levitron!

Another option is use the bubble level method, which provides a faster adjustment of the pegs and a more precise levelling of the base.

Figure 13-1: Bubble levelling of the magnetic base.

Once the level of the base has been reached, the next step is choosing the mass of the Levitron that allows a stable hovering by means of the washers of the set.

It is easier to decide on a good weight by probing at the condition where the top is just a little bit too heavy. When the top is a little bit too heavy, it will almost bounce on the plate but not quite lift off, before spinning out on the plate. For this reason, we should approach the weight issue from the heavy side.

If the Levitron is used for the first time, we should put all of the weight on the spinning top. In all likelihood, the top will not lift off the plate. If this happens, cutting the weight in half is a nice option until the top either almost lifts off the plate or hovers for a little bit before flying off in random directions.

Once the top does one of these two things, it is time for small weight changes:

- If the top is too heavy, try removing a small weight or extra o-ring.
- If the top is really bouncing on the plate, it will probably only need one o-ring removed.
- If it is barely too light, try adding the smallest weight or o-ring. The o-rings make a bigger difference than one would expect. Eventually, the correct weight will be found.

If the Levitron has been used before, we can start with the weight that was previously on the top and use the same method outlined in the previous lines.

An important consideration is that the magnetic field is temperature dependent, and so the necessary weight is as well. If it is a colder day, it will be necessary the addition of some weight. If it is warmer, we will probably need to remove weight.

13.2. Flow chart

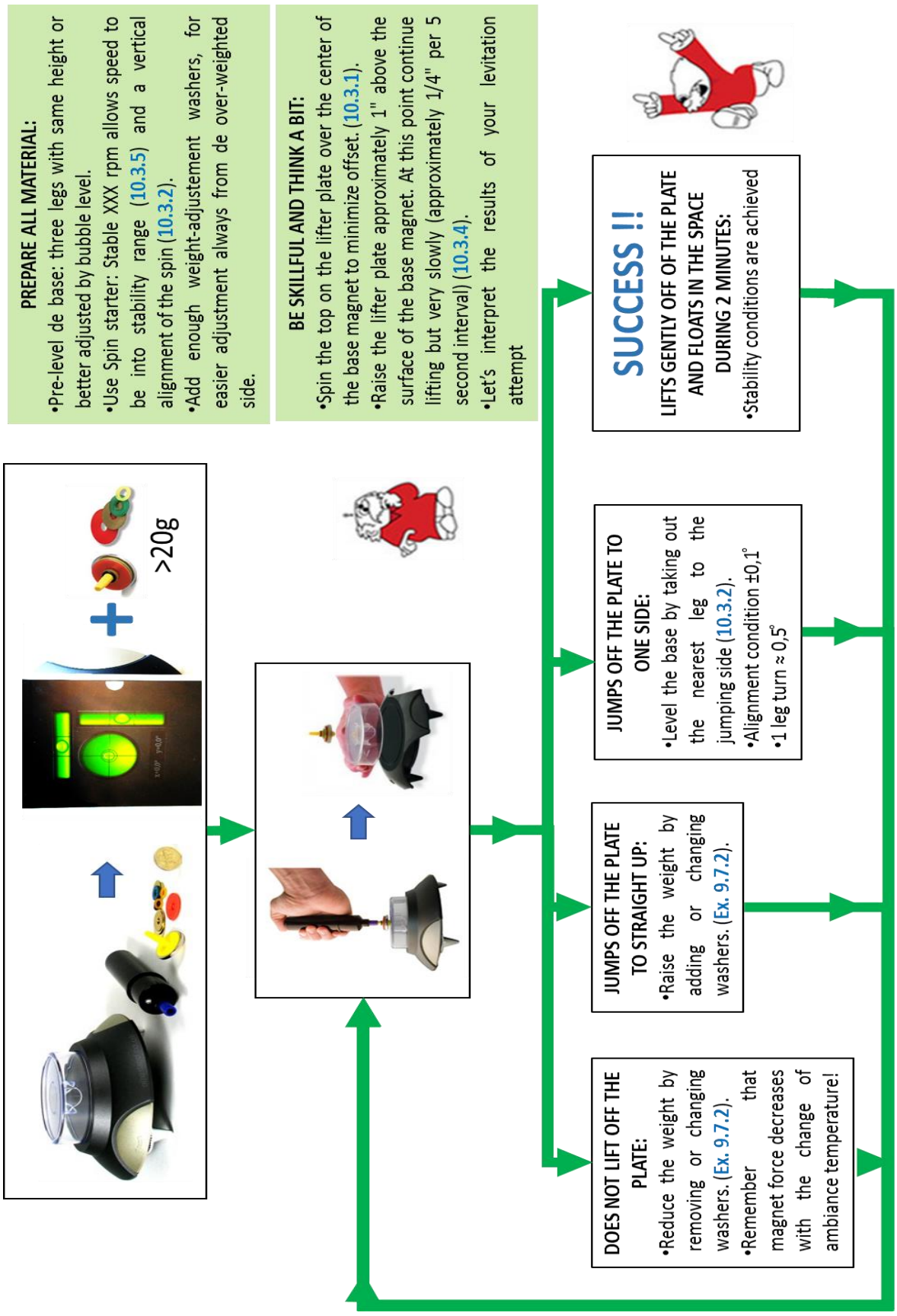

Figure 13-2: Flowchart to achieve levitation.

14 CONCLUSIONS AND FUTURE STEPS

During this project, an analytical study of the hovering magnetic system (known as Levitron) has been developed:

- In chapter 1, we describe the typical contents of a Levitron kit, how the toy works and briefly expose the history of the device.

- In chapter 2, an analysis of the free-motion, in absence of the external magnetic field and solely submitted to the action of gravity is performed using the Classical Euler angles. We derive the constants of the free-motion and describe the motion in term of the axoids (also known as body and space cones). We also see that Classical Euler angles provide a nice visualization of the problem, but the set of equations is singular for $\theta = 0°$.

- In chapter 3, we present the Tait-Bryan angles, describing the system with a yaw-pitch-roll sequence in order to solve the singularity previously mentioned. We obtained the relation between the fixed frame '1' and the local body-frame '4', and computed the angular velocity $\vec{\omega}$, kinetic moment $\vec{L}_G$ and kinetic energy T using this set of angles.

- In chapter 4, we find the expression of the magnetic field at $0Z_1$ axis, derive the equations of the magnetic field $\vec{B}$ for points near the axis and first approximate the spinning top as a magnetic dipole of magnetic moment $\vec{\mu}$.

- In chapter 5, we analyze the static stability of the system. Firstly, the potential energy is computed and we see that its expression validates Earnshaw's theorem. Nevertheless, we see that the Laplacian of the potential energy considering the alignment between $\vec{\mu}$ and $\vec{B}$ because of gyroscopic effect is positive, so that the previous theorem is not verified. Finally, we compute the potential energy $0Z_1$ axis and found the minimum height for which hovering is posible.

- In chapter 6, the equations of motion of the system are derived using vector mechanics. Newton's and Euler's Second law provide a second-order differential set of equations, that is also rewritten as a first-order set.

- In chapter 7, we get the same set of equations using the Lagrangian formulation of the analytical mechanics and Hamilton's equations are derived. The Hamiltonian framework allow us to work with a first-order set of ten equations, as we can ignore the equation for ψ.

- In chapter 8, nondimensional variables are defined in order to perform numerical integrations and we give the expressions for the vector mechanics and Hamilton's set of equations in term of these variables.

- In chapter 9, the analysis of the linear stability is performed. We linearize the first-order set of equations about the position of equilibrium in the $0Z_1$ axis, solve the linear system with real variables, complex exponentials and complex variables and find a basis of solutions to express any other as a combination of them.

Moreover, we derive mass, stiffness and gyroscopic matrixes to describe the system and its characteristic equation, that allow us to find the stability region in which stable hovering is possible. We also numerically solve two examples for different height of levitation, obtaining Campbell's diagrams and the natural frequencies for a certain rotational speed.

Computing the eigenvectors of the linear matrix, we explain the interpretation of the complex conjugate eigenvectors and find the five normal modes of the system. An analysis of these modes is also done, showing their trajectories and the time evolution.

Finally, we numerically show the trajectories for two given initial conditions and numerically validate the stable rotational speed for a height of levitation centered in the stability region.

- In chapter 10, we study the nonlinear system, verifying the linear and the nonlinear coupling. Moreover, we numerically solve the set of equations with initial conditions that try to reproduce the real situations that one faces when plays with the toy.

- In chapter 11, constants of the motion are presented. We numerically check the constancy of the mechanical energy and demonstrate the constancy of L_{0Z_1} and L_{GZ_3}.

- In chapter 12, a simple model is presented to consider the effect of air friction. We compute the drag force, Magnus force and drag torque and their corresponding generalized forces are included in the Hamiltonian system. The values of three coefficients, C_{drag}, C_{mag} and C_{torque} are found in order to provide a time of levitation around one minute.

- Finally, in chapter 13 we give some instructions in order to use the toy properly and we present a flowchart that summarizes all the situations that can be found when playing with the toy, indicating the corresponding chapter where we numerically study the situation.

Some recommendations for a future research should be given:

- Our analytical study is valid near the $0Z_1$ axis, as the expressions of the magnetic field can only be used for $\rho \ll 1$. Therefore, a study using the exact expressions of the magnetic field should be done.
- We have considered the spinning top as a magnetic dipole, neglecting its real size. This is another effect that should be taken into account in next studies.
- A more detailed model of the air friction is another possibility for future works.

ADDENDUM I: EXPERIMENTAL ADJUSTMENT

To make the experimental adjustment of the magnetic field, the experimental data taken in the job 'Efectos de pequeñas corrientes de aire sobre un Levitron' [8], which was obtained using a teslameter, is going to be used:

z(mm)	B(mT)	z(mm)	B(mT)	z(mm)	B(mT)	z(mm)	B(mT)
10	8,40	31	7,36	52	7,29	73	5,01
11	-7,21	32	7,54	53	7,17	74	4,91
12	-5,61	33	7,70	54	7,05	75	4,83
13	-4,55	34	7,82	55	6,95	76	4,73
14	-3,14	35	7,90	56	6,83	77	4,63
15	-1,84	36	7,98	57	6,74	78	4,53
16	-1,01	37	8,03	58	6,64	79	4,46
17	0,10	38	8,06	59	6,52	80	4,37
18	0,91	39	8,07	60	6,40	81	4,27
19	1,73	40	8,07	61	6,29	82	4,18
20	2,52	41	8,06	62	6,16	83	4,10
21	3,25	42	8,01	63	6,05	84	4,03
22	3,90	43	7,98	64	5,95	85	3,95
23	4,46	44	7,93	65	5,85	86	3,86
24	5,05	45	7,87	66	5,74	87	3,79
25	5,54	46	7,78	67	5,64	88	3,70
26	5,87	47	7,72	68	5,53	89	3,63
27	6,25	48	7,65	69	5,44	90	3,58
28	6,52	49	7,55	70	5,32	91	3,49
29	6,91	50	7,47	71	5,20		
30	7,16	51	7,39	72	5,11		

One has to find the values of the parameters A, b and z_0 in the following expression:

$$\vec{B}_0(z) = A\left(\frac{b^2}{(b^2+(z-z_0)^2)^{3/2}} - \frac{a^2}{(a^2+(z-z_0)^2)^{3/2}}\right)\vec{k}_1$$

1- The inner radius of the platform a is approximately equal to 25 mm.

2- To calculate b and z_0, we solve the set of equations given by (AI. 1) and (AI. 2)

$$B_0 = 0 \qquad \text{(AI. 1)}$$

$$\frac{\partial B_0}{\partial z} = 0 \qquad \text{(AI. 2)}$$

obtaining $b = 67.6864$ mm and $z_0 = -11.4067$ mm

3- Parameter A can be obtained evaluating those points where B_0 reaches its maximum value. Hence,

$$A = 1.9608 \cdot 10^3 \text{ mm} \cdot \text{mT}$$

In figure, we can see a comparison between the distribution of points experimentally obtained and the adjustment given by eq.

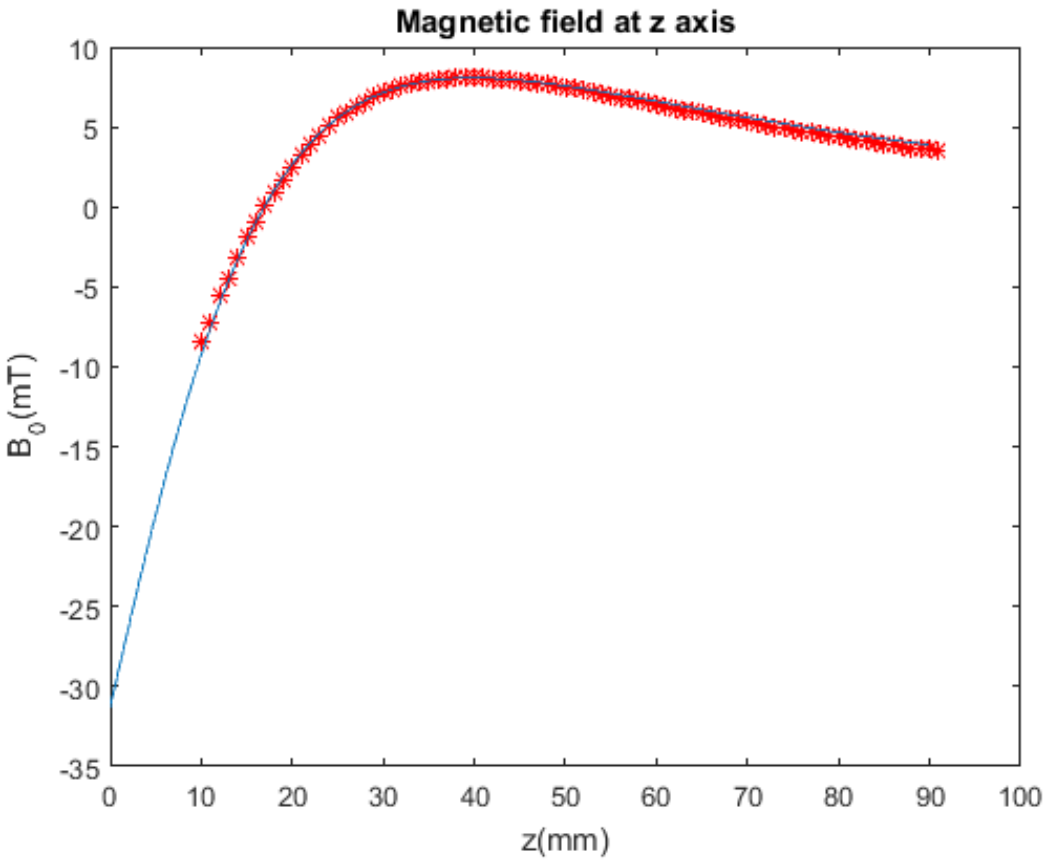

Figure AdI-1: Experimental adjustment.

ADDENDUM II: ANALYSIS WITH QUATERNIONS AND EULER PARAMETERS

In the previous chapters, we studied the Euler angles to relate the angular velocities to the rotation angles ϕ, θ, ψ and their rates. These equations have singularities, which makes it difficult to do any numerical work with them.

Even with the advantage of the yaw-pitch-roll sequence, which eliminated the problem in the denominators by shifting the singularity to $\theta = \frac{\pi}{2}$, the equations are highly nonlinear.

To alleviate these difficulties, we are going to express the motion of system with another set, called Euler parameters. These parameters increase the number of variables from three to four, but in many cases they eliminate the nonlinearities and many of the numerical problems.

Because a set of three variables (ϕ, θ, ψ) is being expressed in terms of four variables, the use of Euler parameters introduces a redundancy. This implies that there is no unique way of expressing the Euler parameters, existing other commonly used quantities which are, essentially, different forms of these parameters. The vector formulation, known as quaternions, was developed by Heaviside.

Nevertheless, from the inspection of the Hamiltonian system of equations derived in chapter 7.2, one can see that there are some equations with cosine functions in the denominators. This fact allays the significant advantage provided by the use of quaternions.

The most important ideas and expressions of quaternions used to derive the equations of motion are

- Generalization of complex numbers to 4D

$$\mathrm{q} = q_0 + \vec{q} = q_0 + q_x\vec{\imath} + q_y\vec{\jmath} + q_z\vec{k}$$

- Conjugate quaternion:

$$\mathrm{q}^* = q_0 - \vec{q}$$

- Scalar and vector parts of a quaternion q:

$$q_0 = S(\mathrm{q}) = \frac{\mathrm{q} + \mathrm{q}^*}{2}$$

$$\vec{q} = V(\mathrm{q}) = \frac{\mathrm{q} - \mathrm{q}^*}{2}$$

- Product of two quaternions q and p:

$$\mathrm{qp} = (q_0 p_0 - \vec{q} \cdot \vec{p}) + (q_0\vec{p} + p_0\vec{q} + \vec{q} \times \vec{p})$$

- Modulus of a quaternion

$$|\mathrm{q}| = \sqrt{\mathrm{q}\mathrm{q}^*} = \sqrt{q_0^2 + |\vec{q}|^2}$$

- Inverse

$$\mathrm{q}^{-1} = \frac{\mathrm{q}^*}{|\mathrm{q}|^2}$$

- The direction cosine matrix $\bar{\bar{R}}$, in terms of the parameters

$$\{q_0, q_x, q_y, q_z\}$$

has quadratic expressions

$$\bar{\bar{R}} = \begin{pmatrix} q_0^2 + q_x^2 - q_y^2 - q_z^2 & 2(q_x q_y - q_0 q_z) & 2(q_x q_z + q_0 q_y) \\ 2(q_x q_y + q_0 q_z) & q_0^2 - q_x^2 + q_y^2 - q_z^2 & 2(q_x q_y - q_0 q_z) \\ 2(q_x q_z - q_0 q_y) & 2(q_y q_z + q_0 q_x) & q_0^2 - q_x^2 - q_y^2 + q_z^2 \end{pmatrix}$$

- The consideration of unit quaternions leads to

$$|\mathrm{q}| = 1 \Rightarrow q_0^2 + q_x^2 + q_y^2 + q_z^2 = 1$$

Following Euler's rotation theorem, a rotation through an angle θ about an axis defined by the unit vector $\vec{u}$

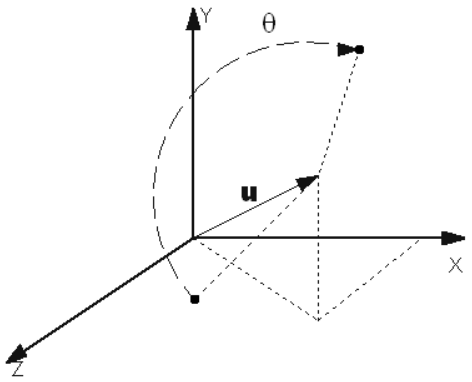

Figure AdII-1: Euler's rotation theorem.

can be written as

$$\mathrm{q}_\theta = \cos\left(\frac{\theta}{2}\right) + \sin\left(\frac{\theta}{2}\right)\vec{u}$$

Denoting as $\vec{r}_0$ and $\vec{r}$ the initial and final positions, we have the following relations

$$\vec{r} = \mathrm{q}\vec{r}_0\mathrm{q}^*$$
$$\vec{r}_0 = \mathrm{q}^*\vec{r}\mathrm{q}$$

As we saw in chapter 3, we use the yaw-pitch-roll sequence to describe the motion of the spinning top, so that we arrive from frame '1' to the body-frame '4' by means of the successive rotations:

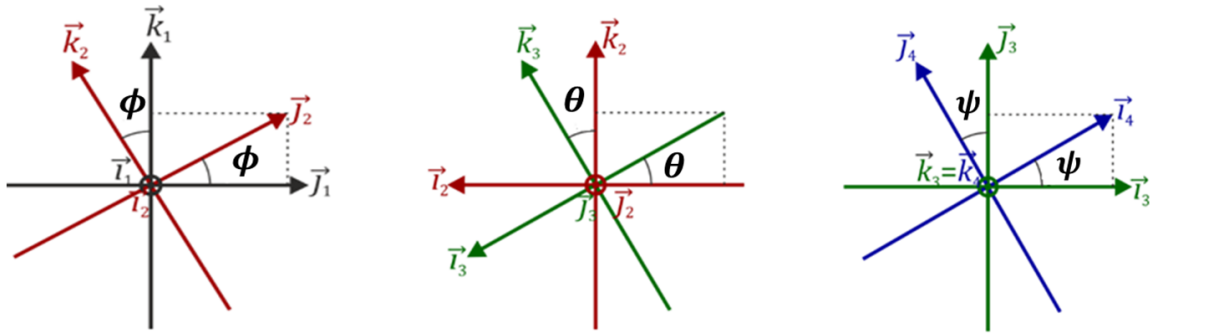

$$\mathrm{q}_{\phi} = \cos\left(\frac{\phi}{2}\right) + \mathrm{sen}\left(\frac{\phi}{2}\right)\vec{\imath} \qquad \mathrm{q}_{\theta} = \cos\left(\frac{\theta}{2}\right) + \mathrm{sen}\left(\frac{\theta}{2}\right)\vec{\jmath} \qquad \mathrm{q}_{\psi} = \cos\left(\frac{\psi}{2}\right) + \mathrm{sen}\left(\frac{\psi}{2}\right)\vec{k}$$

Figure AdII-2: Successive rotations in terms of the quaternions.

In terms of the quaternions, we can compound these three rotations by multiplying the quaterions:

$$\mathrm{q} = \mathrm{q}_{\phi}\mathrm{q}_{\theta}\mathrm{q}_{\psi}$$

Differentiating with respect to time

$$\vec{r} = \mathrm{q}\vec{r}_0\mathrm{q}^*$$

we have

$$\dot{\vec{r}} = \dot{\mathrm{q}}\vec{r}_0\mathrm{q}^* + \mathrm{q}\vec{r}_0\dot{\mathrm{q}}^* = \dot{\mathrm{q}}\mathrm{q}^*\vec{r} + \vec{r}\mathrm{q}\dot{\mathrm{q}}^* = V(2\dot{\mathrm{q}}\mathrm{q}^*\vec{r})$$

The angular velocity can be written as

$$\vec{\omega} = 2\dot{\mathrm{q}}\mathrm{q}^*$$

Therefore, we arrive to the following relation between the time derivatives of Euler parameters and the angular velocity components.

$$\dot{\mathrm{q}} = \frac{1}{2}\vec{\omega}\mathrm{q}$$

As we saw in chapter 6.1, the traslational motion of the system is given by Newton's Second law

$$m\vec{a} = m\vec{g} + \nabla\left(\vec{\mu}\cdot\vec{B}\right)$$

and the rotational motion, studied in 6.2

$$\frac{\mathrm{d}\vec{L}_G}{\mathrm{d}t} = \vec{\mu}\times\vec{B}$$

The components of the magnetic field $\vec{B}$ and the magnetic moment $\vec{\mu}$ verify

$$\vec{B} = B_x\vec{\imath}_1 + B_y\vec{\jmath}_1 + B_z\vec{k}_1$$
$$\vec{\mu} = -\mu\vec{k}_4 = -\mu\bar{\bar{R}}^{-1}\vec{k}_1$$

Using all the previous ideas, we arrive to the following set of equations:

$$\begin{cases} \dot{x} = v_x \\ \dot{y} = v_y \\ \dot{z} = v_z \end{cases} \tag{AdII.1}$$

$$\begin{cases} \dot{v}_y = \dfrac{1}{m}\dfrac{\partial}{\partial x}(B_x\mu_x + B_y\mu_y + B_z\mu_z) \\ \dot{v}_y = \dfrac{1}{m}\dfrac{\partial}{\partial y}(B_x\mu_x + B_y\mu_y + B_z\mu_z) \\ \dot{v}_z = -g + \dfrac{1}{m}\dfrac{\partial}{\partial z}(B_x\mu_x + B_y\mu_y + B_z\mu_z) \end{cases} \tag{AdII.2}$$

$$\begin{cases} I_1\dot{\omega}_X + (I_3 - I_1)\omega_Y\omega_Z = \mu B_Y \\ I_1\dot{\omega}_Y - (I_3 - I_1)\omega_X\omega_Z = \mu B_X \\ I_3\dot{\omega}_Z = 0 \end{cases} \tag{AdII.3}$$

$$\begin{cases} \dot{q}_0 = (-\omega_X q_X - \omega_Y q_Y - \omega_Z q_Z)/2 \\ \dot{q}_X = \ \ (\omega_X q_0 - \omega_Y q_Z + \omega_Z q_Y)/2 \\ \dot{q}_Y = (-\omega_X q_Z + \omega_Y q_0 + \omega_Z q_X)/2 \\ \dot{q}_Z = \ \ (\omega_X q_Y + \omega_Y q_X + \omega_Z q_0)/2 \end{cases} \tag{AdII.4}$$

ADDENDUM III: DESCRIPTION OF OTHER SYSTEMS

In this addendum, we are going to study the dynamics and derive the equations of motion of some interesting systems that share resemblances with the Levitron:

- A classical spinning top and the Earth, where the gyroscopic effect plays a decisive role as in the case of our toy. Using the 'classical' Euler angles, which were presented in chapter 2.1, the main characteristics of the motion are described.

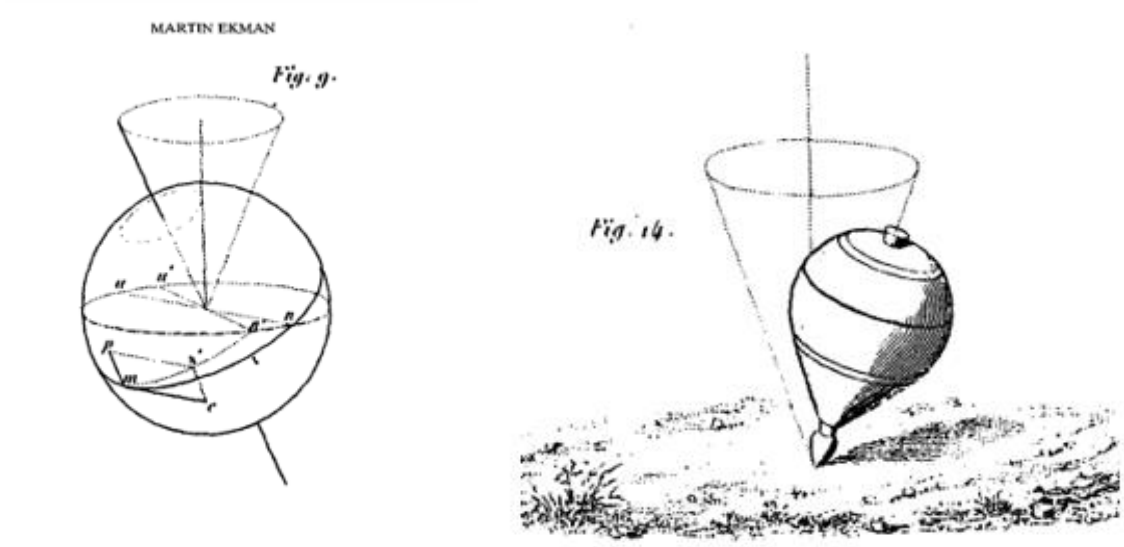

Figure AdIII-1: Martin Ekman: precession-nutation and polar motion.

- An introduction to the magnet-mechanical problem of the nuclear fusion, an investigation line of great cientific repercussion.

AdIII.1 Motion of a spinning top

An interesting case to consider is the motion of a spinning top. It consists basically on a body that possesses rotational symmetry and that pivotes about a sharp point fixed (called the apex or vertex), moving on a gravitational field. The axisymmetric design increases stability and reduces the friction due to the air mass around the top.

The physical reason why the motion of the top is stable is due to the balancing of the gravitational moment about the apex by the gyroscopic moment. We assume that the apex does not translate and it is in continuous contact with the horizontal plane (the translational motion would be caused by the initial translational motion given, as well as the roughness and unevenness of the plane on which the top moves).

Here, we will derive the equations of motion using analy1tical mechanics and briefly analyze the integrals of the motion and qualitatively assess the behavior of the top.

The constraint on the apex to be a fixed point reduces the number of degrees of freedom to three. Therefore, we can use the Euler angles to completely specify the motion of the top. A 3-1-3 transformation will be used, so that the values for the angular velocities as a function of the Euler angles are the same to those used in the chapter 2.1.

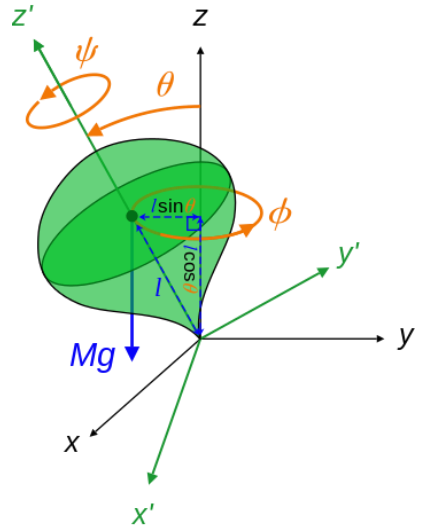

Figure AdIII-2: Classical spinning top.

The top being an axisymmetric body, the kinetic energy can be written as

$$T = \frac{1}{2}\left(I_X\omega_X^2 + I_Y\omega_y^2 + I_Z\omega_Z^2\right) \tag{AdIII.1}$$

and in term of the Euler angles

$$T = \frac{1}{2}\left[I_X\left(\dot{\theta}^2 + \dot{\phi}^2\sin^2(\theta)\right) + I_Z\left(\dot{\psi} + \dot{\phi}\cos(\theta)\right)^2\right] \tag{AdIII.2}$$

The potential energy is

$$V = mgl\cos(\theta) \tag{AdIII.3}$$

The only other forces acting on the spinning top are those at the point of contact, which do not work, as they are being applied to a fixed point. The Lagrangian of the system is then

$$\mathcal{L} = \frac{1}{2}\left[I_X\left(\dot{\theta}^2 + \dot{\phi}^2\sin^2(\theta)\right) + I_Z\left(\dot{\psi} + \dot{\phi}\cos(\theta)\right)^2\right] - mgl\cos(\theta) \tag{AdIII.4}$$

It can be seen that $\mathcal{L}$ does not involve the angles ϕ and ψ, which indicates that these coordinates are cyclic. Therefore, the integrals of motion of the system are the total energy and generalized momenta associated with precession and spin. These integrals of the motion are

$$\begin{aligned} p_\phi &= I_X\dot{\phi}\sin^2(\theta) + I_Z\left(\dot{\phi}\cos(\theta) + \dot{\psi}\right)\cos(\theta) = constant \\ p_\psi &= I_Z\left(\dot{\phi}\cos(\theta) + \dot{\psi}\right) = I_Z\omega_Z = constant \end{aligned} \tag{AdIII.5}$$

These constants represent the components of the angular momentum along the Z and Z' axes (see figure AdIII-3). Using Lagrange's equations, the equation of motion for θ is

$$I_X\ddot{\theta} - (I_X - I_Z)\dot{\phi}^2 \sin(\theta)\cos(\theta) + I_Z\dot{\phi}\dot{\psi}\sin(\theta) - mgl\sin(\theta) = 0 \tag{AdIII.6}$$

Solving from equations (AdIII.7) for the precession and spin rates, we have

$$\begin{aligned} \dot{\phi} &= \frac{p_\phi - p_\psi \cos(\theta)}{I_X \sin^2(\theta)} \\ \dot{\psi} &= p_\psi \left(\frac{1}{I_Z} + \frac{\cos^2(\theta)}{I_X \sin^2(\theta)} \right) - p_\phi \frac{\cos(\theta)}{I_X \sin^2(\theta)} \end{aligned} \tag{AdIII.8}$$

Substituting into eq.(AdIII.9), we can solve for θ. Once the nutation angle is solved for, the precession and spin rates can be calculated.

The equation of motion for θ can also be derived using the Routh's method for ignorable coordinates (ϕ and ψ in our problem). Defining the Routhian as

$$\mathcal{R} = \mathcal{L} - p_\phi \dot{\phi} - p_\psi \dot{\psi} \tag{AdIII.10}$$

and substituting the expressions for $\dot{\phi}$ and $\dot{\psi}$, one obtains

$$\mathcal{R} = \frac{1}{2} I_X \dot{\theta}^2 - \frac{\left(p_\phi - p_\psi \cos(\theta)\right)^2}{2 I_X \sin^2(\theta)} - \frac{p_\psi^2}{2 I_Z} - mgL\cos(\theta) \tag{AdIII.11}$$

We can therefore define T' and U' as

$$\begin{aligned} T' &= \frac{1}{2} I_X \dot{\theta}^2 \\ U' &= \frac{\left(p_\phi - p_\psi \cos(\theta)\right)^2}{2 I_X \sin^2(\theta)} + \frac{p_\psi^2}{2 I_Z} + mgL\cos(\theta) \end{aligned} \tag{AdIII.12}$$

and the energy integral

$$E = T' + U' \tag{AdIII.13}$$

Introducing the following constant quantities

$$\alpha' = \frac{2}{I_X}\left(E - \frac{p_\psi^2}{2 I_Z} \right)$$

$$\beta' = \frac{2mgL}{I_X}$$

$$a' = \frac{p_\phi}{I_X}$$

$$b' = \frac{p_\psi}{I_X}$$

E can be written as

$$\sin^2(\theta)\dot{\theta}^2 = \sin^2(\theta)(\alpha' - \beta'\cos(\theta)) - (b' - a'\cos(\theta))^2 \quad \text{(AdIII.14)}$$

To simplify the expression, we define the variable $u = \cos(\theta)$, which is a nondimensional quantity that describes the elevation of a point on the symmetry axis that is at a distance unit from the apex.

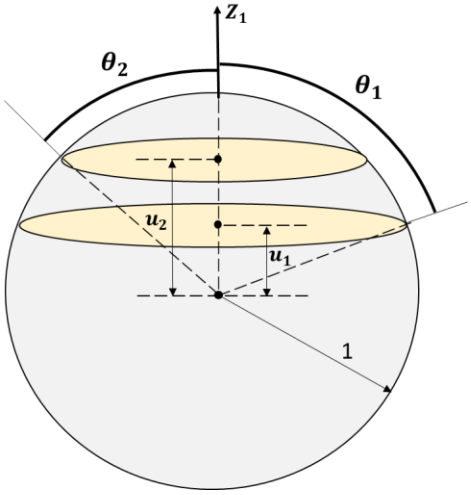

Figure AdIII-0-4: Intepretation of variable u.

The energy integral can thus be written as the following cubic function

$$\dot{u}^2 = f(u) = (1 - u^2)(\alpha - \beta u) - (a - bu)^2 \quad \text{(AdIII.15)}$$

The characteristics of the motion can be qualitatively studied analyzing the function $f(u)$.

A very interesting case corresponds to zero nutation rate, i.e, $\dot{u} = 0$. The values of u that lead to zero nutation rate can be obtained by solving $f(u) = 0$. Because u is defined as $u = \cos(\theta)$, we are interested in the roots of $f(u)$ in the range $-1 \leq u \leq 1$. Moreover, we have to consider the values of u that are larger tan zero, as a negative value implies that the top would be spinning below the platform it is on.

We next study the characteristics of $f(u)$

1- Both $f(1)$ and $f(-1)$ are less tan zero

2- As u becomes larger, $f(u) \simeq \beta u^3 > 0$, since $\beta > 0$

With this information, an approximate plot of $f(u)$ is

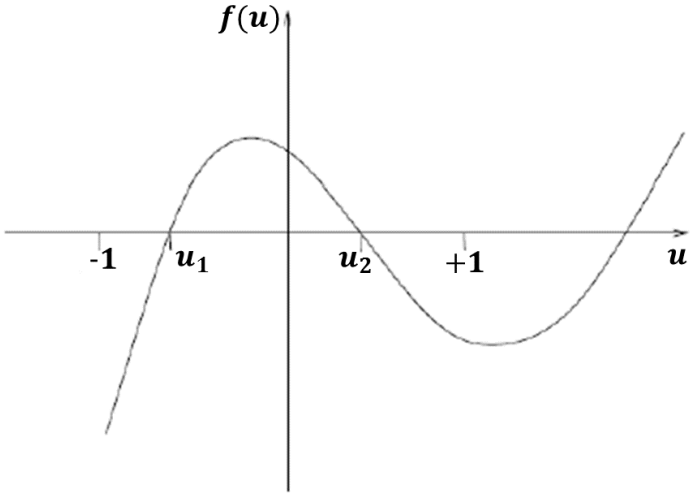

Figure AdIII-5:Plot of $f(u)$

The precession rate, from eq. is

$$\dot{\phi} = \frac{a - bu}{1 - u^2} \tag{AdIII.16}$$

so that this rate depends on the value $a - bu$. Defining the quantity u_0, based on initial conditions as

$$u_0 = \frac{p_\phi}{p_\psi} = \frac{a}{b} = \frac{I_X \sin^2(\theta_0)\dot{\phi}_0}{I_Z\left(\dot{\phi}_0 \cos(\theta_0) + \dot{\psi}_0\right)} \tag{AdIII.17}$$

It turns out that characteristics of the motion of the top depend on u_0, u_1 and u_2. We have the following different types of motion based on the initial conditions:

Unidirectional precession $u_0 > u_2 \; or \; u_0 < u_1$ | Looping precession $u_1 < u_0 < u_2$ | Cuspidal motion $u_0 = u_2$

Figure AdIII-6: Types of precession.

AdIII.2 Forced precession and nutation of Earth

In this section, we follow [22] in order to obtain a model to describe precession and nutation motions and compute the precession and nutation periods of our planet. To do this, we use again the proper or classic Euler angles (chapter 2.1).

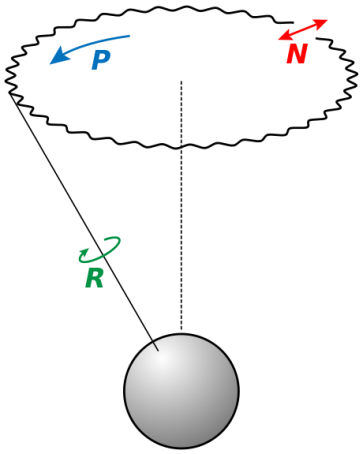

Figure AdIII-7: Earth motions in term of the Classic Euler angles.

We start considering the Sun-Earth system and then we increase the accuracy of the model adding the moon influence. The potential energy of the Earth-Sun system, using McCullough's formula, is

$$U = -\frac{GM_S M}{a_S} + \frac{GM_S(I_Z - I_X)}{a_S^3} P_2(\cos\gamma_S) \tag{AdIII.18}$$

where M_S is the mass of the Sun, M the mass of the Earth, I_Z the Earth's moment of inertia about its axis of rotation and I_X the Earth's moment of inertia about an axis lying on its equatorial plane. Function $P_2(x)$ is given by

$$P_2(x) = \frac{1}{2}(3x^2 - 1) \tag{AdIII.19}$$

and γ_S is the angle subtended between $\vec{\omega}$ and the position vector of the Sun relative to the Earth. Being a_S the radius of the apparent orbit and λ_S the ecliptic longitude , $\vec{r}_S$ is given by

$$\vec{r}_S = a_S(\cos\lambda_S\,, \sin\lambda_S, 0) \tag{AdIII.20}$$

Computing the dot product to obtain $\cos\gamma_S$, we have

$$\vec{\omega}\cdot\vec{r}_S = |\vec{\omega}||\vec{r}_S|\cos\gamma_S \rightarrow \cos\gamma_S = \frac{\vec{\omega}\cdot\vec{r}_S}{|\vec{\omega}||\vec{r}_S|} = \sin(\theta)\sin(\gamma_S) \tag{AdIII.21}$$

In figure AdIII-8 we can see all the magnitudes previously defined:

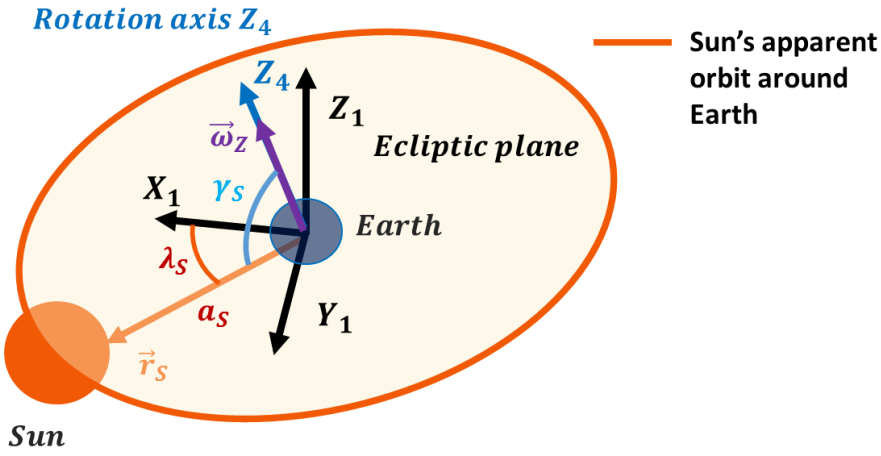

Figure AdIII-9: Sun-Earth system.

Potential energy is therefore

$$U = -\frac{GM_S M}{a_S} + \frac{GM_S(I_Z - I_X)}{2a_S^3}(3\sin^2(\theta)\sin^2(\lambda_S) - 1) \tag{AdIII.22}$$

As we are primarily interested in the motion of the Earth's axis of rotation on timescales that are much longer than a year, we can average the expression over the Sun's orbit, using that the average of $\sin^2(\lambda_S)$ over a year is ½

$$U = -\frac{GM_S M}{a_S} + \frac{GM_S(I_Z - I_X)}{2a_S^3}\left(\frac{3}{2}\sin^2(\theta) - 1\right) \tag{AdIII.23}$$

After some mathematical manipulation, we get

$$U = -\frac{GM_S M}{a_S} - \frac{3GM_S I_Z(I_Z - I_X)}{8a_S^3 I_Z}\left(\frac{1}{3} + \cos(2\theta)\right) \tag{AdIII.24}$$

The preceding expression can be rewritten as

$$U = U_0 - \tilde{\epsilon}\alpha_S \cos(2\theta) \tag{AdIII.25}$$

U_0 is a constant that will disappear when we derive the equations of motion. Moreover, the following constants have been introduced:

$$\alpha_S = \frac{3}{8} I_Z \omega_S^2$$

where ω_S is the Sun's apparent orbital angular velocity, whose expression can be obtained by equating the gravitational force to the centripetal force of the Earth

$$\frac{GM_SM}{a_S^2} = M{\omega_S}^2 a_S \rightarrow \omega_S = \frac{d\lambda_S}{dt} = \left(\frac{GM_S}{a_S^3}\right)^{\frac{1}{2}}$$

Finally, $\tilde{\epsilon}$ is the Earth's dynamical ellipticity and its value is determined from the Earth's observed flattening

$$\tilde{\epsilon} = \frac{I_Z - I_X}{I_Z}$$

The rotational kinetic energy is

$$T = \frac{1}{2}\left(I_X\omega_X^2 + I_Y\omega_Y^2 + I_Z\omega_Z^2\right) \tag{AdIII.26}$$

and in terms of the Classic Euler angles

$$T = \frac{1}{2}\left[I_X\left(\dot{\theta}^2 + \dot{\phi}^2\sin^2(\theta)\right) + I_Z\left(\dot{\psi} + \dot{\phi}\cos(\theta)\right)^2\right] \tag{AdIII.27}$$

Hence, neglecting any constant terms, the Earth's Lagrangian is

$$\mathcal{L} = \frac{1}{2}\left[I_X\left(\dot{\theta}^2 + \dot{\phi}^2\sin^2(\theta)\right) + I_Z\left(\dot{\psi} + \dot{\phi}\cos(\theta)\right)^2\right] + \tilde{\epsilon}\alpha_S\cos(2\theta) \tag{AdIII.28}$$

As $\mathcal{L}$ does not depend on the angular coordinate ψ, it follows that the corresponding conjugate momentum is a constant of the motion, implying that ω_Z is also a constant of the motion. Note that ω_Z is the Earth's angular velocity of rotation about its axis

$$p_\psi = \frac{\partial\mathcal{L}}{\partial\dot{\psi}} = I_Z\omega_Z$$

Using Lagrange equation for θ

$$\frac{d}{dt}\left(\frac{\partial\mathcal{L}}{\partial\dot{\theta}}\right) - \frac{\partial\mathcal{L}}{\partial\theta} = 0$$

we have

$$I_X\ddot{\theta} - \frac{\partial\mathcal{L}}{\partial\theta} = 0 \tag{AdIII.29}$$

To compute the precession period, we consider steady precession of the rotation axis of the Earth about the normal of the ecliptic plane. In terms of the Proper Euler angles, this means

$$\dot{\phi} = constant \rightarrow \ddot{\phi} = 0$$
$$\theta = constant \rightarrow \dot{\theta} = \ddot{\theta} = 0$$
$$\dot{\psi} = constant \rightarrow \ddot{\psi} = 0$$

and therefore

$$\frac{\partial \mathcal{L}}{\partial \theta} = 0 \rightarrow \frac{1}{2} I_X \dot{\phi}^2 \sin(2\theta) - I_Z \omega_Z \dot{\phi} \sin(\theta) - 2\tilde{\epsilon}\alpha_S \sin(2\theta) = 0 \quad \text{(AdIII.30)}$$

Using that ω_Z is much larger than precession speed, i.e $|\dot{\phi}| \ll \omega$, the first term of the previous equation can be neglected and obtain $\dot{\phi}$ as a function of the rest of the variables:

$$\dot{\phi} = -\frac{4\tilde{\epsilon}\alpha_S \cos(\theta)}{I_X \omega} = -\frac{3\tilde{\epsilon}\omega_S^2}{2\omega_Z}\cos(\theta) = -\Omega_\phi \quad \text{(AdIII.31)}$$

with

$$\Omega_\phi = \frac{3\tilde{\epsilon}\omega_S^2}{2\omega_Z}\cos(\theta) \quad \text{(AdIII.32)}$$

Thus, Earth's axis of rotation describes a steady precession about the normal of the ecliptic plane with speed $-\Omega_\phi$. Minus sign means that the precession sense is opposite to the Sun's apparent orbit and the Earth's diurnal rotation:

$$T_\phi = \frac{\omega_S}{\Omega_\phi} = \frac{\omega_S}{\frac{3\tilde{\epsilon}\omega_S^2}{2\omega_Z}\cos(\theta)} = \frac{2\omega_Z/\omega_S}{3\tilde{\epsilon}\cos(\theta)} \quad \text{(AdIII.33)}$$

with

$$\frac{\omega_Z}{\omega_S} = \frac{366.26\ rev/year}{1\ rev/year} = 366.26$$

For the rest of the parameters

$$\tilde{\epsilon} = 0.00335$$

$$\theta = 23.44° \text{ (mean value)}$$

Therefore, we get

$$T_\phi \simeq 79400 \text{ years}$$

Nevertheless, the observed precession period of the Earth's axis of rotation about the normal to the ecliptic plane is approximately 25.800 years, so we need to refine the model considering the influence of the Moon.

The potential energy of the Earth-Moon system is

$$U = -\frac{GM_m M}{a_m} + \frac{GM_m(I_Z - I_X)}{a_m^3} P_2(\cos\gamma_m) \quad \text{(AdIII.34)}$$

where M_m is the lunar mass, $a_m$the radius of the Moon's orbit (assuming that is approximately circular) and γ_m is the angle subtended between the Earth's angular velocity $\vec{\omega}$ and the position vector of the Moon relative to the Earth $\vec{r}_m$.

The Moon's orbital plane is slightly inclined to the ecliptic plane, being the angle of inclination $I_m = 5.16°$

$$\vec{r}_m = a_m(\cos\lambda_m\,, \sin\lambda_m, \sin(I_m)\sin(\lambda_m - \alpha_n))$$

Approximating to first order in I_m, we can write:

$$\vec{r}_m \simeq a_m(\cos\lambda_m\,, \sin\lambda_m, I_m\sin(\lambda_m - \alpha_n))$$

where λ_m is the Moon's ecliptic longitude and α_n is the ecliptic longitude of the lunar ascending node, which is defined as the point of the lunar orbit where the Moon crosses the ecliptic plane from south to north. All these variables can be seen in figure AdIII-10 and AdIII-11:

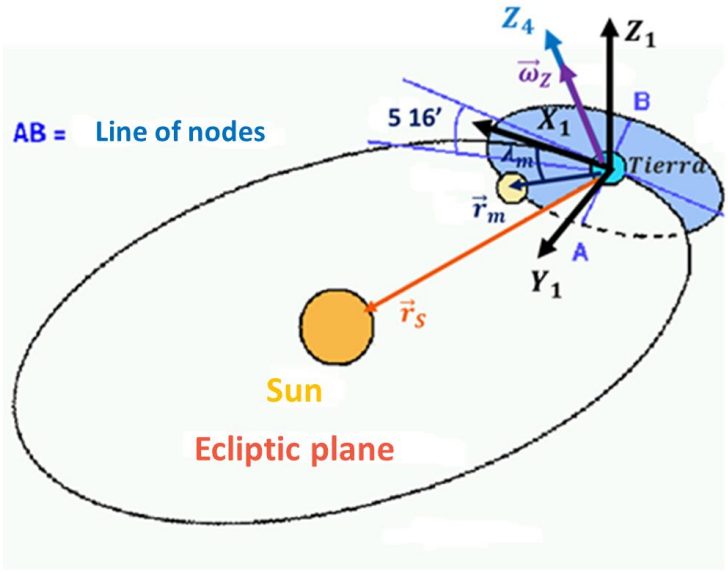

Figure AdIII-12: Sun-Earth-Moon system.

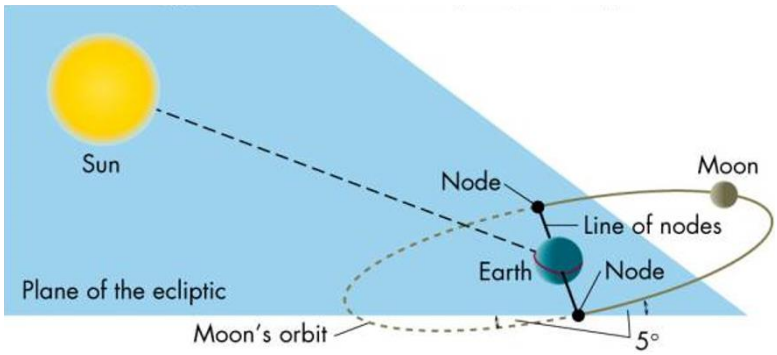

Figure AdIII-13: Sun-Earth-Moon system.

Computing Moon's apparent angular velocity ω_m and $\cos\gamma_m$

$$\omega_m = \frac{d\lambda_m}{dt} = \left(\frac{GM}{a_m^3}\right)^{\frac{1}{2}}$$
$$\vec{\omega}\cdot\vec{r}_m = |\vec{\omega}||\vec{r}_m|\cos\gamma_m \rightarrow \cos\gamma_m = \frac{\vec{\omega}\cdot\vec{r}_m}{|\vec{\omega}||\vec{r}_m|} = \sin(\theta)\sin(\lambda_m-\phi) + I_m\cos(\theta)\sin(\lambda_m-\alpha_n) \quad \text{(AdIII.35)}$$

The potential energy of Moon's-Earth system is

$$U = -\frac{GM_mM}{a_m} + \frac{GM_m(I_Z-I_X)}{2a_m^3}[3\sin^2(\theta)\sin^2(\lambda_m-\phi) + 3I_m\sin(2\theta)\sin(\lambda_m-\phi)\sin(\lambda_m-\alpha_n) - 1] \quad \text{(AdIII.36)}$$

We are interested in the motion of the Earth's axis of rotation on timescales that are much longer than a month

$$U = -\frac{GM_mM}{a_m} + \frac{GM_m(I_Z-I_X)}{2a_m^3}[3\sin^2(\theta)\sin^2(\lambda_m-\phi) + 3I_m\sin(2\theta)\sin(\lambda_m-\phi) - 1] \quad \text{(AdIII.37)}$$

where it has been used that the average of

$$\sin^2(\lambda_m-\phi) = 1/2$$
$$\sin(\lambda_m-\phi)\sin(\lambda_m-\alpha_n) = \frac{1}{2}\cos(\alpha_n-\phi)$$

Moreover, defining

$$\alpha_m = \frac{3}{8}I_Z\gamma_m\omega_m^2$$
$$\beta_m = \frac{3}{4}I_ZI_m\gamma_m\omega_m^2$$

Therefore, Moon's-Earth potential energy can be shortened to

$$U = U_0{}' - \tilde{\epsilon}\alpha_m\cos(2\theta) + \tilde{\epsilon}\beta_m\sin(2\theta)\cos(\alpha_n-\phi) \quad \text{(AdIII.38)}$$

To compute the total potential energy of the Earth we use that gravity is a superposable force, so we can add the potential energy of the Earth-Sun and Eath-Moon systems:

$$U = U_0{}'' - \tilde{\epsilon}\alpha_S\cos(2\theta) - \tilde{\epsilon}\alpha_m\cos(2\theta) + \tilde{\epsilon}\beta_m\sin(2\theta)\cos(\alpha_n-\phi) \quad \text{(AdIII.39)}$$

where $U_0{}''$ is another constant

Therefore, the Lagrangian of the Earth, considering the influence of Sun and Moon, is

$$\mathcal{L} = \frac{1}{2}\left[I_X\left(\dot{\theta}^2 + \dot{\phi}^2\sin^2(\theta)\right) + I_Z\left(\dot{\psi} + \dot{\phi}\cos(\theta)\right)^2\right] + \tilde{\epsilon}\alpha\cos(2\theta) - \tilde{\epsilon}\beta_m\sin(2\theta)\cos(\alpha_n-\phi) \quad \text{(AdIII.40)}$$

Following in an analogous way to [13], Lagrange's equations

$$\frac{d}{dt}\left(\frac{\partial \mathcal{L}}{\partial \dot{\theta}}\right) - \frac{\partial \mathcal{L}}{\partial \dot{\theta}} = 0$$
$$\frac{d}{dt}\left(\frac{\partial \mathcal{L}}{\partial \dot{\phi}}\right) - \frac{\partial \mathcal{L}}{\partial \phi} = 0$$

provide

$$T_\phi \simeq 24800 \text{ years}$$
$$T_\theta \simeq 18.6 \text{ years}$$

Both stimations are quite close to the mark. The inaccuracies are due to small eccentricities of the Earth's orbit around the Sun and the Moon's orbit around the Earth, that have been neglected, and the consideration of the Earth as a homogeneous body.

AdIII.3 Trajectories of particles in a heli-toroidal magnetic field

Nuclear fusion is a magnet-mechanical problem with cylindrical symmetry (as the Levitron case) of great cientific repercussion.

We are going to construct a simplified model of a Tokamak reactor in order to study the motion of a single particle. For that purpose, a constant magnetic field acting in the Z-direction B_Z and an azimuthal component B_θ are going to be considered (the real problem is, of course, so much complex).

A basic scheme of the reactor can be seen in figures AdIII-14 and Figure AdIII-0-15

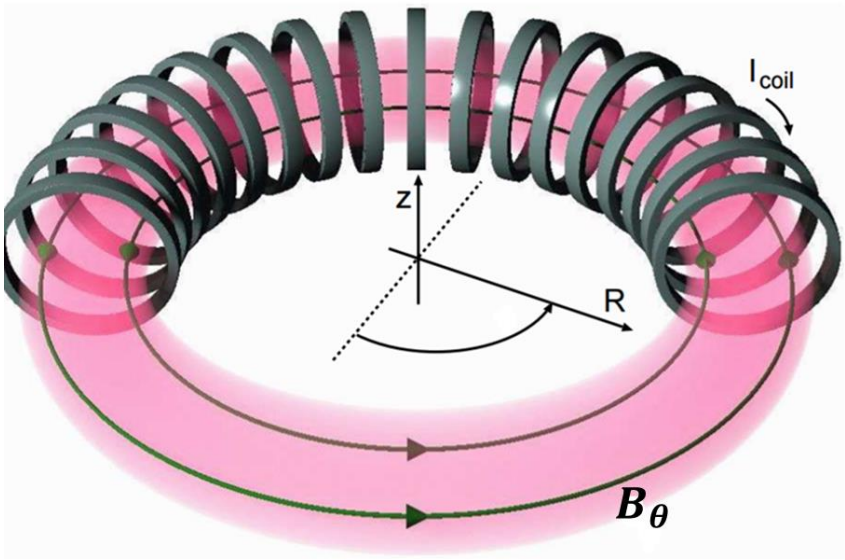

Figure AdIII-16: Scheme of a Tokamak reactor.

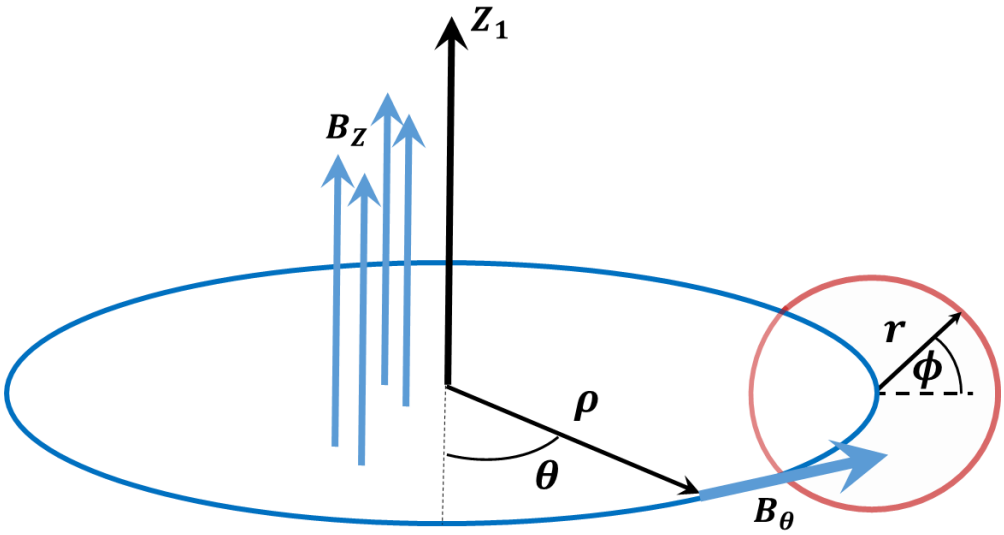

Figure AdIII-17: Scheme with constant vertical and azimuthal magnetic fields.

We assume that both fields are constants

$$B_Z = constant\ 1$$
$$B_\theta = constant\ 2$$

In a more detailed model, the variable r in figure AdIII-18 would represent small variations around the stationary solution (circumference about Z_1-axis).

To take into account the magnetic field acting in the azimuthal direction, we can use the Ampere's circuit law, which relates the integrated magnetic field around a closed loop (our simplified Tokamak) to the electric current passing through the loop:

$$\oint \vec{B}d\vec{l} = \mu_0 \sum_i I_i^{int} \rightarrow B_\theta \cdot 2\pi\rho = \mu_0 I \qquad \text{(AdIII.41)}$$

Therefore,

$$B_\theta = \frac{k}{\rho}$$
$$\text{with } k = \mu_0 I/2\pi$$

Using cylindrical coordinates, $\vec{B}$ can be expressed as

$$\vec{B} = B_\theta \vec{u}_\theta + B_Z \vec{k}$$

The acceleration of the particle is

$$\vec{a} = \begin{pmatrix} \ddot{\rho} - \rho\dot{\theta}^2 \\ \rho\ddot{\theta} + 2\dot{\rho}\dot{\theta} \\ \ddot{z} \end{pmatrix} \qquad \text{(AdIII.42)}$$

To compute the force acting on the particle of charge q due to the magnetic field $\vec{B}$ we use the expression of the Lorentz force:

$$\vec{F} = q\vec{v} \times \vec{B} = q \begin{vmatrix} \vec{u}_\rho & \vec{u}_\theta & \vec{k} \\ \dot{\rho} & \rho\dot{\theta} & \dot{z} \\ 0 & B_\theta & B_Z \end{vmatrix} = q \begin{pmatrix} \rho\dot{\theta}B_Z - \dot{z}B_\theta \\ -\dot{\rho}B_Z \\ \dot{\rho}B_\theta \end{pmatrix} \tag{AdIII.43}$$

This leads to the second-order differential equations

$$\begin{cases} m(\ddot{\rho} - \rho\dot{\theta}^2) = q(\rho\dot{\theta}B_Z - \dot{z}B_\theta) \\ m\left(\rho\ddot{\theta} + 2\dot{\rho}\dot{\theta}\right) = -q\dot{\rho}B_Z \\ m\ddot{z} = q\dot{\rho}B_\theta \end{cases} \tag{AdIII.44}$$

In order to perform numerical integrations, we rewrite it as a first-order set of equations

$$\begin{cases} \dot{\rho} = v_\rho \\ \dot{\theta} = v_\theta \\ \dot{z} = v_z \\ \dot{v}_\rho = \dfrac{\rho v_\theta^2}{m} + \dfrac{q}{m}(\rho v_\theta B_Z - v_z B_\theta) \\ \dot{v}_\theta = \dfrac{-2v_\rho v_\theta}{\rho} - \dfrac{q v_\rho B_Z}{\rho} \\ \dot{v}_z = q v_\rho B_\theta \end{cases} \tag{AdIII.45}$$

In the following figures, we can see that the motion consists on the superposition of the helical trajectory caused by B_Z and the contribution due to the azimuthal field B_θ

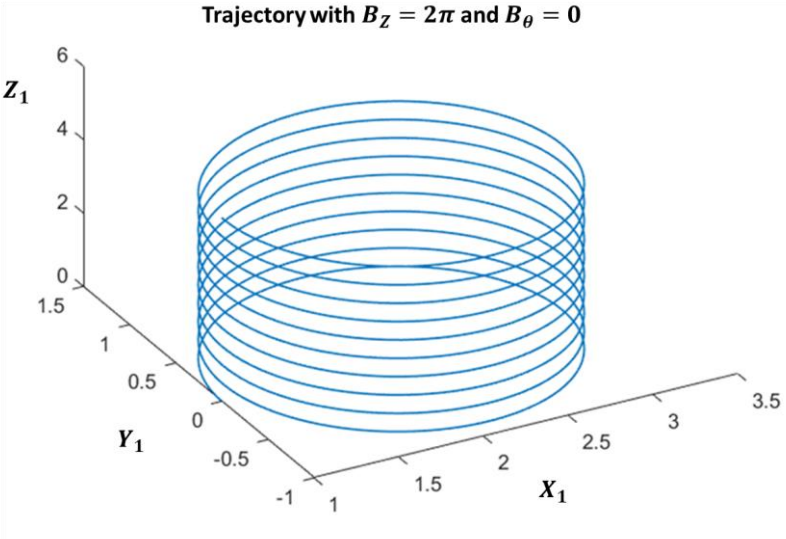

Figure AdIII-19: Helical trajectory considering vertical constant magnetic field.

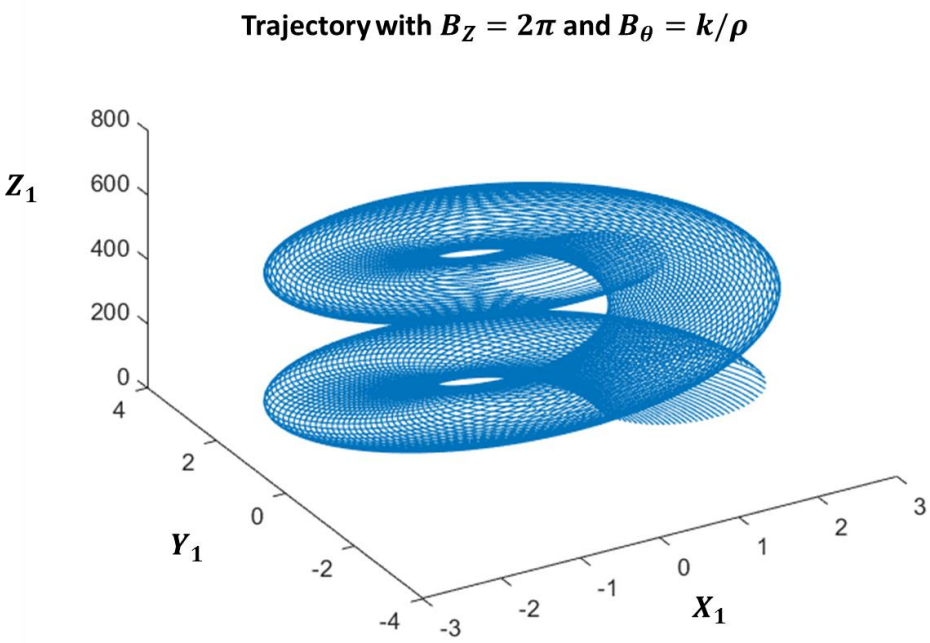

Figure AdIII-20: Trajectory considering vertical and azimuthal magnetic fields.

BIBLIOGRAPHY

[1] Wikipedia The free enciclopedia (July, 2017). Levitron (Online).
Available: https://en.wikipedia.org/wiki/Levitron

[2] Mike & Karen Sherlock, *The hidden history of the Levitron.*

[3] M. V. Berry: *The Levitron ™: an adiabatic trap for spins*, Proc. R.Soc. London, Ser. A 452, 1207–1220 (1996).

[4] G. Genta, C. Delprete, and D. Rondano, *Gyroscopic stabilization of passive magnetic Levitation*, Meccanica 34, 411–424 (1999).

[5] Holger R. Dullin and Robert W. Easton, *Stability of Levitrons*, Physica D 126, 1–17 (1999).

[6] S. Gov, S. Shtrikman, and H. Thomas, *On the dynamical stability of the hovering magnetic top*, Physica D 126, 214–224 (1999).

[7] A. T. Pérez and P. García-Sánchez, *Dynamics of a Levitron under a periodic magnetic forcing,* Departamento de Electrónica y Electromagnetismo, Universidad de Sevilla, Facultad de Física, 2014.

[8] Daniel Núñez Álvarez, *Efecto de pequeñas corrientes de aire sobre un Levitron®*, Trabajo Fin de Grado GIA, Tutor: Antonio González Fernández.

[9] Kirk T. McDonald, *The Levitron®,* Joseph Henry Laboratories, Princeton University, Princeton.

[10] S. I. Rubinow, Joseph B. Keller, *The transverse force on a spinning sphere moving in a viscous fluid,* Stevens Institute of Technology, Hoboken, New Jersey; Institute of Mathematical Sciences, New York University, New York, N.Y. , 1961.

[11] N. Lukerchenko, Yu. Kvurt, I. Keita, Z. Chara & P. Vlasak, *Drag Force, Drag Torque and Magnus Force coefficients of rotating spherical particle moving in fluid*.

[12] Anisha Deshmane, Karin Fisher, Emily Seitz & Katie Szeto, *How to use the Levitron*. Online Available: http://web.mit.edu/viz/levitron/How_To.html

[13] Richard Fitzpatrick, *Forced precession and nutation of Earth*, (Online).
Available: http://farside.ph.utexas.edu/teaching/celestial/Celestialhtml/node74.html

[14] Martin D. Simon, Lee O. Helfinger, and S. L. Ridgway, *Spin stabilized magnetic levitation*, Am. J. Phys. 65(4), 286–292 (1997).

[15] Antonio González Fernández, *Dinámica de un Levitron,* Universidad de Sevilla, 2016.

[16] T. B. Jones, Masao Washizu, and Roger Gans, *Simple theory for the Levitron*, J. Appl. Phys. 82, 883–888 (1997).

[17] [P. Flanders, S. Gov, S. Shtrikman, and H. Thomas, *On the spinning motion of the hovering magnetic top*, Physica D 126, 225–235 (1999).

[18] Manuel Toscano Jiménez, *Mecánica para ingenieros industriales,* Universidad de Sevilla, 2008.

[19] Jim Van Verth, *Understanding quaternions*, Game developers conference, 2013

[20] Jürgen Geiser, *Multiscale methods for levitron problems: Theory and applications*, EMA University of Greifswald, Department of Physics, 2012

[21] Haim Baruh, *Analytical Dynamics*, Mc-Graw Hill, 1999.

[22] Mark D. Ardema, *Analytical Dynamics, Theory and Applications*, 2005.

[23] Chloe Elliot, *The spinning top*, 2009.

[24] J. Jackson, *Classical Electrodynamics*, 2nd ed., Wiley, New York, 1975.

[25] MIT Open Courseware, nuclear engineering, chapter 2, *Motion of charged particles in fields*. (Online). Available: https://ocw.mit.edu/courses/nuclear-engineering/22-611j-introduction-to-plasma-physics-i-fall-2003/lecture-notes/chap2.pdf